

MASTER THESIS

A BIOLOGICALLY REALISTIC MEAN-FIELD MODEL OF THE THALAMUS

JORIN OVERWIENING



UNIVERSITY OF MÜNSTER
INSTITUTE FOR THEORETICAL PHYSICS



FRENCH NATIONAL CENTER FOR SCIENTIFIC RESEARCH
PARIS-SACLAY INSTITUTE FOR NEUROSCIENCES

SUPERVISORS:

Dr. Alain Destexhe
&
Dr. Svetlana Gurevich

CO-SUPERVISORS:

Dr. Federico Tesler
&
Dr. Domenico Guarino

FIRST ASSESSOR:

Dr. Svetlana Gurevich

SECOND ASSESSOR:

Dr. Alain Destexhe

DATE OF PRESENTATION:

-/-/-

LOCATION:

Münster

TIME FRAME:

23/04/2024 – 23/10/2024

*The thing we must do intensely is be human together.
People are more important than things*

— Frank Herbert

AUTHOR'S NOTE

I want to give a few opening remarks on this thesis:

Due to the interdisciplinary nature of this physics thesis, minimal prior knowledge of neuroscientific topics and definitions is assumed. The neuroscience-focused chapter on relevant aspects of the thalamus and its functions and cells ([Chapter 2](#)) is designed to be mostly self-contained. However, for additional support, a *Neuroscience primer* (in [Section A.1](#)) and a *Glossary* are provided at the end of this thesis.

The project's topic was initially outlined by Alain Destexhe, Federico Tesler, and Domenico Guarino, and subsequently approved by Svetlana Gurevich. The master project, comprising a two-set module at the *University of Münster*, was primarily conducted at the *Institut des Neurosciences Paris-Saclay*. During this time, I was fully integrated into Alain Destexhe's research group, while the remainder of my work was completed at the *Institute for Theoretical Physics* in Münster, where I was part of Svetlana Gurevich's and Uwe Thiele's group.

I am deeply grateful to several individuals who made this project possible. First and foremost, I thank Svetlana Gurevich for allowing me to undertake this project in an unconventional manner, for her constant support and helpfulness, and for integrating me into her research group. I extend my heartfelt gratitude to Alain Destexhe for providing this opportunity, inviting me to his laboratory, and granting me considerable freedom in pursuing my research goals. My co-supervisors, Federico Tesler and Domenico Guarino, deserve special mention for their balanced guidance. I also want to express my appreciation to the entire team at the institute, especially my newfound friends Mikal, Maria, Drex, and Farzin, with whom I shared wonderful experiences both within and outside the institute. Lastly, I am profoundly thankful for my family and friends at home, whose unwavering support has shown that distance can strengthen, rather than diminish, connections.

DISCLAIMER: This master thesis project resulted in a publication [[51](#)], which contains results nearly identical to those presented in this thesis. The publication is solely my own work, including all text, code, figures, and simulations. Alain Destexhe, Federico Tesler, and Domenico Guarino provided supervision and commentary. Main figures in this thesis are adapted from [[51](#)]. Some sections, particularly in the main results chapter ([Chapter 4](#)) and the final discussion ([Chapter 5](#)), as well as the following abstract, are adapted from the publication with some modifications.

ABSTRACT

The thalamus, serving as the brain's central relay station and gateway to the external world, orchestrates both sensory processing and cognitive functions. However, the relationship between thalamic responses at different scales to various stimuli and brain states remains poorly understood. To address this, we developed a biologically realistic dynamical mean-field model of the thalamus, integrating the complex single-cell dynamics of thalamocortical relay (TC) and thalamic reticular (RE) neurons with their collective behavior. Using this model, we conducted a multi-scale study of thalamic responsiveness and its dependence on cellular and brain states. Our findings, based on existing single-cell experiments, reveal that: (1) Awake and sleep-like states can be defined via the absence/presence of the neuromodulator acetylcholine (ACh), which controls bursting in TC and RE. (2) Thalamic response to sensory stimuli is linear in awake state and becomes nonlinear in sleep state, while cortical input generates nonlinear response in both states. (3) Cortical input modulates stimulus response, suppressing responsiveness in the awake state while enhancing it during sleep, promoting a linear response effectively *waking up* the thalamus. (4) Synaptic noise induces a global linear responsiveness, reducing the difference in response between thalamic states. Finally, the model replicates spindle oscillations within a sleep-like state, drastically changing its responsiveness. This novel thalamic mean-field model provides a valuable tool for incorporating detailed thalamic dynamics into large-scale brain simulations.

KURZFASSUNG

Der Thalamus ist die zentrale Relaisstation des Gehirns. Dieser steuert alle sensorische Verarbeitung als auch höhere kognitive Funktionen. Wie die Funktion des Thalamus von verschiedenen internen und externen Zuständen abhängt, ist jedoch nicht gut verstanden. Um ein umfassendes Verständnis zu erlangen, ist es notwendig, die komplexe Dynamik der thalamischen Neuronen (TC&RE) mit ihrem kollektiven Verhalten zu integrieren. Zu diesem Zweck stellen wir ein biologisch realistisches Mean-Field-Modell des Thalamus vor. Mit diesem führen wir eine multiskalige Studie der thalamischen Funktion und ihrer Abhängigkeit von zellulären und Gehirn-zuständen durch. Aufbauend auf bestehenden Einzelzellexperimenten zeigen wir, dass: (1) Wach- und schlafähnliche Zustände können durch die Abwesenheit bzw. Anwesenheit des Neuromodulators Acetylcholin (ACh) definiert werden, welcher Bursting in TC und RE kontrolliert. (2) Die thalamische Reaktion auf sensorische Reize ist im Wachzustand linear und wird im Schlafzustand nichtlinear, während der kortikale Input sowohl im Wach- als auch im Schlafzustand eine nichtlineare Reaktion erzeugt. (3) Die Reizantwort wird durch den kortikalen Input gesteuert, der die Reaktionsfähigkeit im Wachzustand unterdrückt, während er den Thalamus im Schlafzustand effektiv aufweckt und eine lineare Antwort fördert. (4) Synaptisches Rauschen führt zu einer globalen linearen thalamischen Reaktion. Schließlich repliziert das Modell erfolgreich Spindeln in einem schlafähnlichen Zustand. Dieses thalamische Mean-Field-Modell bietet ein neues und wichtiges Instrument zur Einbeziehung detaillierter thalamischer Dynamik in groß angelegte Gehirnsimulationen.

CONTENTS

1	Introduction	1
2	Aspects of the Thalamus	3
2.1	Anatomy and function	3
2.2	Neurons and their network	5
2.2.1	TC cells	7
2.2.2	RE cells	9
2.3	Characteristics	10
2.3.1	Bursting	10
2.3.2	Noise and responsiveness	12
2.3.3	Sleep and acetylcholine	15
2.3.4	Spindle oscillations	16
3	Modeling approaches	18
3.1	Modeling preliminaries	18
3.2	Neuron model	19
3.2.1	Integrate and fire model	20
3.2.2	The AdEx model	22
3.3	Mean-field model	24
3.3.1	Network models	24
3.3.2	Master equation framework	27
3.3.3	Statistical moments	29
3.3.4	Transition function	31
3.3.5	Mean-field with adaptation	33
3.3.6	Transfer function	35
3.4	Analysis and simulations	41
4	Results and Analysis	44
4.1	Thalamic model	44
4.1.1	Cell level	44
4.1.2	Population level	46
4.1.3	Validation of the mean-field	48
4.2	Responsiveness	50
4.2.1	Tonic and burst firing modes	50
4.2.2	Cortical and sensory input	54
4.2.3	Synaptic noise	55
4.3	Spindles	59
5	Discussion	63
6	Conclusion and Outlook	66
A	Appendix	68
A.1	A neuroscience primer	68
A.2	Mathematical appendix	70
A.3	Auxiliary calculations	75
	Bibliography	80

LIST OF FIGURES

Figure 2.1	Anatomy and placement of the thalamus	4
Figure 2.2	Thalamic inner structure	7
Figure 2.3	Hyperpolarization promotes burst firing of TC and RE cells.	9
Figure 2.4	Burst firing changes thalamic response	12
Figure 2.5	Synaptic noise removes TC dependency on voltage	13
Figure 2.6	Synaptic noise removes TC dependency on frequency	15
Figure 3.1	AdEx oscillations	23
Figure 4.1	TC and RE single cell dynamics	46
Figure 4.2	Employed network and connectivity structure	47
Figure 4.3	Transfer function fit	48
Figure 4.4	Validating the mean-field with spiking networks	49
Figure 4.5	Firing adaptation and bursting of TC cells.	51
Figure 4.6	Bursting of TC cells renders thalamic response nonlinear	53
Figure 4.7	The thalamus responsiveness depends on external input origin	55
Figure 4.8	Synaptic noise modulates the dependence of thalamic response on voltage	56
Figure 4.9	Synaptic noise removes the dependence of thalamic response on frequency	58
Figure 4.10	Spindle oscillations are generated by TC-RE connections and missing excitatory-excitatory links in the thalamus	59
Figure 4.11	Spindle oscillations in a sleep-like state generate a highly unresponsive thalamic state	61
Figure A.1	Global parameter analysis for mean-field and spiking network .	77
Figure A.2	Parameter space fit for TC without ACh	78
Figure A.3	Parameter space fit for TC with ACh	78
Figure A.4	Parameter space fit for RE without ACh	79
Figure A.5	Parameter space fit for RE with ACh	79

LIST OF TABLES

Table 3.1	Formalism requirements	41
Table 4.1	Cell and synaptic parameters for TC and RE cells	45
Table 4.2	Fitting parameters for the mean-field	48
Table 4.3	Fitting parameters for the spindle-adapted mean-field	60

PUBLICATIONS

- [1] J Overwiening et al. “A Multi-Scale Study of Thalamic State-Dependent Responsiveness”. In: *bioRxiv* (preprint, 2024). In review. doi: [10.1101/2023.12.02.567941](https://doi.org/10.1101/2023.12.02.567941). URL: <https://www.biorxiv.org/content/early/2024/06/29/2023.12.02.567941>.

ACRONYMS

ACh	acetylcholine
AdEx	adaptive exponential integrate and fire (model)
AMPA	α -amino-3-hydroxy-5-methyl-4-isoxazolepropionic acid
AI	asynchronous-irregular
E-I	excitation-inhibition (balance)
CLT	central limit theorem
CNS	central nervous system
DMN	default-mode-network
EPSP	excitatory postsynaptic potential
GABA	γ -aminobutyric acid
HH	Hodking-Huxley (model)
IF	integrate and fire (model)
ISI	interspike interval (1/firing rate)
IPSP	inhibitory postsynaptic potential
LGN	(thalamic) lateral geniculate nucleus
NMDA	<i>N</i> -methyl-D-aspartate
PNS	peripheral nervous system
PSP	postsynaptic potential
RE	thalamic reticular (cell)
REM	rapid-eye-movement (sleep phase)
RN	thalamic relay nucleus
SR	synchronous-regular
SN	spiking network
TC	thalamo-cortical (relay cell)
TRN	thalamic reticular nucleus
MAE	mean absolute error (metric)
MF	mean-field (model)

1 | INTRODUCTION

The thalamus is a well-preserved structure found in all mammals [57]. As the core relay hub of the brain, it processes almost all information from the outside world and the body before routing it to respective processing sites in the brain. Additionally, all outgoing motor commands from the cortex are distributed by the thalamus to their respective motor neurons in the body. Thus, the thalamus is often referred to as the *gate* between the central nervous system and the periphery [41].

Beyond its relay function, the thalamus plays a principal role in whole brain dynamics, such as spindle oscillations and slow waves in non-REM sleep or anesthesia [10, 30, 60], connecting to sleep functions and memory consolidation. Recent studies have also shown that thalamic integration with cortical pathways suggests a significant and active role of the thalamus in many higher brain functions, including sensation, attention, and cognition [49, 83].

Despite its crucial importance, the thalamus's inner mechanisms and functions in the brain are remarkably little understood. Experimental studies are notoriously challenging to perform in the thalamus due to its relatively small size and deep central location, shielded by other brain regions and the cerebral cortex. Moreover, most studies focus on single-cell experiments on thalamic neurons with their highly complex and unique behavior. However, this approach alone is insufficient to explain the function of the thalamus as a whole and its impact on general brain function, which operates on population coding principles at larger scales [55].

Investigating the interaction between thalamic neurons at various levels is therefore crucial for deciphering the interplay of the brain with the outside world and its inner workings. To this end, it is necessary to analyze thalamic neurons, their interactions, and their corresponding population activity via multi-scale models.

To this end, we for a first time propose a biologically realistic mean-field model of the thalamus incorporating the complex dynamics and interplay of thalamic cells. This model is build based on a combination of earlier works [23, 44, 87] and connects single cell characteristic at the population scale. Validated on in-vitro experiments, the proposed model captures the most important behaviors of thalamic neurons and their interaction with cortical and sensory input. Additionally, this approach incorporates three crucial nonlinear biological features: (1) *Irregular spiking* activity of neurons is believed to be important for transfer efficiency [24] and the correct baseline for neurons in both awake-like asynchronous (AI) states [6] as well as in sleep-like synchronous (SI) states [68]. (2) Synaptic conductances allow for realistic bi-stability and self-sustained activity [79] as well as modeling the fluctuation-driven regime [20]. (3) *Adaptation* mechanisms are the main generators of the different firing behaviors in the brain and important to include into models for generating realistic firing rate saturation and especially the bursting behavior of thalamic cells.

Finally, this novel thalamic mean-field model is constructed so it can readily be integrated with previously developed models of cortical and subcortical brain regions [23, 32, 74, 75] to effectively build macro-scale (to whole-brain-scale) models. This provides a starting point for the computational analysis of sleep, attention, and related brain

disorders with micro-scale variable models, connecting whole brain dynamics to single cell behavior and especially neuromodulation effects.

WE PROCEED IN THREE PARTS: In [Chapter 2](#) the thalamus and its function and cell types as well as its importance for the brain are described. In [Chapter 3](#) the modeling theory is motivated and derived. Then, we investigate in [Chapter 4](#) the state-dependent responsiveness of the thalamus employing the built models. We integrate the interplay between different brain scales, from single-cell to the meso-scale, while building upon existing single-cell experiments. In more detail, we show that: First, the transition from tonic to burst firing of TC cells via ACh renders thalamic response nonlinear ([Section 4.2.1](#)). Second, sensory stimuli generate a linear response, while cortical inputs generate a nonlinear response of the thalamus ([Section 4.2.2](#)). Third, cortical input and noise suppress thalamic response and noise diffuses thalamic state transitions and removes the thalamic response dependency on both voltage and frequency ([Section 4.2.3](#)). Finally, we demonstrate that the proposed model is capable of generating realistic self-sustained spindle oscillations, drastically changing responsiveness in this state ([Section 4.3](#)).

2

ASPECTS OF THE THALAMUS

In all vertebrates, and especially in mammals, the thalamus is the core relay hub of the brain. Almost all information from the outside world and the rest of the body must pass through the thalamus to reach their respective processing sites in the brain. The inner structure of the thalamus and its connections to other brain regions are highly preserved and change remarkably little across all mammalian species. The thalamus connects both to older evolutionary structures (like basal ganglia, cerebellum, and hippocampus) and newer ones, especially the cerebral cortex, connecting primal and sub-conscious functions with attentive and cognitive ones. There is also convincing evidence that the thalamus plays an important role in consciousness and memory. Lastly, the thalamus can control and generate whole brain dynamics, especially during emergency and sleep states.

Here, we will provide a broad biological and anatomical overview of the thalamus and its structure and neurons (loosely following Sherman and Guillery [61]). At the end, thalamic core functions at different scales and its macroscopic role in the brain are detailed – with a focus on how to include these in computational models.

2.1 ANATOMY AND FUNCTION

The thalamus forms a well-preserved structure occupying a central position in the brain [57]. Sitting at the top of the – evolutionarily old – brain stem, the thalamus is directly surrounded by the main information highway of the brain (corpus callosum), fundamental brain regions attributed to memory (hippocampus), motor control (cerebellum, basal ganglia), and emotions (amygdala), and finally the cortex (see [Figure 2.1](#) right).

The thalamus is structurally and functionally well separated into smaller substructures of connected neuron groups, so-called *nuclei*. These can be grouped into roughly three thalamic subdivisions [40]. The **anterior** thalamus combines nuclei which are targeted by pathways from older brain structures (i.a. cerebellum, hippocampus, and basal ganglia). The **medial** thalamus serves as a relay station from cortex to brain stem, playing the intermediary in *downstream* projection from higher to lower (cognitive) brain regions. Finally, the **lateral** thalamus contains extrinsic nuclei which each serve as a transmitter of exclusive sensory signals to a structurally and functionally distinct cortical area. This strong feedforward *thalamo-cortical* pathway is the main input to the neocortex – assigned with all higher order brain functions in mammals, rendering the thalamus (esp. lateral thalamus) as our gate to the outside world. Evolutionarily speaking, development and increase in size of cortical processing areas in mammals have always corresponded to an increase in the size of the related thalamic nucleus.

In this study, we will focus on the lateral nuclei. This is due to the fact that thalamic nuclei are structurally very similar and contain the same general types of neurons and their connections. Especially the lateral nuclei between themselves can be nearly identical while only being related to different sensory types. Further, the lateral nuclei are the most important for understanding brain function and processing. Here, the nucleus receiving all visual input from the retina, the lateral geniculate nucleus (LGN; see [Figure 2.1](#) left,

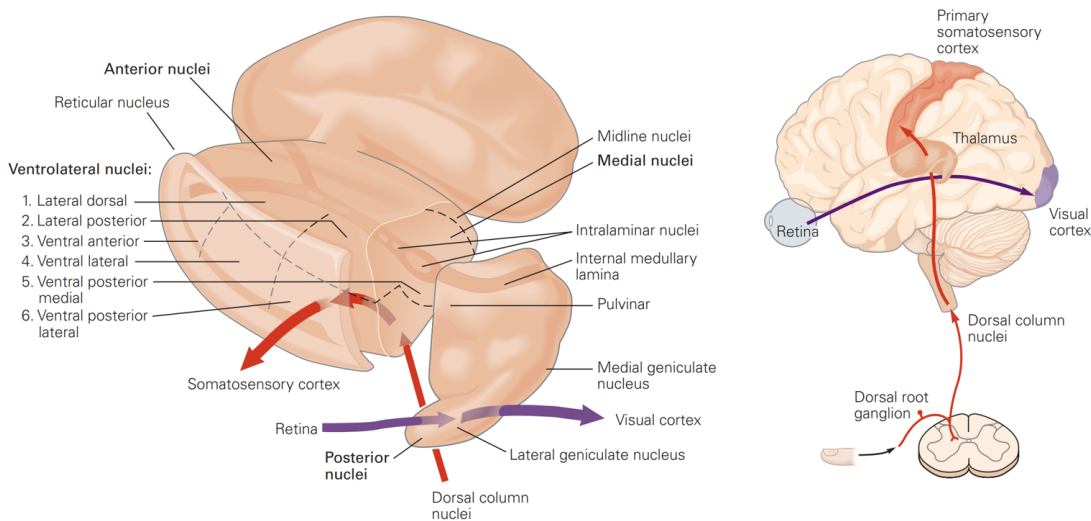


Figure 2.1: Anatomy and placement of the thalamus. **Left:** Close-up look at the thalamus and its ordering in structurally and functionally distinct substructures or *nuclei*. The two *down streams* in red and purple mark somatosensory (touch) and visual sensory input, respectively. **Right:** The thalamus sits at the center of the brain, with all peripheral information going through it. E.g., the somatosensory (red) and visual (purple) down streams being transferred from their respective receptors (skin and retina) to their individual processing site in the cortex (Primary somatosensory and visual cortex, respectively). (Figure taken from [41])

purple stream), is the most experimentally well-investigated nucleus. In addition, with most experiments in electrophysiology using visual stimuli and the role of visual input playing arguably the most important role in human observation and interaction with the outside world, this leads to the LGN as the prime nucleus of many experimental and theoretical studies. We follow this convention, and in this thesis focus on a general lateral nucleus while mostly comparing to experiments performed in the LGN.

The above described *classical view* of the thalamus [81] renders it as simply a linear map of information between different brain regions and the periphery. For visual, auditory, and somatosensory pathways, the respective sensory surfaces (retina, cochlea, skin surface) are mapped in a topographic order. This leads to a remarkable topographical organization which is continuous from thalamus to cortex [63].

This classical view, however, is to be expanded by newer findings: First, different neocortical areas connect back to not only their upstream lateral nuclei exerting a strong feedback influence, but also to different neighboring nuclei. The cortex is indeed the major source of connections (synapses) within the thalamus. For example, the cortex accounts for 50% of synapses found in the LGN, whereas only 20% of synapses derive from major ascending (sensory) pathways [62]. This extensive upstream input and activation from cortex to thalamus indicates a substantial role of the cortex in thalamic activity.

Second, the thalamus does not only consist of nuclei which solely relay subcortical (e.g., sensory) messages to the cortex but also of nuclei with activation from the cortex itself. The extension of only *first order* relay to *higher order* relays hints at a significant feedback loop between cortex and thalamus, and that the thalamus transfers – parallel to sensory information – also higher cognitive (cortico-cortical) messages. For example, in primates, higher order nuclei make up more than half of the thalamus and nearly all lateral nuclei [61]. Recent studies showed that both types of messages from the thalamus

play a significant role in higher cognitive brain function such as decision-making [86]. Additionally, *deep brain stimulation* of the central thalamus restores consciousness in anesthetized patients [73], suggesting a deep nesting of first and higher order connections crucial for attention and conscious access.

Third, one can distinguish between two functionally different types of afferents to the thalamus. *Drivers* induce direct activity and define the main qualitative nature of a message input to the thalamus. All downstream inputs from the periphery are drivers. A second, distinct type of afferents are *modulators*, which do not yield a sustained, recognizable signal, but modify and interact with the relay of messages or activity induced by drivers. One possible function is to reduce or even destroy a to-be-relayed signal. For example, when a cortical driver is blocked, the transmission of the corresponding receptive field is completely blocked as well; however, when a connected modulator is blocked, the receptive field survives. Modulators are found in all thalamic nuclei and are mostly originating in the cortex. This further suggests a strong influence of the cortex on thalamic relay of sensory information but also on its own feedback loop [15].

Fourth, the connections of the thalamus and the cortex with a specialized cell structure, the *thalamic reticular nucleus* (TRN) which anatomically sheaths the thalamus, have to be taken into account (see Figure 2.1 left). The TRN is activated on-the-way by both thalamocortical and corticothalamic connections (axons). It connects back and inhibits the thalamic relay nuclei. If the classical view's linear topographical mapping were correct, the TRN should act in distinct and linear function on both pathways. However, the TRN axons not only inhibit their driving thalamic relay nuclei but also neighboring ones. This extends to connecting even between "far-apart" anterior, medial, and lateral nuclei, and ultimately links sensory input to motor commands even before the signal is being processed in the cortex, opening the philosophical "*Chicken-or-Egg?*" question of the interplay between action and perception (see also [34]). Additionally, the TRN inhibitorily connects densely to itself, rendering its function highly complex and nonlinear.

Last, thalamic substructure and inner connectivity is highly complex with some of the most extreme phase transitions in its neuron dynamics, depending on states of the neurons themselves and the rest of the brain. This, together with the different functional inputs and feedback connections, suggests significant impact of especially microscale variables governing cell and synaptic states. Experimental studies in most nuclei show that there are distinct cells or even cell populations heavily diverging from the functional or connectional conceptualization of their corresponding nucleus according to the classical view. In this study, we will therefore model not a complete nucleus but a nucleus subpopulation. This is in agreement with newer studies suggesting multiple distinct parallel pathways per nucleus, with also interactions between themselves. Furthermore, our computational models will be built from the cell level upwards, including the evident significant role of individual cells and their parameters for thalamic function.

2.2 NEURONS AND THEIR NETWORK

Neurons are the brain's fundamental processing unit and are not only highly complex objects on their own but are interlinked with $\sim 10^{10}$ other neurons to make the brain function. (The ontological use of *cell*, *nerve cell*, and *neuron* will be used interchangeably, and other non-neuronal cell types will be marked explicitly.) Neurons alone are still not sufficient when one hopes to decipher the brain's function, as there are non-neuron cell types, chemical and biological processes, and many more –some still heavily unexplored–

mechanisms at play (see [Section A.1](#)). All of this makes understanding and especially modeling the brain a daunting task. We can, however, apply proven approximations. Especially with this thesis being a purely computational one, we will take into account computational-focused approximations in the form of two conjectures. The neuron and mean-field models proposed are built on top of these conjectures. We will discuss those in detail at the beginning of the modeling [Chapter 3](#) but briefly state them here to justify talking mostly about cells which will be of matter using these conjectures in the following sections: We reduce the complexity of the brain's tissue structure by implying that its computational basis is irreducibly representable by only neurons and their synaptic connections. Further, a "correct" distinguishing of neuron types can be made only when taking into account their position, connections, and full morphology. In principle, this is also needed when separating into distinct functional groups of neurons. We, however, will focus mostly on electrophysiological properties, referring to the success of this approximation in experimental and computational studies. Lastly, we conjecture that action potentials are the key feature for relay of information and consequently computation in the brain (see [Section 3.1](#)). Henceforth, we will also focus on experiments based on firing rate and spike times to compare to the (*firing-based*) models in this thesis. This is supported further when taking into account that we are mostly concerned about the thalamus as a relay hub, and thus action potentials are the sole way how information can be (directly) transferred between the thalamus and other far-away brain regions, especially the cortex.

Moving to **thalamic neurons**, we stay in this framework and focus on cells of the relay and reticular nuclei, their properties, and their connections. As outlined in the last section, thalamic substructure with its distinct cell types and their interplay as a network are crucial for deciphering thalamic function in the brain at all scales. In this section, we will classify and have a closer look at these cells and their connections.

One basic but helpful classification is between cells with axons projecting to thalamic-external locations such as the cortex and cells with axons only projecting locally to other thalamic neurons of the surrounding or the same nucleus [40, 62]. These neurons are termed *relay cells* and *interneurons*, respectively. Their axonal and dendritic branching, and their morphology are readily distinguishable. Furthermore, and resulting in completely separate functions, relay neurons are (glutamatergic) *excitatory* whereas interneurons are (GABAergic) inhibitory. A third distinct type of cell found in the thalamus are cells occupying the TRN. These so-called *reticular cells* (RE) are GABAergic as well and only have (strong) axonal projections to the thalamic relay nuclei and –to a lesser extent– locally inside the TRN to other RE cells [61, 62].

The inner structure of the thalamus with its nuclei remains a valid classification even at the cell level. In [Figure 2.2](#), there is depicted exemplarily the inner structure of the thalamus. It consists of two generic lateral thalamic relay nuclei and their connections to the TRN, with the three general thalamic cell types of *thalamo-cortical* (TC) relay cells, interneurons, and RE cells. In the figure, there is also depicted the corresponding targeted cortex area with both *thalamo-cortical* and *cortico-thalamic* connections.

Interneurons have the smallest cell bodies in the thalamus with only localized GABAergic connections to relay neurons. They make up a minor part (<25%) of thalamic relay nuclei's cell population and their representation and connections are not well investigated [61]. There is also no clear evidence about a specific role of interneurons in thalamic pathways. Together with evidence that local placement and connection to interneurons of different relay cells in the same nuclei show remarkably little discrepancy in their respective functional role, this suggests –without new experimental findings–

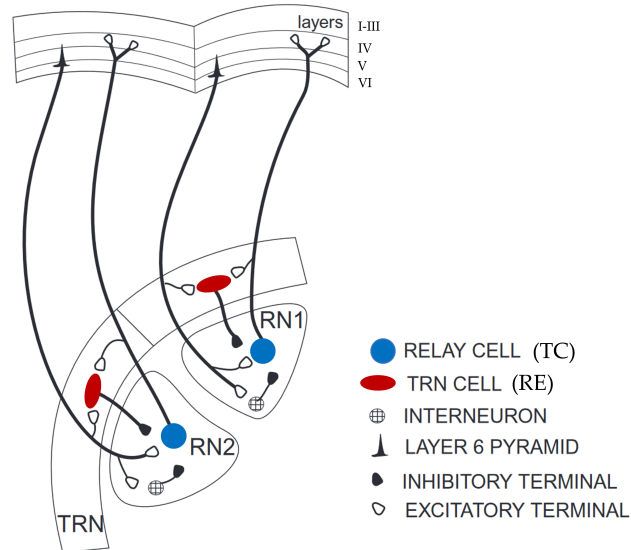


Figure 2.2: Thalamic inner structure. Schematic view of two generic thalamic relay nuclei (RN1, RN2) and their connections with a targeted cortical area, and the thalamic reticular nucleus (TRN). In RN1 and RN2 there are depicted two TC relay cells (blue) and their axons projecting here to layer IV of their distinct cortical areas and on-the-way to the TRN. Shown are also two exemplary cortical layer VI neurons connecting back to both relay and reticular neurons. Not pictured is the self-connection inside the TRN, first order inputs to the relay nuclei, nor possible connected cortical neurons of layer V. (Figure adapted from [61])

neglecting interneurons in modelling approaches. A developmental theory supports this, hypothesizing that interneurons are migrated perigeniculate cells and therefore also developmentally and morphologically similar to RE neurons. (See [61]) With this conjecture and the in-principle same GABAergic inhibitory role on relay cells, we can also hope to integrate interneurons passively by modelling RE neurons only. This will be supported by capturing significant in-vitro or in-vivo behavior which includes interneurons, or alternatively would support the view which marks interneurons as irrelevant for population dynamics in the thalamus. With these points, we will from here on only discuss and include TC and RE cells, neglecting interneurons in the rest of this thesis

2.2.1 TC cells

Nearly all lateral thalamic nuclei in mammals contain relay cells projecting to the neocortex, rendering these *thalamicocortical* (TC) *cells* the primary focus of this thesis (under the assumption that the thalamic main function is the connection to the cortex). These cells also represent the majority of cells, ranging from 70% to 99% in mammals [61].

A further strong hint at the structural connection between the thalamus and the cortex is that rapid and severe retrograde degeneration occurs in TC cells when cortical regions –corresponding to their axon terminals– are damaged by local lesions. With this method, TC cells can be categorized based on their cortical connections, and a strong thalamocortical dependency is evident [50]. Interestingly, this characteristic is, in its severity, unique for the thalamo-cortical connection in the brain and leads to nearly full neuronal degeneration in the whole thalamus when the cortex is globally damaged.

To classify *functionally* different subgroups of TC cells, there are two possible ways: First, looking at distinct integrative properties produced by the cells themselves. Here, especially morphology, axonal branching, and receptive field function are established characteristics. In this way, three types of relay cells could be distinguished. However, in this thesis' modeling approach, we will use heavily reduced neuron models so that the functional differences between these types are negligible, and we aim to describe a homogeneous TC cell population. This is supported by the second way of classifying TC cells in the literature: Namely, imposing that all relay cells have the same integrative function for information transfer from their respective inputs to the cortex. Then they differ only because of external properties such as distinct modulatory and driving functions or cortical distribution, feedback, and control. This view is evident especially in experiments in the LGN and lateral nuclei in general.

The connection to the cortex is the most pronounced and well investigated in the primary sensory cortices. These are organized into 6 distinct layers (layers I-VI, with layer I at the surface of the cerebral cortex), distinguishable by cell morphology, density, and their axonal and dendritic branching and connections. All TC afferents end in layer IV where they serve as drivers, while some additionally branch into lower (V-VI) and sometimes higher (I-III) layers, playing a more modulatory role [66]. Recent studies show that TC neurons can be classified into two groups separated by axonal branching in the cortex and by their information flow. *Core* TC neurons mostly do not branch and connect predominantly to sensory cortices; these make up most cells in the lateral nuclei. On the other side, *matrix* TC cells branch like cascades and can also branch into different cortical areas. These connect mostly to higher order regions, with especially strong connections to cortex areas in the *default-mode-network* (DMN), where the thalamus directly controls cognitive functions such as decision-making [86].

The cortico-thalamic input is mostly coming from pyramidal neurons in layers V and VI. These cells are mostly tuned to low frequencies (2-4Hz, RS cells). As described above (Section 2.1), the cortico-thalamic connections are only reciprocal and send axons back to their respective thalamic relay nuclei. Interestingly, all relay nuclei receive afferents from layer VI, while only some receive afferents from layer V. Importantly, input from layer V serves as a thalamic driver, while layer VI acts as modulatory input. Some lateral nuclei (i.a. LGN) receive only (modulatory) input from layer VI but no input from layer V. These receive strong ascending afferents from the periphery, whereas nuclei with layer V-input receive only a diminishing amount of such input.

FIRING BEHAVIOR OF TC CELLS While in a natural or unaltered state (mostly referring to the membrane potential being at *rest* or equilibrium level), TC neurons show *tonic* firing behavior, with nearly no *spike adaptation* in play slowing down the rate of emitted action potentials. Tonic firing means there is a near constant *interspike interval* (ISI) and the firing response of a neuron to a constant stimulus, such as an injected current, is a constant rate of action potentials. This means that TC cells transmit incoming spike information linearly, agreeing with terming them relay neurons, and in accordance with the classical view [63]. However, thalamic relay neurons have so-called *T-channels* [38]. These voltage-gated *ion-channels* in the cells' membrane induce Ca^{2+} currents into the cell when its membrane potential is at a low threshold or *hyperpolarized* level (Section A.1). These T-channels induce rich behavior into relay cells, with the most significant impact that the Ca^{2+} currents support the timed depolarization coming from presynaptic (input) spikes. In this way the cell fires not only one action potential in response to one incoming spike but a *burst* of a few action potentials [48]. This renders the firing response of relay cells

highly nonlinear and much more susceptible to small inputs which will be transferred and amplified to e.g., the cortex. T-channels activate when the cell's membrane potential is hyperpolarized (see Figure 2.3 A).

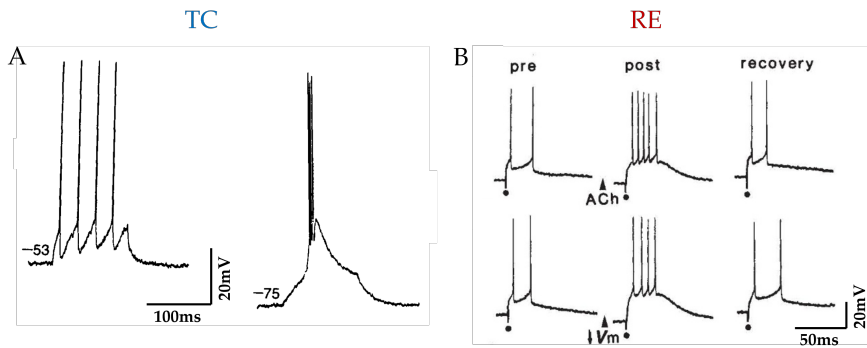


Figure 2.3: Hyperpolarization (ACh) promotes burst firing of TC and RE cells. A TC relay cells at hyperpolarized membrane potentials experience T-channel (Ca^{2+}) currents I_T which trigger a burst of action potentials (burst firing). Depolarizing the membrane potential inhibits burst firing by inactivating the low threshold I_T current (not shown). At depolarized or rest levels an input current generates a train of constant-phase action potentials (regular or *tonic* spiking). B In RE cells the application of membrane potential hyperpolarization (lower row, upper row is with ACh), changes the firing response of the cell to a δ synaptic stimulus (dot): A *weak* burst of two action potentials in depolarized or resting state (pre) is changed to a strong burst response of multiple spikes (post). Similar to artificial hyperpolarization (via current injection), ACh causes membrane hyperpolarization through an increase in K^+ conductance thus resulting in a very similar phase transition between firing modes. Remark: In A, a prolonged input current was provided while in B only a synaptic δ -like stimulus was applied. If a shorter δ stimulus would be applied to TC cells (A) the response at resting polarization would be one spike only. (Figure A and B adapted from [46, 48], respectively.)

2.2.2 RE cells

Thalamic reticular (RE) cells represent the only cell type present in the TRN, sheathing all thalamic relay nuclei from the cortex. All thalamo-cortical and cortico-thalamic axons have to go through the TRN and innervate RE cells via excitatory *gap junctions* (see Glossary). Outside the TRN, RE cells project axonally only to thalamic relay cells and inhibit them in the same manner as interneurons. However, there are axonal and dendritic inhibitory connections between RE cells themselves. Because of their large cell bodies, there are surprisingly many connections via usually scarce gap junctions. RE cells' dense disc-like dendritic branching inside the nucleus results in a highly interconnected population, rendering it impossible to morphologically classify distinct TRN sections. This dense net, together with the fact that there is no evident mapping in the TRN similar to the thalamic relay nuclei, and that different thalamic and/or cortical regions can connect to the same RE cells, shows that the TRN –substantially more than even the matrix cell part of the relay nuclei– merges all incoming and outgoing pathways of the thalamus [40, 53]. Via the strong inhibition on all relay cells, the TRN gives a gating and controlling (or modulating) role to inputs from the thalamus itself or cortical regions. This, and especially the fact that modulation of all sensory input to the brain is dependent on not only cortical gating but also the input itself, and via the wide area-

wide activation of RE cells of thought-to-be separate brain functions, marks the TRN as crucially important for modeling not only the thalamus but all macroscopic brain dynamics.

FIRING BEHAVIOR OF RE CELLS RE cells exhibit bursting responses across all physiological states [63]. Sufficient incoming activation almost invariably produces a train of action potentials (burst) in response to each presynaptic spike. This property allows the TRN to robustly modulate relay neurons even with subtle activation from, e.g., the cortex. This bursting behavior also facilitates interesting oscillatory dynamics within the thalamus, which can propagate to the whole brain, for example during sleep. Additionally, –and similar to thalamic relay neurons– RE cells possess T-type calcium channels [38]. In RE cells, these T-channels are also activated only at hyperpolarized membrane potentials [46]. However, unlike in TC cells where T-channels induce a phase transition between tonic and burst firing, in RE cells they primarily enhance the existing bursting pattern. This enhancement results in a slightly more prolonged response window and an increased number of action potentials within the same burst in response to a single stimulus, such as a presynaptic spike (see [Figure 2.3](#) B, lower row).

2.3 CHARACTERISTICS

With the computational modeling focus of this thesis, the most important features of the investigated (thalamic) cells are those connected to the creation and transfer of action potentials and TC cells' firing dynamics (following the conjectures described above, and detailed in [Chapter 3](#)). Of particular interest is how the firing behavior is dependent on different states at all scales, such as membrane or synaptic parameters, different inputs, or overall brain state. We focus on the distinction between the two most obvious firing behaviors, namely tonic and bursting states. In this section, we describe the major characteristics intrinsic to the thalamus with respective experimental studies: (1) How bursting affects thalamic response and relay. (2) How noise affects response and bursting. (3) How we can connect the firing modes to the physiological brain states of awake and sleep. (4) And that the thalamus generates whole brain oscillations during sleep. These characteristics have significant impact not only on the thalamus behavior and responsiveness but also on whole brain dynamics and how brain states at different scales shape the way we interact with the outside world. This will later on guide validation and exploration with the proposed models ([Chapter 4](#)).

2.3.1 Bursting

We saw in the last section that TC cells show tonic firing at resting or depolarized membrane potentials. Most brain cell types, and especially cortical neurons, exhibit only tonic firing in response to various types of stimuli, rendering their response of spike and information transfer direct and linear. Furthermore, bursting mostly occurs only in altered or non-equilibrium states induced via external factors. This renders the strong and robust bursting behavior of RE cells special within the brain. Additionally, –and as described above– the capability of both major thalamic neuron types (RE and TC) to burst strongly and in a prolonged manner in a state of hyperpolarized membrane potential is quite unique for brain structures, especially one mostly playing a role in

relaying sensory information, which should best be done linearly according to naive information theory.

So why does the thalamus have two distinct firing modes, and how do these affect the response and relay function of the thalamus? In the last section, we saw that the *bifurcation* parameter for the transition between tonic and bursting modes is the membrane potential: hyperpolarization allows T-channel currents (IT) to create strong and prolonged depolarization which, in turn, creates a burst of action potentials. In [Section 2.3.3](#), we will see that tonic and burst modes can be attributed to the physiological states of awake and sleep, and that the neuromodulator acetylcholine (ACh) can be used as their link and as a natural way the brain achieves hyperpolarization and the switch between tonic and bursting modes in the thalamus. First, however, we are more generally interested in how TC cells in bursting mode react to realistic stimuli differently from their tonic mode and how this affects the way information is relayed.

As evident from the definition of tonic and bursting behavior and from [Figure 2.3](#), the tonic mode suggests a more linear and faithful way of relaying information than the burst mode. Experiments show, however, that both modes respond to sensory stimuli vigorously and that both modes convey more or less equal absolute amounts of information about the presented stimulus. However, two important distinctions are that: (1) Cells in burst mode mostly convey time- and phase-dependent information, whereas tonic mode leads to a strong linear response, conveying more reliable amplitudes. (2) Information transfer in burst mode is more *efficient*, such that cells react less to noise and the output is also less noisy.

Regarding (2), in the upper row of [Figure 2.4](#), there is depicted the spontaneous activity of a general TC cell (in-vivo cat). We see that in the absence of targeted stimuli, the spontaneous activity of the cell is substantially lower in the burst mode. This is due to the fact that hyperpolarization reduces the chance that low amplitude inputs or fluctuations generate an action potential via (high-)voltage gated Na^+ channels. Additionally, IT currents are only being activated efficiently by membrane potential gradients which are pronounced enough. These effects effectively create an amplitude threshold for inputs, which reduces the impact of noise while only letting through and also promoting significant inputs.

In [Figure 2.4](#), the lower row, the same TC cell's response to a grating visual stimulus (dashed gray line) in both tonic and burst modes was recorded. According to (1), we see that indeed in tonic mode, the response is a linear representation faithfully following the stimulus (this also allows for superposition of distinct inputs [[61](#)]). In contrast, in burst mode, the response is strongly non-linear and occurs only at an initial phase of the stimulus, conveying frequency but not amplitude. However, when taking into account the relative strength of the response by comparing it to the spontaneous activity, we see that in tonic mode, the response is more or less of equal average amplitude, while in burst mode –because of the highly reduced spontaneous activity– the response is magnified 10-fold.

Summarizing, both modes respond to stimuli and efficiently relay information to the cortex. However, tonic mode allows for more efficient stimulus distinction and more reliable signal analysis in the receiving cortex, while burst mode is pronouncing stimulus detection. This suggests that burst mode is used by the brain during sensory-searching as a target acquisition mechanism and in modes of less or undirected attention, where a burst acts as a *wake-up call*. We can connect this well to the general states of awake and sleep ([Section 2.3.3](#)) and the brain's natural phase transition between these states. Additionally, experiments show that relay cells in burst mode often exhibit *rhythmic*

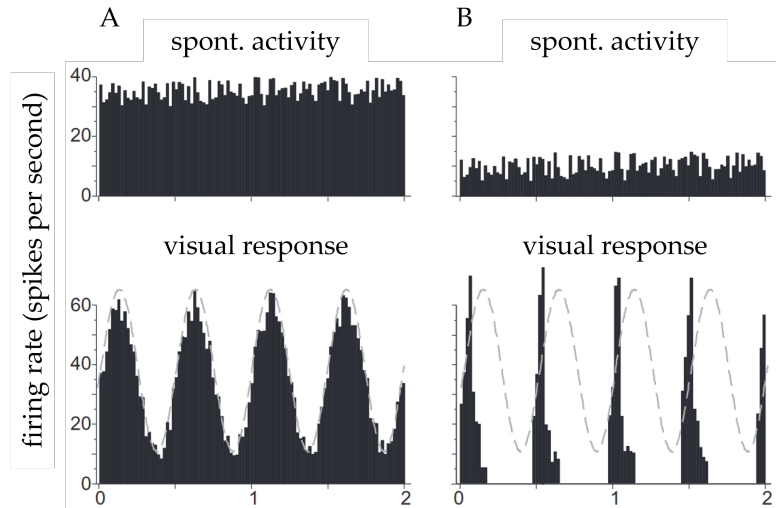


Figure 2.4: Burst firing drastically changes thalamic response. Responses of a TC relay cell in a cat's lateral geniculate nucleus (LGN) to an oscillatory visual stimulus. The cell was recorded in a lightly anesthetized state while the stimulus was a drifted sinusoidal grating across the cell's receptive field in the retina. Current was injected into the cell through the recording electrode to alter the membrane potential. In **A**, the injected current was adjusted so that the cell without visual stimulation represents tonic firing, because of a mostly inactivated T-channel currents (I_T) at this membrane potential. In **B** the current injection was adjusted to a more hyperpolarized level, permitting burst firing via activated I_T . Shown are the cell's response histograms, as the over many trials averaged mean firing rates. **Top row:** The cells spontaneous activity with no stimulus presented. Note the significantly reduced activity during burst mode (B). **Bottom row:** The response of the cell to the aforementioned oscillatory stimulus in its receptive field. The grating stimulus is shown as a dashed gray line. Note that the response in A captures the sinusoidal shape while in B it does not. However, the effective response amplitude in burst mode (B) is magnified 10-fold. (Figure adapted from [61])

bursting. In this case, multiple neurons or populations of neurons are found to be synchronized, generating the same (rhythmic) bursting [71]. This also connects back to sleep and is dependent on the TRN. This will be discussed in [Section 2.3.4](#).

2.3.2 Noise and responsiveness

Following up on the above general discussion about tonic and burst modes and their effects on thalamic responsiveness, we will in this section focus on noise, which has crucial impact on said transition and can serve as a peek into the brain's, and especially cortical, control of thalamic function.

Noise, or *subthreshold fluctuations* of a cell's membrane potential, can be seen as the result of various sources such as brain state, neurotransmitters and neuromodulators, and spontaneous activity input from connected *modulatory* brain areas. Here, especially, we will focus on how noise impacts the responsiveness of TC cells to sensory stimuli. Synaptic noise can be interpreted also as modulating cortical input shaping thalamic responsiveness [5]. This would represent the internal state and include some form of memory via the cortical feedback into stimulus response. Additionally, external noise adds biologically realistic response variability, especially important for the thalamus [55]. However, the generality of noise regarding its origin allows investigating noise

in an abstract manner without implying the noise source. This will be used to get the most general information about thalamic responsiveness dependent on possible internal states via noise.

Following, we will mainly focus on the experiments conducted by Wolfart et al. [84]: Similar to most neuron types, the (spike-) response function of TC cells follows a generic sigmoid distribution. In states with absent noise, most input amplitudes in terms of their synaptic conductance produced either a spike or no spike with a binary probability distribution and a steep slope of the response function. Here, two noise-less states were used: The *quiescent* state with no external input conductance and the *static* state with constant excitatory and inhibitory input conductance injected. When noise is applied via fluctuations in both excitatory and inhibitory input conductance, the response function was linearized and adopted intermediate values, thus reducing gain but also increasing sensitivity to small inputs (see Figure 2.5a).

The input conductance or *synaptic noise* directly correlates with its induced subthreshold fluctuations in the cell's membrane potential. This voltage variance (σ_V) shows a linear relationship to the slope of the response function or gain (see Figure 2.5b), suggesting that synaptic noise can modulate response in a multiplicative manner.

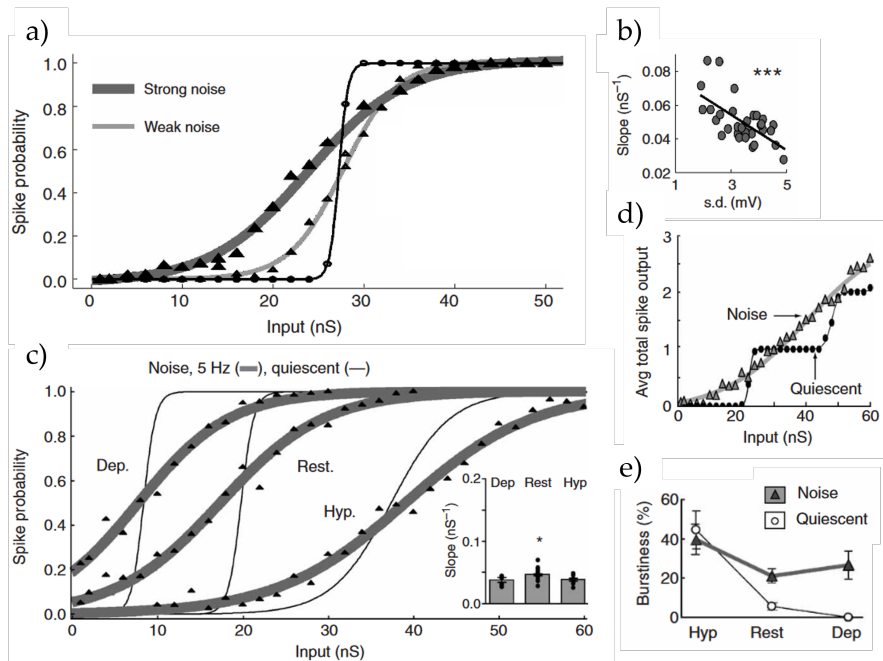


Figure 2.5: Synaptic noise removes TC dependency on voltage. (a) Decreasing the variance of noise g values (Strong, Weak) increased the input-output slope. (b) The response gain was correlated with the noise-induced voltage variance (s.d.). (c) Thick gray curves: response probabilities during noise mode, 5 Hz stimulation, at depolarized (Dep.), resting (Rest.) and hyperpolarized potentials (Hyp.). Thin black lines: quiescent curves (same cell). The response gain (slope) during noise was almost equally low at all potentials (inset). (d) Plotting the average total number of spikes per burst response against the input shows that noise linearized the staircase-like transfer function across the whole input range. (e) Percent bursts per spike-evoking stimulation with different input frequencies and membrane potentials. Noise increased burstiness at resting and depolarized potentials (here exemplarily at 5Hz input frequency). This effect was smaller with higher input frequencies. Noise did not increase the burstiness at hyperpolarization. (Figure adapted from [84])

Following the distinction between the two modes of tonic and bursting firing in TC cells dependent on the cell membrane's polarization, Figure 2.5c depicts the TC cell's response function with and without noise (quiescent) for three levels of polarization. Depolarized and resting membrane potentials lead to the same modulation via noise where only the response function is shifted. However, at hyperpolarization, the gain is reduced and more similar between quiescent and noise conditions. This is in contrast to cortical neurons and also not in line with our previous findings about T-channels, which are expected to increase gain via the all-or-none response of the induced bursting mode (Section 2.3.1). However, the inactivation time of T-type channels is usually of the order of 10^2 ms such that with input spikes of frequency ≥ 5 Hz the constant I_T currents effectively depolarize the cell, resulting in no bursting behavior as long as the ISI is of the order of the inactivation time [84]. Noise, however, equalizes the gain across different membrane potential levels, thus rendering TC cell's response independent of voltage in two manners: independent of input conductance and independent of polarization.

Bursting in TC cells can also be created by very strong synaptic inputs and not only via activated T-channels, even at resting potential. Now a double sigmoid function marks the shape of response, including a *burst response* of two emitted spikes at high conductance, and here too, noise linearizes the response slopes (Figure 2.5d). This bursting, however, would need a significant increase of input conductance, *in vivo* mostly via a drastic change in the amount of neurotransmitters, which is usually far from the biological modus operandi. These levels of synaptic conductance for both glutamatergic and GABAergic neurotransmitters are typically only reached in neurons in feedforward pathways where information is primarily transmitted and not extensively processed, such as nerve cells in the spinal cord, whereas neurons in densely connected, higher order brain regions generally show less input conductance and rely more on multiple inputs to reach threshold [62]. This relation between input conductance and network size (or connectivity) was also shown computationally [18].

T-channel bursting is not effected by noise, but strong noise generates bursting at resting and depolarized potentials via induced subthreshold fluctuations (σ_V) acting similar to prolonged I_T currents (Figure 2.5e).

Summarizing, noise renders thalamic response and the phase transition between its firing modes largely independent of voltage. However, for the above experiments, only constant Poisson-distributed spike trains were used as input [84]. Next to voltage, the frequency of inputs is one of the most important factors shaping response in neural systems. In Figure 2.6a, we see that TC cells at resting potential respond primarily to high-frequency spike trains. A single spike does not evoke an output action potential, but multiple near-simultaneous spikes create sufficient membrane potential depolarization to activate voltage-gated Na^+ channels. In contrast, at hyperpolarized levels, the same cell responds similarly to imposed spikes but also responds to single spikes. This is due to the activated IT currents. Following the same explanation as above: The interspike interval (ISI) needs to be long enough such that an inactivation of IT can occur before the next input spike. We can see that this time window is approximately 200 ms, corresponding to an input frequency of about 5 Hz. Adding noise, we observe that synaptic noise substantially reduces the frequency dependence for both resting and hyperpolarized potentials of TC cells (in Figure 2.6b).

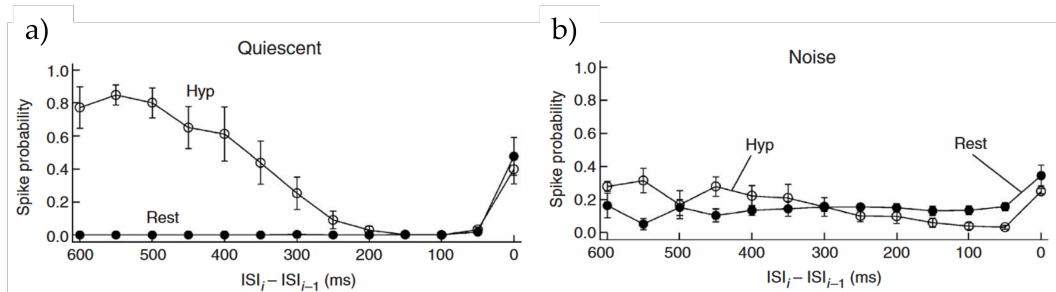


Figure 2.6: Synaptic noise removes TC dependency on frequency. (a) The probability of evoking at least one spike was plotted against the ISI's. Whereas at resting potential spiking probability was increased only with high-frequency inputs, at hyperpolarized potentials the spiking probability increased strongly with low frequency inputs. (b) During the injection of noise, the difference in frequency-dependent response behavior of thalamocortical cells was strongly reduced. Spiking probabilities were approximately equal at all input frequencies in the presence of noise. (Figure adapted from [84])

2.3.3 Sleep and acetylcholine

The two most prominent states in the brain, which have a direct impact on our daily lives, are wakefulness and sleep. Sleep, in particular, whose role is still not fully understood, is a remarkable state that quietly occupies approximately one-third of our lifetime. We know it is crucial for the metabolic recovery and regeneration of neurons and brain tissue, as well as for cognitive functions, especially memory consolidation [41, ch. 44].

The thalamus, acting as a gate for sensation and perception, is intrinsically linked to the distinction between awake and sleep states. Recent research has demonstrated that deep brain stimulation (DBS) of the central thalamus can restore both arousal and awareness following loss of consciousness. In a study involving anesthetized non-human primates, central thalamic stimulation induced arousal in an on-off manner and increased functional magnetic resonance imaging (fMRI) activity in prefrontal, parietal, and cingulate cortices. Moreover, DBS restored a broad dynamic repertoire of spontaneous resting-state activity, previously described as a signature of consciousness [73].

Sleep is typically studied via polysomnography, which includes three primary physiological measures: brain activity through electroencephalography (EEG), eye movements through electrooculography (EOG), and muscle fiber activity through electromyography (EMG). The transition between sleep and wakefulness is regulated by the brain through interacting homeostatic and circadian processes, with various neuromodulators playing crucial roles in this complex regulation.

Neuromodulators are signaling molecules that generally alter a cell's excitability by modifying the properties of ion channels and receptors. They typically act on relatively long time scales and are often regulated by whole brain states or cycles, in contrast to the rapid, point-to-point communication of action potentials. Due to their broad influence on neural activity, neuromodulators are a primary focus in neurological and psychiatric drug research and application, such as with antidepressants. Examples of neuromodulators include dopamine, serotonin, and norepinephrine (see [Section A.1](#)). In the thalamus, the neuromodulator **acetylcholine** (ACh) is particularly important. ACh is active in both the peripheral nervous system (PNS) and the central nervous system

(CNS), with significant roles in subcortical regions such as the brainstem and thalamus. Its significance in the thalamus is twofold:

First, ACh generates and strengthens bursting of both TC and RE cells in a natural and highly specialized way. Biochemically, ACh enhances Na^+ and Ca^{2+} permeability, while also increasing K^+ conductance. This results not only in hyperpolarization (K^+) [46], but also directly strengthens (Ca^{2+} -based) T-channel activation. Adding to this, the cells are generally more excitable via improved action potential creation (Na^+). This results in highly responsive cells that exhibit burst-like firing (as in [Figure 2.3](#)). However, ACh – mainly by shifting the membrane potential away from equilibrium – also renders the cells more adaptive. The ion channels attempt to rebalance the chemical equilibrium, causing the cell to counteract the highly depolarized state during action potential generation. Ultimately, ACh enhances firing and especially burst firing, but also induces cessation of firing via adaptation currents that try to restore the membrane potential. In this manner, ACh leads to bursts not only in response to brief (δ -like) stimuli but also to prolonged stimuli.

Secondly, ACh can be attributed a key role in the regulation and distinction of wake and sleep states in subcortical areas such as the brainstem and thalamus [70, 85]. This is further supported by the impact of ACh on processes intrinsically linked to the wake-sleep cycle, such as attention [35] and memory consolidation [28], which are predominantly associated with either the wake or sleep phase, respectively. Given that ACh induces phase transitions in all thalamic cells and drastically alters their behavior, we can infer that the cholinergic state of the thalamus is strongly correlated with wake and sleep states [39]. However, it's important to note that while ACh plays a crucial role, the wake-sleep cycle is regulated by a complex interplay of multiple neuromodulatory systems.

In the context of our thalamic mean-field model, we utilize ACh as a microscale variable and bifurcation parameter for the transition between tonic and bursting modes, which we associate with awake and sleep states, respectively. This approach provides a more biologically realistic mechanism than artificial manipulation of the membrane potential and allows us to represent the two predominant functional states of the thalamus and its constituent cells.

Recent research has challenged earlier hypotheses about thalamic cell firing modes in sleep-wake states. While it was previously thought that awake animals had depolarized thalamocortical cells operating in tonic mode and sleeping animals had hyperpolarized cells in burst mode, the reality is more complex. Ramcharan, Gnadt, and Sherman [54] demonstrated that tonic firing remains dominant even during some sleep phases. Moreover, bursting is not limited to sleep; it becomes more prevalent as animals transition from wakefulness to sleep but can occur in both states. It was also shown that cells in burst mode can fire arrhythmically and respond to stimuli, contradicting the notion that burst mode represents a complete relay failure [61]. In fact, cells in burst mode can reliably respond to visual stimuli, with bursts following the temporal properties of the stimulation [62]. These findings indicate that the relationship between thalamic firing modes and sleep-wake states is more nuanced than initially believed, necessitating more sophisticated models of thalamic function across brain states.

2.3.4 Spindle oscillations

The thalamus, beyond its gating function, plays a principal role in whole brain dynamics, particularly in the generation and maintenance of spindle oscillations and slow waves

during non-REM sleep and anesthesia [10, 30, 60]. These oscillatory patterns are crucial for sleep-dependent memory consolidation and cortical plasticity [56].

Spindle oscillations, characterized by waxing-and-waning 7-15 Hz oscillations lasting from less than one second up to a few seconds, are one of the primary activity dynamics of the thalamus during slow-wave sleep or anesthesia. They strongly influence thalamic responsiveness in these states and are considered a defining characteristic of stage 2 non-REM sleep [69]. The generation of spindle oscillations originates from the interplay of multiple cellular and circuit properties, with the intrinsic loop between thalamocortical (TC) relay and thalamic reticular (RE) cells playing a pivotal role. This thalamic circuit acts as a pacemaker and oscillator, with the crucial mechanism being the rebound bursting of TC cells following hyperpolarization induced by RE cell inhibition [71].

In ACh depleted conditions, such as during non-REM sleep, several key factors contribute to spindle generation: T-type calcium channel currents promote bursts after hyperpolarization, as modeled by [19] using a Hodgkin-Huxley model (see [Section 3.2](#)). Barrages of inhibitory postsynaptic potentials occur in strongly connected subgroups within the thalamic reticular nucleus (TRN) [65]. Two self-sustained loops are created: an inhibitory self-loop within TRN neurons, and a loop connecting RE and TC cells. This circuit arrangement generates rebound bursts, which are the foundation of spindle oscillations, as demonstrated by both experimental studies and computational models [21, 69].

In-vitro and in-vivo experiments have shown that relay cells in burst mode often exhibit rhythmic bursting, with multiple neurons or populations of neurons synchronizing to generate the same rhythmic pattern [71]. The TRN is crucial for this collective oscillation, with frequency ranges typically between 0.3-10 Hz. Importantly, this burst mode is observed in-vivo only during sleep states and not in awake or alert states. Recent studies have further elucidated the precise mechanisms of spindle generation and propagation. Fernandez and Lüthi [26] demonstrated that spindles are initiated in the thalamus and propagated to the cortex through thalamocortical projections. The cortex then provides feedback to the thalamus, creating a thalamocortical dialogue that shapes the spatiotemporal properties of spindles.

Understanding the mechanisms of spindle oscillations has important clinical implications. Alterations in spindle characteristics have been associated with various neurological and psychiatric disorders, including schizophrenia and developmental disorders. Furthermore, enhancing spindles through pharmacological or non-invasive brain stimulation techniques has shown promise in improving memory consolidation (see, for example, [27] for schizophrenia).

TO SUMMARIZE: The thalamus is a distinct group of cells primarily concerned with relaying and modulating information to the cortex, thus earning its designation as the brain's gate to the outside world. This relay and distribution of information is subject to a wide range of modulatory inputs and overall brain states, including neuromodulation, that modify how the thalamus responds to stimuli and transmits information to the cortex for further processing. In awake-like states, this relay occurs without significantly altering the fundamental properties or nature of the transmitted information. In contrast, during states of reduced consciousness, such as sleep-like states, the thalamus effectively filters information reaching the cortex and also generates or supports whole-brain oscillations such as spindles, directly interacting with and influencing global brain states.

3 | MODELING APPROACHES

Numerous experimental findings impose constraints on computational approaches to investigating the thalamus, particularly the cortico-thalamic loop. Although experimental manipulations of this loop, both *in vitro* and *in vivo*, are accessible to modelers, they provide only partial insights into the functional roles of this feedback mechanism. As a result, current computational simulations of the thalamus and cortico-thalamic loop tend to focus narrowly on specific aspects of cortico-thalamic computation, usually examining only one or a few facets at a time. This limited scope results in partial interpretative frameworks, restricting our comprehensive understanding of the system.

According to existing computational literature and ongoing research on the cortico-thalamic loop (from [34]), two broad modeling approaches have been delineated: (1) Emphasis on functional specificity, dependent on the nature of sensory stimuli presented to the system. In this approach, the loop is modeled to regulate the quantity, content, and temporal organization of information transmitted to other brain regions. (2) focus on dynamic behavior, concentrating on the system's state rather than specific functions. In this framework, the cortico-thalamic loop is implicated in generating and propagating various rhythmic activities across the brain (see [Section 2.3.4](#)).

The complexity of the cortico-thalamic loop necessitates the development of comprehensive and large-scale interpretative frameworks. To this end, we aim to lay the foundation for highly interpretative and biologically realistic models. To accomplish this, we apply previously developed and highly predictive single-cell models [9, 44, 88] and mean-field models [23, 25, 87], originally applied only to cortical tissue, to the thalamus and its constituent cells. The main objective of this thesis is to combine these approaches for the thalamus and, for the first time, investigate thalamic behavior in a multi-scale study.

3.1 MODELING PRELIMINARIES

Before delving into the applied modeling theory, we will first discuss and derive the main assumptions and conjectures that form the general framework of much of computational neuroscience.

We will focus solely on electrophysiological properties, acknowledging the success of this approximation in both experimental and computational studies. Within this framework, non-electrophysiological mechanisms can be incorporated by modeling their effects on a neuron's electrophysiology; prominent examples include neurotransmitters and neuromodulators. We employ the hypothesis that: *Neurons in general brain tissue can be classified and categorized into finite homogeneous groups distinguished by their influence on network dynamics via measurable electrophysiological properties.* Furthermore, we also reduce neurons to point-like structures in the computational grid by focusing on action potentials, commonly referred to as *spikes* ([Section A.1](#)). We assume that: (1) the critical aspects of the brain's computation are performed explicitly through the transfer and pro-

cessing of spikes; and (2) for computational purposes, spikes are identical stereotypical events that transfer information solely via their timing [64].

This approach is supported by the general success of computational neuroscience, particularly when considering the thalamus as a relay hub. In this context, action potentials are the primary means by which information is directly transferred between the thalamus and other brain regions, especially the cortex. This further justifies the reduction to electrophysiological properties of membrane potentials and currents, as these govern action potential generation. Other modes of non-spike-based information transfer, such as indirect neuromodulation or changes in brain state, operate on timescales beyond the scope of the models employed here and are more closely associated with physiological states not central to this thesis.

Thus, neurons within the central nervous system predominantly interact through action potentials, or spikes, which manifest as stereotypical electrical impulses. Early electrophysiological investigations empirically established that the frequency of spikes generated by nerve fibers is modulated by the strength of stimulation. The classical perspective on neural computation posits that the fundamental unit of information processing is the firing rate, rather than individual spikes, with little regard for their precise temporal occurrence. Conversely, numerous studies contend that effective neural computation hinges upon the temporal coordination of spikes. Various theoretical frameworks have been proposed to elucidate this phenomenon, encompassing synchrony-based models, asynchronous firing models, and predictive spike coding (e.g., [8, 17, 37]). These divergent lines of neural theory are commonly classified as *rate-based* and *spike-based* paradigms.

The fundamental question, as posed by Brette [8], is whether individual spikes and their precise timings are crucial for computation, or if the essence of neural computation can be adequately captured by firing rates, with spikes serving merely as physical manifestations of this representation.

This inquiry reveals that much of the ambiguity in this discourse stems from framing the question solely in terms of coding—that is, the correlation between stimuli and specific observables such as spike trains or firing rates. However, the crux of the matter lies not in whether these observables exhibit variability in response to stimuli, but in whether they play a causal role in the functioning of the nervous system. In essence, can a functional model of the nervous system be constructed based solely on firing rates, or are spikes indispensable? Given that firing rates are essentially aggregates of spikes, this inquiry ultimately delves into whether a realistic model grounded in spikes can be approximated by a rate-based model. We will address this question in the following sections by constructing our models and comparing spike-based and rate-based approaches, examining the requirements for transitioning from microscopic spiking models to mesoscopic firing models (the mean-field).

With these considerations in mind, this modeling chapter is divided into two sections: one concerned with modeling single neurons (Section 3.2), and another focused on building the mean-field model based on these single-cell models (Section 3.3).

3.2 NEURON MODEL

The biophysical and chemical mechanisms underlying neuronal activity and information transfer are well established. Leveraging this knowledge, numerous neuron models have been proposed, ranging from highly detailed models incorporating various biological

properties—such as specific ion channels and synapse types—to simplified and abstract mathematical models with only one or a few variables.

The first and most elaborate model to comprehensively describe neuronal activity at the single-cell level was the *Hodgkin-Huxley* (HH) model [36]. This conductance-based model provides a detailed description of a neuron's membrane potential and action potential generation by modeling different types of ion channels. This approach allows for the inclusion of a wide range of behaviors, as described in [Section 4.2.1](#), and, in principle, enables the modeling of all neuron types distinguished by their ion channel properties.

The HH model is a single-compartment model with specifically defined values for the different gated conductances $g_i(v)$ and reversal potentials E_i of a cell's ion channels i . The time evolution of the membrane potential v depends on the influx of two different currents into the cell membrane: the current describing all ion channel-induced currents, I_m , and an external current, I_e , similar to electrophysiological stimulation during experiments. This leads to

$$c_m \frac{dv}{dt} = \underbrace{\sum_i (E_i - v) g_i(v)}_{I_m} + I_e \quad (3.1)$$

where i runs over the cell's ion channels with their respective $g_i(v)$ and E_i , and c_m is the specific membrane capacitance. As with all single-compartment models, this equation is rescaled with respect to an ordinary cell's unit area [17]. The difference between the reversal potential of a channel and the current membrane potential, $(E_i - v)$, is the *driving force* of channel i .

The conductances are functions of the membrane potential and include voltage-gated variables defining the opening and closing of ion channels. With this high degree of complexity, the HH model is able to very accurately fit cellular recordings and simulate action potential propagation.

However, the large number of parameters and the nonlinear voltage-dependent currents make the HH model difficult to analyze. This high degree of freedom results in interpretational challenges when comparing single parameters to biological behavior. Especially for simulating large networks of neurons, the HH model is not well suited due to its computational complexity and fundamental problems that arise when using overly detailed single-cell models to describe neuron population dynamics (see [Section 3.3.1](#)).

A much simpler model is the *Integrate-and-Fire* model, which founded a whole new area of neuron models based on the same computational principle. As we will see, this model greatly simplifies computation, rendering it the most employed model in network computational neuroscience.

3.2.1 Integrate and fire model

The *Integrate and Fire* model (IF) relies on a simple premise: Between cells in the CNS, there exists a strong similarity regarding the level of membrane potential required (threshold) to activate voltage-gated ion channels producing action potentials. This allows us to apply a computational trick to mimic action potentials as numerically accounted spikes: emit a spike if the membrane potential reaches a specific threshold V_t , modeling the onset of, for example, voltage-gated calcium (Ca^{2+}) ion channels, and reset the membrane potential to a reset value V_r , modeling the repolarization following action potentials. This is supported by the fact that real cells show relatively similar

action potential depolarization and hyperpolarization shapes, regardless of cell type [17].

With this approach, spikes are recorded as (postsynaptic) spike times t_s , and we are concerned only with the membrane potential evolution without explicitly modeling the action potentials themselves. Thus, membrane potential *fluctuations* are modeled, focusing on the dynamics of the subthreshold membrane potential induced by external input.

Explicitly, we assume just one general ion channel modeling all channels responsible for creating the cell's equilibrium or resting membrane potential, thus taking $i = 1$ in (3.1). The general IF model then follows to [42]

$$c_m \frac{dv}{dt} = g_L(E_L - v) + I_e \quad (3.2)$$

with effective resting or leakage potential E_L and corresponding leakage conductance g_L , both constants, and with the equilibrium driving force ($E_L - v$). While the effect of specific action potential-generating channels (e.g., Ca^{2+}) is now modeled via the numerical spiking mechanism, g_L represents non-specific ion channels that generate the membrane potential equilibrium, usually permeable to multiple ions (mostly K^+ and Na^+).

We can define an important model parameter, the membrane time constant $\tau_m \equiv c_m/g_L$, which states the time scale of membrane potential fluctuations and will be an important parameter for building statistical models later on.

From (3.2), we can calculate the firing rate ν of an IF neuron and connect directly a spiking neuron model with the neuron's firing rate, which is defined as the inverse interspike interval (ISI), or $\nu \equiv \Delta_{\text{isi}}^{-1}$ (see Section A.3 for derivation).

The benefit of the IF model lies mainly in its simplicity and ease of integration into networks of IF neurons. However, as soon as networks are considered or realistic synaptic input needs to be modeled, the artificial external current I_e needs to be adjusted. In neural networks, the input current to a neuron integrates the high bombardment of synaptic events and maps incoming presynaptic spike times t_s to a synaptic current I_{syn} , changing the membrane potential. Such synaptic bombardment can lead to distinct dynamical and integrative properties observed in neurons *in vivo* [20]: (1) Neuron's responsiveness is enhanced via an active balance of membrane potential fluctuations. (2) Neurons gain increased temporal resolution via a smaller τ_m . (3) The response of neurons becomes stochastical in nature leading to precise and discriminate population responses.

Points (1) and (3) are especially important to include in our population modeling approaches, while (1) and (2) are necessary for modeling realistic firing responses with spiking model neurons.

To effectively include this high-conductance state and model the membrane potential changes induced by incoming spike times, we replace I_e in equation (3.2) with I_{syn} . The synaptic current I_{syn} models excitatory (e) and inhibitory (i) synapses with a synaptic driving force and the spike-induced change in membrane conductance:

$$\begin{aligned} I_{\text{syn}}(t) &= (E_e - v_\mu)G_{\text{syn}}^e(t) + (E_i - v_\mu)G_{\text{syn}}^i(t) \\ G_{\text{syn}}^{(e,i)}(t) &= Q_{(e,i)} \sum_{t_s^{(e,i)}} \theta(t - t_s^{(e,i)}) e^{-\frac{t-t_s^{(e,i)}}{\tau_{(e,i)}}}, \end{aligned} \quad (3.3)$$

where $G_{\text{syn}}(t)$ is the kernel of membrane conductance with a synaptic conductance increment Q at each spike time t_s and an exponential decay with (synaptic) time constant $\tau_{(e,i)}$ for excitatory and inhibitory synapse, respectively.

3.2.2 The AdEx model

The simple IF model is to-date quite popular in the computational neuroscience community, because of its computational efficiency and ease to analyze. However, the rich biophysics of neurons, synapses, and ion channels leads to important biological characteristics which can not be captured by this model. Further, the shape of the IF model can not be fitted reliably to recorded cell traces and does not allow to distinguish different neuron types. This is due to two biological properties: (1) The shape of the membrane potential at the onset of a spike, when i.e. Ca^{2+} channels gradually begin to open, drastically changes the trace of a neuron. (2) Adaptation mechanisms via i.e. K^+ channels (see [Section 2.2](#) for their importance in the thalamus) or axial conductances of dendritic neuron compartments [76]. Where the spike-onset is mainly needed for systematic fitting, adaptation is a crucial property generating the observed firing rates of neurons, such as RS neurons in the cortex and especially for the bursting properties of neurons in the thalamus (refer back to [Section 2.3.1](#)).

This lead to different two-variable extensions to the IF model (e.g., [9, 37]), which are able to reproduce a large range of experimentally evident electrophysiological properties.

We will focus here on the *Adaptive Exponential integrate and fire model* (AdEx) as described in [9], because it shows many model parameters translatable to observables and thus attainable via experiments. Additionally, this conductance based model proved to be a good balance between computability and biological realism in terms of capturing all firing modes observable in real cells [37] and significantly in thalamocortical cells including TC and RE neurons [18].

The AdEx being a conductance-based model also elevates multiple advantages such as being especially reliable in high-conductance states which are necessary for modeling realistic neuron behavior and connect firing rates of population models to the integrative properties of cells membrane potentials and ion channels [20].

The AdEx, describing the two variables of membrane potential $v(t)$ and adaptation current $\omega(t)$ and with the same spike reset mechanism as for (3.2), is defined as

$$\begin{aligned} c_m \frac{dv}{dt} &= g_L(E_L - v) + g_L \Delta e^{\frac{v-V_t}{\Delta}} - \omega + I(t) \\ \frac{d\omega}{dt} &= -\frac{\omega}{\tau_\omega} + b \sum_{t_s} \delta(t - t_s) + a(v - E_L), \end{aligned} \quad (3.4)$$

where Δ is the amplitude of the spike onset and V_t is the spike-onset threshold both describing the initial phase of action potential generation, in contrast to the simple IF model (3.2) with the rest of parameters the same. I is a general input current which can either be an injected current (as via current and patch clamp techniques) or modeled as a synaptic current integrating all presynaptic spikes (3.3).

For the adaptation the parameters are the adaptation time constant τ_ω governing the time scale of adaptation effects and τ_m/τ_ω being the ratio of timescales between membrane and adaptation changes. Heuristically, the adaptation decays exponentially with time τ_ω and increases via the two adaptation parameters $\{a, b\}$. The the spike-triggered adaptation b incrementally increases ω as response to presynaptic incoming spike times t_s and the subthreshold adaptation a linearly increases adaptation when the cell is polarized ($v - E_L$). These two mechanism capture the two main ways how adaptation of ion channels or dendritic compartments can influence a neuron. In comparison to the model parameters governing the membrane potential, $\{a, b\}$ are more abstract and can not be gathered from electrophysiological data but have to be found via e.g. fitting.

We will now follow Touboul and Brette [76] and analyze the dynamics of the AdEx, which will be used to restrict some parameters for both single cell, network, and mean-field model later on.

We start by nondimensionalizing (3.4) in units for time of τ_m and for voltage of Δ and V_t . This leads to only four free model parameters plus the input current I , which are $\{a/g_L, \tau_m/\tau_\omega, V_r, b\}$ (see [Section A.3](#)).

The dynamics are governed by the two nullclines of (3.4) for both v and ω . The ω -nullcline is a linear function while the v -nullcline is a convex function resulting in the possible set of number of fixpoints $N_{FP} = \{0, 1, 2\}$. The v -nullcline is linearly shifted by the input current I , where a sufficiently large I results in intersections of the nullclines and consequently in fixpoints. This threshold of I marks the point at which spikes are generated and the bifurcation structure determines the type of spiking and excitability. Next to this I also serves as the bifurcation parameter evoking either bursting via a homo-clinic bifurcation or tonic firing via a saddle-node Hopf bifurcation [76, 82].

Next to the current, also the free parameters V_r and b govern the spiking pattern. They lead from single spikes to bursting and at some point chaos via period-doubling [76]. However, because these parameters are only accessible via fitting, they are not so interesting for us as we inherently achieve the correct spiking pattern via the fit on realistic data.

The parameters a/g_L and τ_m/τ_ω are of more interest as they are at least restrictable from data. They govern the subthreshold dynamics, controlling the temporal encoding and generation of spikes which will be of major importance for the construction of the mean-field in the next section. With these two excitability classes can be found, separating the parameter space ([Figure 3.1A](#)).

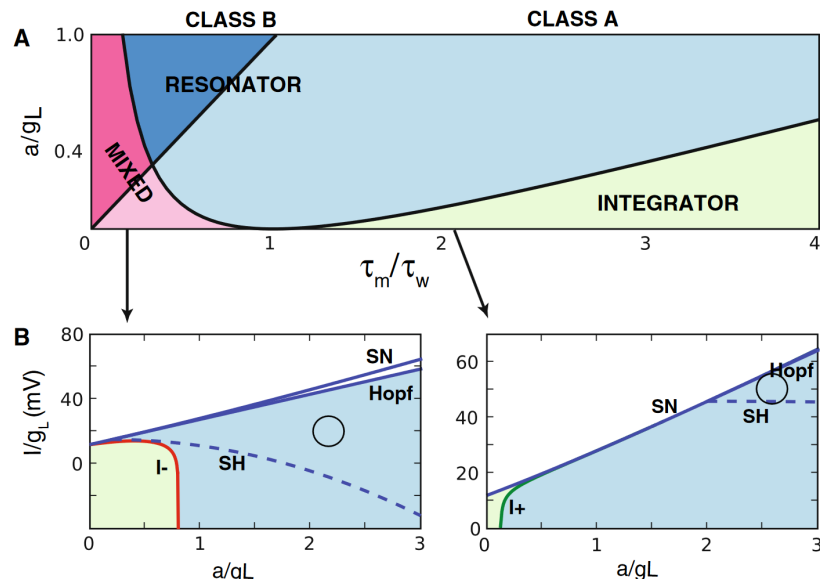


Figure 3.1: Employed network and connectivity structure. A Dynamical regimes of the AdEx as a function of the free parameters a/g_L and τ_m/τ_ω controlling membrane fluctuations. Resonator means emerging oscillations for almost all or all values of I . Mixed refers to a regime where only sufficiently high I generate resonator-like oscillations. B Active firing behavior of the AdEx dependent on input current I for the free model parameter a/g_L and (left:) $\tau_m/\tau_\omega = 0.2$ and (right:) $\tau_m/\tau_\omega = 2$. White area indicates spiking and the circle marks a (repulsive) limit cycle. (Figure taken from [76])

This together with I generating the spike-producing bifurcations results in two different mechanisms for spiking in the AdEx: Spiking occurs when either the current I is above the saddle-node curve or the Hopf curve, depending on the excitability class ([Figure 3.1](#) with SN the saddle-node curve and Hopf the Hopf curve; see [[76](#)] for more details).

The excitability separation in parameter space in [Figure 3.1](#) limits the parameter values for especially τ_m/τ_ω . With confining $\tau_m < \tau_\omega$ we guarantee a rich spiking and response regime for nearly all levels of a and g_L and the spike-dependent free parameters (see [[76](#)]; as listed in [Table 3.1](#)). Additionally, for $\tau_m < \tau_\omega$ low input currents show richer dynamics including both spiking and bursting and also negative currents can induce spiking. These two factors are crucial because: Low I allow for neurons in a balanced and fluctuation driven regime which builds the basis of the employed network and mean-field model. And negative I in principle allow for rebound bursts via hyperpolarization as found in TC cells and significant for the bursting properties ([Section 4.2.1](#)) and large scale oscillations of the thalamus ([Section 4.3](#)).

3.3 MEAN-FIELD MODEL

Most existing neuronal field models can be separated in two groups: either phenomenological models (e.g. [[4, 7, 59](#)]), or more abstract mathematical models (e.g. [[2, 14, 78](#)]). Phenomenological models replicate biological behavior and are capable of modelling particular brain regions, cell types or whole brain recordings. However, these can not couple significant effects or characteristics to model parameters which makes it impossible to use such models far from the fitting point and renders analytical analysis impractical. Conversely, abstract mathematical models couple the dynamical aspects of neuronal activity directly to model parameters and allow analytical or fast-forward numerical analysis, but model parameters are often not well linked to biological observables.

In this section we will discuss theory and background behind the mean-field and network models employed in this thesis. The mean-field model is a combination of, and build upon, three earlier works [[23, 25, 87, 88](#)] where it was employed to model cortical tissue only. As evident from [Chapter 2](#), the thalamus exhibits some unique behaviors – especially regarding phase transitions and bursting – and has a distinct structure compared to the cortex. These intricacies and how we implement them in neuron, network, and mean-field models will be the matter in [Section 4.1](#). In the following, we will start by generally introducing networks of neurons and how to take the step from single neuron models to network models via valid approximations. There we will move from simple inter-connected neuron models to firing rate mass models to stochastic and finally to mean-field models. This will be quite general but of importance for justifying steps in constructing the employed mean-field formalism later in the main part of this section.

3.3.1 Network models

The most direct way in constructing network models of neurons is to employ for each neuron a model as discussed in [Section 3.2](#) and *synaptically* connect them appropriately, e.g. via a synaptic kernel ([3.3](#)). This would be the most instructive and representative way – especially when considering more biologically realistic neuron models such as the HH model, but it comes with substantial informational, computational, and interpretational

problems rendering it impractical for most usecases and especially for exploration and large scale modeling. Therefore, we employ these *spiking networks* (SN) mostly for comparison and validation for the mean-field.

In accordance with our electrophysiological and spike-based approximations, we focus on network models with neurons as their smallest unit, but we further reduce and replace action potentials and precise spike timings with population *firing rates*. These firing-based models avoid the short timescale of channel dynamics and action potential generation completely, simplifying computational load drastically. The conjecture here is that populations of neurons – at the meso- to macroscale – respond with the amount of spikes per time (firing rate) instead of with second order statistics between single spikes. Firing-based models also allow for purely analytic investigation of network dynamics which is near impossible with more intricate model types. A second argument for firing models is that the response of neurons is natural stochastically because if the amount of noise apparent in the brain and networks of neurons [17]. Single neuron models (Section 3.2), however, respond deterministic to current and synaptic input, which would require an impossible perfect knowledge about the input. Additionally, SN's have the problem that because of their amount of free parameters, they mostly only are employable if many neurons in the network form a homogenous subgroup sharing the exact same cell and connection parameters. This can lead to unrealistic strong synchronisations which are far from observed dynamics in the brain.

We refer here again to the success of firing rate-based models at population scale and hypothesise that rates are sufficiently for describing network dynamics in the limit of large networks: If input spike trains are uncorrelated then it holds for the mean and standard deviation of firing rates ν that $\langle \nu \rangle \propto N_{\text{syn}}$ and $\sigma_\nu \propto \sqrt{N_{\text{syn}}}$, where N_{syn} is the number of synapses a neuron receives input from. Thus in large networks with sufficiently little correlation, as is the case in balanced networks and the firing pattern becomes irregular and asynchronous (AI) [80], firing rate works as a good approximation. (For more discussion on this refer to [8, 17].)

Firing-based models can in general be constructed in two steps. The fundamental idea is that a *transfer function* $F(t)$ of a neuron type can be found which maps the input frequency ν_{in} to the cells output frequency ν_{out} . A spike-based transfer function ρ would consist of superpositions of δ -functions at spike times $(t_s) - \rho(t) = \sum_s \delta(t - t_s)$, rendering it impractical for analysis and calculations. A firing based, frequency transfer function in contrast is merely the trial-average of many $\rho(t)$'s for the same neuron. We will see that the resulting shape of F is sigmoidal and necessarily continuous. The second step is to define a *total synaptic current* $I_{\text{syn}}(\nu_{\text{in}})$ which maps the input frequency to the change in membrane potential of a neuron such that F can be defined as a function of this current for a generic neuron type μ

$$\nu_{\text{out}} \equiv F(I_\mu) = \frac{1}{1 + \exp(-I_\mu)},$$

where the exact form of F usually assumes the most general shape of transfer, namely a sigmoid function [17].

Now I_μ can be defined in ways of incoming spikes and subsequently also via incoming firing rate

$$I_\mu(t) \equiv \int_\tau d\tau K(\tau - t)\rho(t) \rightarrow \int_\tau d\tau K(\tau - t)\nu_{\text{in}},$$

where K is the synaptic kernel, describing the synaptic current response to incoming spikes. Here I_μ is just a generalized (3.3)!

We can formulate a firing-rate model when assuming that synaptic input does not change v_{out} instantaneously, and that the firing rate has an equilibrium point where the total synaptic current I_s via F induces fluctuations which will be followed by the firing rate in time constant T which determines the time-window of change of the firing rate v . A good starting point for T would be the membrane time constant of single neurons of the same neuron type as the firing-rate model, namely τ_m . Then it follows that

$$T \frac{d\nu_\mu}{dt} = -\nu_\mu + F_\mu(I_\mu). \quad (3.5)$$

Just with (3.5) it is possible to model a firing based single neuron, but also to assume a homogenous population consisting of the same neuron type. As discussed above, this holds when the network is large enough and homogenous enough.

However, these simple models do not capture the whole landscape of dynamics which should be observed and additionally they do not provide accurate description for the entire range of possible input parameters such as amplitude and frequencies [17].

E-I networks with (3.5) take this very simple model which lacks biological usability in taking two populations or units where each one population is either excitatory or inhibitory (exclusively positive or negative weights or synaptic conductances). These show rich dynamical behavior for their simplicity and ease of their analytical use. Especially non-reciprocal (or active or non-variational) coupling will induce a Hopf bifurcation. They can be used to effectively capture the oscillatory behavior of olfactory bulb or the cortex [17].

A second extension addresses the dynamical regime of real neurons. These show temporally asynchronous and irregular firing activity (AI). The hypothesis, supported by many experiments and computational studies in the last decades, is that there exists a balance between excitatory and inhibitory activities (E-I balance). The above oscillations in E-I systems marks the synchronous regime, whereas irregular spiking occurs in a *normal* activity state. It was shown that the AI state allows for linear responses of populations of highly nonlinear neurons, different responses to nearly the same stimuli, and chaotic behavior [80].

Up to now we have only considered models of neurons and of neuron networks which are deterministic in nature. But because not all information can be known and neuronal activity in the brain exhibits strong variability via noise and spontaneous activity [3], networks should incorporate inherently stochastic properties. This also allows to model approximated homogenous neuron groups where the inhomogeneities inside the population are included in the stochastic nature of a model, additional to including the irregular spiking activity.

The simplest stochastical model for neurons is a Boltzmann machine [17]. In there, neurons are treated as binary functions

$$\nu_\mu(t) = \begin{cases} 1 & \text{if } \mu \text{ spikes in } t + \Delta t \\ 0 & \text{else.} \end{cases}$$

where ν_μ now is the binary firing rate of neuron μ .

We can demand that then the probability that a neuron fires in time span Δt depends on only the transfer function

$$p[\nu_\mu(t + \Delta t) = 1] = F(I_\mu(t)). \quad (3.6)$$

When taking this probability again and again as a time evolution for p and for large enough time steps ensuring an adiabatic process this chain behaves as an independent Markov process. With this, and in equilibrium, we can make use of general statistical physics to find the probability distribution P of a given firing rate

$$P(\nu_\mu) = \frac{e^{-E(\nu_\mu)}}{Z}, \quad \text{where } Z = \sum_\mu e^{-E(\nu_\mu)},$$

defined via the partition function Z and a general unknown energy function E of the system (see [17]). P is now a Boltzman distribution.

These formulations are inherently stochastic. This renders computation and also interpretation often unnecessarily difficult, especially because they need a stochastic interpretation of inputs. An improvement, which builds upon the same foundation is mean-field theory. Mean-fields can be seen as approximations of the Boltzmann machine but which are constructed as deterministic evolutions depending on also deterministic inputs. The output is still probabilistic and we can find a general mean-field distribution for ν_μ based on the transfer function [17]

$$Q(\nu_\mu) = \prod_\mu F(I_\mu)^{\nu_\mu} (1 - F(I_\mu))^{1-\nu_\mu}, \quad (3.7)$$

which follows just a binomial distribution with probabilities set to the transfer function via (3.6).

We will dive deeper into the construction of a mean-field based on statistical formalisms in the following section describing the derivation of the employed mean-field formalism. There we will come back to many of the points mentioned and briefly discussed in this section.

3.3.2 Master equation framework

In this and the next sections, we will describe the employed mean-field formalism which follows a master equation approach developed in El Boustani and Destexhe [25]. The current section will state the main framework of this approach and its assumptions.

The main conjecture of this mean-field derivation is that network activity can be modeled as a Markov chain (Section A.2) if the timestep is in the order of the activities autocorrelation decay time. We will discuss this assumption and its effects theoretically in the next sections and phenomenologically in Chapter 4.

We start constructing the model by assuming that neurons in general brain tissue can be classified and categorized in finite homogenous groups distinguished by their influence on network dynamics via measurable electrophysiological properties. This extends to all distinctive brain structures. A general network of neurons exists of K of such homogenous neuron populations. This also holds for most importantly the cortex, and the thalamus as discussed in Section 2.2 (with $K = 2$ with one population of each TC and RE neurons).

Following our firing rate-based generalization we define the absolute population activity as the number of spikes emitted of that population $n(\Delta_t)$ in a finite duration Δ_t . The *effective* network activity for all populations $\gamma \in \{1, \dots, K\}$ in a network is then, with taking into account explicit time-dependence,

$$m_\gamma(t) \equiv \lim_{\Delta_t \rightarrow 0} \frac{n_\gamma(t - \Delta_t, t)}{\Delta_t N_\gamma}, \quad (3.8)$$

where N_γ is a population's size.

To build towards a stochastical model the starting block is the joint probability distribution between possible activity states $\{m_\gamma\}$ for a timestep T

$$P(\{m_\gamma(t)\}|\{m'_\gamma(t-T)\}) \longrightarrow P_T(\{m_\gamma\}|\{m'_\gamma\}),$$

where the arrow refers to the system's assumed time invariance such that it only depends now on the time constant T . Furthermore, we will describe E-I balanced networks in AI state. This allows to neglect correlations between populations at timescales larger than T [11], and accordingly renders P as population independent $P(\{m_\gamma\}) = \prod_\alpha P(m_\alpha)$. With the system being assumed to be memoryless beyond T , we restrict population activity to be in the range of $m_\gamma \in [0, T^{-1}]$. This allows to integrate possible activity transitions over a definite intervall and to employ (and analytically solve) the time-continous *master equation*. It is to remark that this constructed upper limit of activities $m_\gamma(t)$ changes their definition (3.8) slightly: Now it can be more understood as the fraction of neurons in population γ that fired at least once in a period of $\Delta_t \rightarrow T$. With defining a Markovian transition or step operator W , the generalized master equation for the two *time seperate* ensembles of states is then

$$\partial_t P_t(\{m_\gamma\}) = \prod_{\alpha=1,\dots,K} \int_0^{1/T} dm'_\alpha \left[W(\{m_\gamma\}|\{m'_\gamma\}) P_t(\{m'_\gamma\}) - W(\{m'_\gamma\}|\{m_\gamma\}) P_t(\{m_\gamma\}) \right]. \quad (3.9)$$

The time constant T limits the temporal resolution but also the population activity which can be captured by (3.9). The choice for T is thus crucial. It has to be larger than autocorrelation times but a too large value would underestimate activities. However, in AI state the E-I balance forces the network to be restricted to activities well beneath the maximal single neuron firing rate (which would only be assumed at population level if all excitatory but none inhibitory neurons fire, as possible only in extreme SR states). Then, choices of $T < 15\text{ms}$ allow balanced activities of $m \lesssim 65\text{Hz}$ which captures all normal activity values as observed in AI states in cortex or the thalamus [40, 61] and allows even higher values with neglectable activity underestimation (see also Table 3.1). With this upper limit of T and with only one spike per neuron per time span T , the minimal change in network activity (or activity resolution) is then

$$\Delta m = \frac{1}{NT}, \quad (3.10)$$

restricting the size of the network to a lower limit of neurons per population. This resolution will be discussed and adjusted to capture wanted finite size dynamics.

In (3.9) the transition operator W defines the whole dynamics. We can write it in terms of the probabiltiy distribution between states m and m' for an infinitesimal time period T'

$$\begin{aligned} W(\{m_\gamma\}|\{m'_\gamma\}) &\equiv \lim_{T' \rightarrow 0} \frac{P_{T'}(\{m_\gamma\}|\{m'_\gamma\})}{T'} \\ &= \lim_{T' \rightarrow 0} \frac{\prod_\alpha P_{T'}(m_\alpha|\{m'_\gamma\})}{T'}, \end{aligned}$$

where in the second row we used the systems time invariance.

With the system being in AI state and the timescale being small, we can make use of the *adiabatic approximation*. This allows to employ a finite $T' = T$ (fulfilling our above stated limits for T) such that state transition now is a quasi-stationary process reaching

equilibrium from a previous network state a time T earlier. The transition operator is then

$$W(\{m_\gamma\}|\{m'_\gamma\}) = \frac{\prod_\alpha P_T(m_\alpha|m'_\gamma)}{T}. \quad (3.11)$$

This approximation only holds in a specific range of T with the upper limit being the maximal activity of the network and a lower limit defined by the timescale of irrelevant fluctuations. These fluctuations can be defined via the activities autocorrelation time constant τ and it is shown that for sufficiently large networks which are sparse, the autocorrelation for temporal finite-size effects vanishes [11]. Because of these integration limits, T should be adjusted to capture necessary higher order statistics via finite fluctuations which would be excluded if T is too large. In case of a large T the model approaches a first-order description (discussion follows in [Section 3.3.4](#)).

3.3.3 Statistical moments

With the assumptions above and the therein defined master equation (3.9) and its transition operator (3.11), we have build a framework for the systems time evolution. The master equation (3.9) – describing the probability density of the systems activites $\{m_\gamma\}$ – cannot be solved exactly but we can use it to get the time evolution of the systems statistical moments [25]. An occuring problem here is the *closure problem* of statistical physics, which prohibits to use a finite amount of statistical moments because of their interference with higher order moments (for more details see [Section A.2](#)).

However, in adiabatic processes, as in our case via a sufficiently long timestep T , we are only interested in the stationary activity values. In an E-I balanced AI state the activity distribution for m_γ is well described by a Gaussian which allows to define the second statistical moment or the covariance $c_{\mu\nu}$ between two populations $\{\mu, \nu\}$ in terms of the first statistical moment, the mean activities of that populations $\langle m_{\{\mu,\nu\}} \rangle$. We can also look at this via the *central limit theorem* (CLT) such that sufficient long T filter out higher-order activity fluctuations. In both cases the most important requirement is a network which is balanced and stays in AI state, which is only the case for sufficiently large T , and a sparse connected network, e.g. small connection probabiltiy p and large N for an Erdos-Renyi $G(N, p)$ model (see [Section A.2](#)).

With that, the goal is now to find the time evolution for the first two statistical moments: For the mean of the population activity $\partial_t \langle m_\mu \rangle$ and for its covariance matrix $\partial_t c_{\mu\nu}$. The covariance matrix is defined as

$$c_{\mu\nu} = \langle (m_\mu - \langle m_\mu \rangle) \cdot (m_\nu - \langle m_\nu \rangle) \rangle, \quad (3.12)$$

which is dependent only on the second order interferences of the mean, closing the statistical hierarchy as we will see.

We will follow a general Ansatz to describe the statistical moments via *step moments* [77] with the master equation (3.9). We can then find a form for the time derivative of the mean (derivation in [Section A.3](#))

$$\partial_t \langle m_\mu \rangle = \partial_t \prod_\alpha \int_0^{1/T} dm_\alpha m_\mu P_t(\{m_\gamma\}) = \langle a_\mu(\{m_\gamma\}) \rangle, \quad (3.13)$$

with defining the first-order step moment function

$$a_\mu(\{m_\gamma\}) \equiv \prod_\beta \int_0^{1/T} dm'_\beta (m'_\mu - m_\mu) W(\{m'_\gamma\}|\{m_\gamma\}). \quad (3.14)$$

We therefore have to find the average of a_μ . To do this we expand (3.14) and develop it around the populations mean activity $\langle m_\gamma \rangle$ up to second order [77]

$$\begin{aligned} a_\mu(\{m_\gamma\}) &= a_\mu(\{m_\gamma\}) + \partial_\lambda a_\mu(\{\langle m_\gamma \rangle\}) \cdot (m_\lambda - \langle m_\lambda \rangle) \\ &\quad + \frac{1}{2} \partial_\lambda \partial_\eta a_\mu(\{\langle m_\gamma \rangle\}) \cdot (m_\lambda - \langle m_\lambda \rangle)(m_\eta - \langle m_\eta \rangle) + \mathcal{O}(m^3), \end{aligned}$$

where $\partial_\mu \equiv \partial/\partial m_\mu$ refers to the partial derivation with regards to the activity of population μ . With defining m as a firing rate this can be understood as the firing rate derivation. Averaging and disregarding higher order terms then leads to

$$\langle a_\mu(\{m_\gamma\}) \rangle = a_\mu(\{\langle m_\gamma \rangle\}) + \frac{1}{2} \partial_\lambda \partial_\eta a_\mu(\{\langle m_\gamma \rangle\}) c_{\lambda\eta},$$

where $c_{\lambda\eta}$ is the covariance matrix as defined in (3.12), containing the terms with second order moments. Now setting this in (3.13) we obtain the statistical first-order PDE of our framework

$$\partial_t \langle m_\mu \rangle = a_\mu(\{\langle m_\gamma \rangle\}) + \frac{1}{2} \partial_\lambda \partial_\eta a_\mu(\{\langle m_\gamma \rangle\}) c_{\lambda\eta}. \quad (3.15)$$

Now via (3.15) the mean depends only on the first-order moment step function of the mean $a(\langle m \rangle)$ and the covariance. What is left is to get the time evolution for the second order statistical moment, the covariance matrix of (3.12). The last step – in the next section – will then be to find a definition for the transition function P_T which can be used to calculate $a(\langle m \rangle)$ (with $m = \{m_\gamma\}$).

Taking the time derivative of our covariance matrix (3.12) and reordering leads to

$$\partial_t c_{\mu\nu} = \partial_t \langle m_\mu m_\nu \rangle - \langle m_\nu \rangle \partial_t \langle m_\mu \rangle - \langle m_\mu \rangle \partial_t \langle m_\nu \rangle, \quad (3.16)$$

where we can see that next to the first order moment $\langle m \rangle$ we also need the second order interference $\langle mm \rangle$.

Again via the master equation (3.9) we can find a closed form for the derivative of $\langle mm \rangle$ (derivation in Section A.3) which is only dependent on the second-order step moment function $a_{\mu\nu}$

$$\partial_t \langle m_\mu m_\nu \rangle = \langle a_{\mu\nu}(\{m_\gamma\}) \rangle + \langle m_\nu a_\mu(\{m_\gamma\}) \rangle + \langle m_\mu a_\nu(\{m_\gamma\}) \rangle, \quad (3.17)$$

with the second-order step moment

$$a_{\mu\nu}(\{m_\gamma\}) \equiv \prod_\beta \int_0^{1/T} dm'_\beta (m'_\mu - m_\mu)(m'_\nu - m_\nu) W(\{m'_\gamma\} | \{m_\gamma\}). \quad (3.18)$$

Now setting (3.13) and (3.17) into (3.16) and reordering, we get

$$\partial_t c_{\mu\nu} = \langle a_{\mu\nu}(\{m_\gamma\}) \rangle + \langle a_\mu(\{m_\gamma\}) \cdot (m_\nu - \langle m_\nu \rangle) \rangle + \langle a_\nu(\{m_\gamma\}) \cdot (m_\mu - \langle m_\mu \rangle) \rangle. \quad (3.19)$$

All three terms we can again expand and develop around the mean as done above [77], and we get finally the second-order equation of our framework describing the covariance

$$\partial_t c_{\mu\nu} = a_{\mu\nu}(\{\langle m_\gamma \rangle\}) + \partial_\lambda a_\mu(\{\langle m_\gamma \rangle\}) c_{\nu\lambda} + \partial_\lambda a_\nu(\{\langle m_\gamma \rangle\}) c_{\mu\lambda}. \quad (3.20)$$

With (3.15) and (3.20) we close the master equation statistical moments at second order. However to complete a second order framework we need next to the covariance

matrix also the correlation matrix between two populations $C_{\mu\nu}$ [31]. We will only state the procedure here (with some steps in [Section A.3](#), see [25] for details): The procedure is similar to the above derivation but with including an explicit dependence on the time lag τ next to ordinary time t , developing the step moments a around τ , and taking only into account stationary activity values m^{stat} . It follows that

$$\partial_\tau C_{\mu\nu}(\tau) = \partial_\lambda a_\nu(\{\langle m_\gamma^{\text{stat}} \rangle\}) C_{\mu\lambda}(\tau), \quad (3.21)$$

where a is the same step moment as defined in [\(3.14\)](#). Usually it is sufficient to only describe a populations activity via mean and autocovariance. This also will be the main way of comparing to spiking networks and experiments. However the correlation $C_{\mu\nu}$ is especially important to test the employed approximations about the time step being adiabatic and the dynamical regime being in AI state and in E-I balance. To fulfil the requirements ([Table 3.1](#)) the autocorrelation has $C_{\mu\mu}$ for the populations μ has to be compared to the time step T . This will be done in [Section 4.1.3](#) (results).

3.3.4 Transition function

In the last section we successfully found the step moment functions a_μ and $a_{\mu\nu}$ using the master euqation for the probability distribution P_T and we closed the statistical hierarchy at second order by defining mean [\(3.15\)](#), covariance [\(3.20\)](#), and correlation [\(3.21\)](#) via the step moment functions. As we can see in their definitions [\(3.14\)](#),[\(3.18\)](#) they are dependent on only the Markovian transition function W , and where finding this operator will complete the framework.

The transfer function F , as described in [Section 3.3.1](#), maps the input current to the output firing rate of a cell. The input current can be defined in terms of the incoming synaptic events which directly depends on the incoming firing rate in a firing rate based description and especially for statistical models such as in our framework. In the next section we will see that we can define a transfer function via the statistical moments plus autocorrelation time of the subthreshold membrane potential fluctuations and that those can be calculated from only the incoming firing rates. This will allow us to incorporate synaptic parameters into our firing rate-based model which are especially important for the cell types of the thalamus (refer to [Section 2.2](#)).

Rewriting [\(3.6\)](#) and taking the state of the system $\{m_\gamma\}$ instead of the explicit firing rate ν we get for the (stationary) transfer function

$$p_\alpha(\{m'_\gamma\}) \simeq F_\alpha(\{m'_\gamma\})T \leq 1,$$

where now p_α is the probability that population α fires during time T . This works in our framework precisely because of the assumption of adiabatic processes and that the current state is completely characterized by a stationary transfer via F . Mark that the transfer function of population α depends not only on m_α but on all populations activity $\{m_\gamma\}$ which connect to population α .

While staying in time steps of T and continuing to assume that neurons fire only once in this period and are independent of each other [25], we can employ a binomial distribution for the conditional probabiltly P_T of the master equation [\(3.9\)](#) (similar to [\(3.7\)](#)). It follows that

$$P_T(m_\alpha|\{m'_\gamma\}) = \binom{N_\alpha}{m_\alpha N_\alpha T} p_\alpha(\{m'_\gamma\})^{m_\alpha N_\alpha T} (1 - p_\alpha(\{m'_\gamma\}))^{N_\alpha(1-m_\alpha T)}. \quad (3.22)$$

When the population size is sufficiently large $N_\alpha > m_\alpha T$ the noninteger correction becomes small enough to apply a Gaussian approximation via the Stirling formula (see (A.1) and [25]). We get a normal distribution for a single transitional probability density

$$P_T(m_\alpha | \{m'_\gamma\}) \simeq \sqrt{\frac{A_{\alpha\alpha}}{2\pi}} \exp \left[-\frac{1}{2} (m_\alpha - F_\alpha(\{m'_\gamma\}))^2 A_{\alpha\alpha} \right], \quad (3.23)$$

where we defined

$$A_{\mu\nu} \equiv \delta_{\mu\nu} \frac{N_\mu}{F_\mu(\{m'_\gamma\})(1/T - F_\mu(\{m'_\gamma\}))}.$$

Now the binomial function for the probability distribution (3.22) only holds if the described populations μ are indeed explaining for the full system and all its states and state transitions. Because of this it is important that the *independence hypothesis* holds such that interneuron correlations (which are not included in μ) are not substantial. However, for sufficiently large and sparsely connected networks this is given (To be explicit: $G(N, p)$ with $p \approx N^{-1}$, see Table 3.1).

The following normal distribution of P_T in (3.23) also requires – akin to our main conjecture – that the populations μ are homogenous and fully described by the transfer function F_μ . However slight inhomogeneities are taken into account via the employed CLT resulting in $F_\mu \approx \langle m_\mu \rangle$ with a normal distribution, if N is big enough.

Finally we can get the Markovian operator W via integrating P_T over all states and dividing by T via (3.11)

$$W(\{m_\gamma\} | \{m'_\gamma\}) = \sqrt{\frac{\det(A)}{2\pi}} \exp \left[-\frac{1}{2} (m_\mu - F_\mu(\{m'_\gamma\})) A_{\mu\nu} (m_\nu - F_\nu(\{m'_\gamma\})) \right]. \quad (3.24)$$

Now we can connect this back to T our assumptions about the time step. When taking the integral of the transition operator W over the whole state space $\{m_\gamma\} \forall \gamma$ gives trivially $\frac{1}{T}$ [25]. Meaning that this is approximately the total fluctuation of m taken into account, supporting the requirements already restricted on T (Table 3.1). Because a too small or equivalently too big T would now include either infinitesimal fluctuations or remove all fluctuations, respectively, rendering a second order statistical approach unnecessary.

Now with an explicit form of the transition operator we can compute the step moments (3.14), (3.18) and their derivatives. The integration follows over \mathbb{R} with (3.24) being centered on $0 < F < T^{-1}$ and while ignoring corrective terms at the boundary which are $\propto e^{-N}$ and vanish at large enough population size N (This follows naturally from the Gaussian approximation [25]). We get then for the first-order step moment function and its derivatives

$$\begin{aligned} a_\mu(\langle m_\gamma \rangle) &= \frac{1}{T} (F_\mu - \langle m_\mu \rangle) \\ \partial_\lambda a_\mu(\langle m_\gamma \rangle) &= \frac{1}{T} (\partial_\lambda F_\mu - \delta_{\mu\lambda}) \\ \partial_\lambda \partial_\eta a_\mu(\langle m_\gamma \rangle) &= \frac{1}{T} \partial_\lambda \partial_\eta F_\mu, \end{aligned} \quad (3.25)$$

and for the second-order step moment function

$$a_{\mu\nu}(\langle m_\gamma \rangle) = \frac{1}{T} (\delta_{\mu\nu} A_{\mu\nu}^{-1} + T^2 a_\mu a_\nu). \quad (3.26)$$

With the step moments calculated, we can explicitly find the differential equations for mean (3.15), covariance (3.20), and correlation (3.21); completing the master equation framework at second order. Then the differential equations fully describing our statistical system reads

$$T\partial_t \langle m_\mu \rangle = (F_\mu - \langle m_\mu \rangle) + \frac{1}{2} \partial_\lambda \partial_\eta F_\mu c_{\lambda\eta} \quad (3.27)$$

$$T\partial_t c_{\mu\nu} = \delta_{\mu\nu} A_{\mu\mu}^{-1} + (F_\mu - \langle m_\mu \rangle)(F_\nu - \langle m_\nu \rangle) + \partial_\lambda F_\mu c_{\nu\lambda} + \partial_\lambda F_\nu c_{\mu\lambda} - 2c_{\mu\nu} \quad (3.28)$$

$$T\partial_t C_{\mu\nu}(\tau) = [\partial_\lambda F_\nu (\{\langle m_\gamma^{\text{stat}} \rangle\}) - \delta_{\lambda\nu}] C_{\mu\lambda}(\tau), \quad (3.29)$$

where as a sanity check we can see that at first order the system correctly reduces to (3.5).

We see that the whole system is completely explained by the transfer function F which has to be found for each homogenous neuron population μ . This will be the task in the next section. As expected from a relative generic statistical analysis, the system in first-order approximation (3.27) only depends on F as expected, while second-order statistics (3.28) and (3.29) depend on the first derivative of F (this also retroactively proofs our earlier assumption for the normal distribution of (3.23) via the CLT [25]). Even higher order moments would depend on higher derivatives of the transfer function F .

3.3.5 Mean-field with adaptation

With (3.27)–(3.29) the system is fully described, except the explicit transfer functions F . With this cortical tissue can already be successfully modeled with either simple analytical solutions for F [25] and also more phenomenological derivations of F [87]. However, these only describe the statistical moments of network activity m_μ which in our firing-based approach is just the firing rate $\langle m_\mu \rangle = v_\mu$. Adaptation mechanisms play a more or less significant role in different brain areas. In cortex adaptation mechanisms are less important but are important for modeling certain dynamics such as slow-wave oscillations and regular spiking cortical cells. This was investigated in DiVolo et al. [23], where slow adaptation was integrated in the above derived mean-field formalism. Including adaptation mechanisms is not only more elegant to compare to the widely employed AdEx model (3.4), but is also crucial for modeling the thalamus in which adaptation is extremely strong and drastically changes the responsiveness and function of thalamic cells. Therefore, we will in this section follow [23] and sketch their integration of slow adaptation mechanisms into the mean-field formalism of [25] as defined by (3.27)–(3.29).

Starting, we include a mesoscopic variable of adaptation as an adaptation current ω_γ similar to the AdEx single cell adaptation current ω and define it as

$$\omega_\gamma \equiv \frac{1}{N_\gamma} \sum_{n \in N_\gamma} \omega_\gamma^n,$$

with ω_γ^n the adaptation current of a single neuron n in population γ following the evolution of ω of the AdEx (3.4).

The main assumption of this approach is that the timescale of adaptation mechanics is inherently slower than the timescale of network activity/firing rate (this is supported by e.g., [9, 13, 29]). This will allow us to find a deterministic solution for the time evolution

of $\partial_t \omega_\gamma$. From now on we will often neglect the population index γ in ω_γ for readability, such that if ω denotes the single cell adaptation of (3.4) it will be explicitly stated.

It follows that the whole system is now described by the states of network activity m plus adaptation ω , namely the system goes from $\{m_\gamma\} \rightarrow \{m_\gamma, \omega_\gamma\} \forall \gamma$.

Now the three operators completely defining the formalism (namely conditional probability P_T , transition operator W , and transfer function F) should all depend on these new states. Starting, we can just generally induce the new state of adaptation into the master equation (3.9) into the time-dependent P . Further, with the above assumption of $\tau_\omega \gg T$, we can again find a time-independent P_T with assuming a free conditional probability distribution beyond a timescale of T such that ω is independent on fluctuations in m and can be seen as constant at timescales not far bigger than T . This then allows to define the transition operator analogous to (3.11), and we can find general definitions for

$$\begin{aligned} P_T(\{m_\gamma\}|\{m'_\gamma\}) &\rightarrow P_T(\{m_\gamma, \omega_\gamma\}|\{m'_\gamma, \omega'_\gamma\}), \\ W(\{m_\gamma\}|\{m'_\gamma\}) &\rightarrow W(\{m_\gamma, \omega_\gamma\}|\{m'_\gamma, \omega'_\gamma\}). \end{aligned}$$

Additionally, we also define in the new space the transfer function

$$F(\{m'_\gamma\}) \rightarrow F(\{m'_\gamma, \omega'_\gamma\}),$$

which we need for when we explicitly compute the new transition operator. We will see in the next section that this extension is straightforward with the same assumption for the timescale of adaptation τ_ω .

The first of the two steps we have to complete now in order to explicitly integrate adaptation ω into the formalism is to find new step moment functions $\bar{a}(m, \omega)$ which are integrated now also in adaptation space $\omega_\gamma \in \Omega \forall \gamma$. From (3.14) it follows then that for the first order function

$$\bar{a}_\mu(\{m_\gamma, \omega_\gamma\}) \equiv \prod_\beta \int_0^{1/T} \int_\Omega dm'_\beta d\omega'_\beta (m'_\mu - m_\mu) W(\{m'_\gamma, \omega'_\gamma\}|\{m_\gamma, \omega_\gamma\}), \quad (3.30)$$

and analogous, with (3.18), we find the second order step moment

$$\begin{aligned} \bar{a}_{\mu\nu}(\{m_\gamma, \omega_\gamma\}) &\equiv \prod_\beta \int_0^{1/T} \int_\Omega dm'_\beta d\omega'_\beta (m'_\mu - m_\mu)(m'_\nu - m_\nu) \\ &\quad \cdot W(\{m'_\gamma, \omega'_\gamma\}|\{m_\gamma, \omega_\gamma\}). \end{aligned} \quad (3.31)$$

The next step is to find the transition operator W in this space, with which we can explicitly compute the step moments following the same procedure as in the last Section 3.3.4, calculating again and in descending order $P_T \rightarrow W$ via (3.11).

For the conditional probability P_T – for both binomial (3.22) and normal distribution (3.23) – it follows that P_T only has to be extended with a distribution of ω which is a δ -function in Ω because of the assumption of slow adaptation. Then and in (m, ω) -space it follows that

$$P_T(\{m_\gamma, \omega_\gamma\}|\{m'_\gamma, \omega'_\gamma\}) = P_T(\{m_\gamma\}|\{m'_\gamma, \omega'_\gamma\}) \cdot P_\delta(\{\omega_\gamma\}|\{m'_\gamma, \omega'_\gamma\}),$$

with $P_T(\{m\}|\{m', \omega'\})$ the same function as in (3.22)(3.23) except also employing a transfer function dependent on also adaptation $F(\{m'\}) \rightarrow F(\{m', \omega'\})$.

The definition of the transition operator via conditional probability (3.11) now only holds with adiabatic timesteps for T and also $\tau_\omega \gg T$, which ensures the same approximation for both timescales of activity and adaptation. Then, equivalently to before, we get

$$W(\{m_\gamma, \omega_\gamma\}|\{m'_\gamma, \omega'_\gamma\}) = W(\{m_\gamma\}|\{m'_\gamma, \omega'_\gamma\}) \cdot W_\delta(\{\omega_\gamma\}|\{m'_\gamma, \omega'_\gamma\}),$$

where $W(\{m\}|\{m', \omega'\})$ is equivalent to (3.24) except with an adaption-dependent transfer function $F(\{m', \omega'\})$.

Now when the explicit transition operator is integrated over the whole space, namely $(\{m_\gamma, \omega_\gamma\} \forall \gamma)$, to compute the step moments, the δ -function W_δ vanishes via integration in Ω . This leads to the exact same explicit step moments and their derivatives as in (3.25)–(3.26) but with a transfer function $F(\{m', \omega'\})$ describing not only firing rate but also adaptation of a given cell type.

The moments of m_γ depend now also on the value of ω_γ via the transfer function which will be defined in the next section. However, to close this statistical system, now also the statistical moments of ω_γ have to be considered. Adaptation in single cells via the AdEx (3.4) is local and does only influence other cells via its (slow) adaptation on incoming firing rate. When considering a population model this holds again with the employed definition of ω_γ . Additionally, firing rate at a timescale of T is an adiabatic process, and at timescales of τ_ω adaptation is independent on fluctuations in m we only have to find the first statistical moment or mean $\langle \omega_\gamma \rangle$ which should be dependent only on the state of $\{m_\gamma, \omega_\gamma\}$ but no higher order statistics that would describe fluctuations anymore.

Because we have no fluctuations ($\tau_\omega \gg T$) we can simply interpret the PDE describing the evolution of adaptation of a single cell of the AdEx (3.4) as the time evolution of the mean of a whole population of the same homogenous neuro type γ . With a_γ and b_γ the constant of membrane potential and spike frequency adaption of γ , respectively (with the same values as for the single cell AdEx parameters a, b), it follows that

$$\partial_t \langle \omega_\gamma \rangle = -\frac{\langle \omega_\gamma \rangle}{\tau_\omega} + b_\gamma \langle m_\gamma \rangle + a_\gamma \{ \mu_v - E_L \}_\gamma, \quad (3.32)$$

where $\{ \mu_v - E_L \}_\gamma$ is the difference of mean of membrane potential and resting state potential for population γ . With this we now have that P_δ describes the distribution of adaptation as a delta function with mean at a value as predicted by (3.32).

Putting all this together, and with from now on calling $v_\mu \equiv \langle m_\mu \rangle$, $\omega_\mu \equiv \langle \omega_\mu \rangle$, we get the full system of statistical moments describing firing rate v and adaption ω of all populations $\mu = 1, \dots, K$

$$T \frac{\partial v_\mu}{\partial t} = (F_\mu - v_\mu) + \frac{1}{2} \partial_\lambda \partial_\eta F_\mu c_{\lambda\eta} \quad (3.33)$$

$$T \frac{\partial_t c_{\mu\nu}}{\partial t} = \delta_{\mu\nu} A_{\mu\mu}^{-1} + (F_\mu - v_\mu)(F_\nu - v_\nu) + \partial_\lambda F_\mu c_{\nu\lambda} + \partial_\lambda F_\nu c_{\mu\lambda} - 2c_{\mu\nu} \quad (3.34)$$

$$\partial_t \omega_\mu = -\frac{\omega_\mu}{\tau_\omega} + b v_\mu + a((\mu_V)_\mu - E_L), \quad (3.35)$$

where as discussed $F_\mu = F_\mu(\{m'_\gamma, \omega'_\gamma\}) \forall \gamma$. Note we did not state again correlation, which is equivalent to (3.29). The transfer function F will be derived in the next section which will then completely describe the system.

3.3.6 Transfer function

In the last four sections we successfully closed the statistical system at second order and found the differential equations for the statistical moments describing firing rate v and slow adaptation ω using the master equation formalism. We saw that the determinant function which defines the system (3.33)–(3.35), is the transfer function $F(v, \omega)$ which incorporates all biological information and meaning.

The task now is therefore to find a transfer function describing a general neuron population type which can then be also employed for the populations of the thalamus. The core idea here is an extension to the general definition of the transfer function of (3.6). We calculate F based on the fluctuations of the membrane potential as induced by the incoming synaptic currents of spike trains [1] and change

$$F : I(\{\nu_{\text{in}}\}) \rightarrow \nu_{\text{out}} \quad \text{to} \quad F : \int P_v [I(\{\nu_{\text{in}}\})] \rightarrow \nu_{\text{out}},$$

where P_v is a general distribution of membrane potential fluctuations. This approach allows to include into our modeling the realistic *high-conductance* state of neuronal networks. This state alters the integrative properties of neurons in multiple ways [20]: (1) Neuron's responsiveness is enhanced via an active balance of membrane potential fluctuations. (2) Neurons gain increased temporal resolution via a smaller τ_m . (3) The response of neurons becomes stochastical in nature leading to precise and discriminate population responses.

This type of conductance-based transfer function allows to include into the modeling approach active membrane potential mechanisms, which are dependent on channel or synaptic properties, and combine them with fluctuations dynamics via subthreshold integration.

Now the questions left to answer are how to compute the integral over the fluctuation distribution P_v and how to define P_v itself? For this we follow Kuhn, Aertsen, and Rotter [44] and find three variables describing the (statistical) fluctuations in $v(t)$: Their mean μ_v and standard deviation σ_v ; with $v(t)$ describing the *free membrane potential* which is driven by fluctuations via input conductances and only models the subthreshold levels excluding action potentials ($v \leq V_\theta$). This inherently results in a Gaussian distribution for P_v [44].

To construct the transfer function we consider the reorganization of the membrane potential as an adiabatic process at large enough time scales. Then, with the same idea of integrate and fire neuron models, a spike will be emitted by a neuron if the membrane potential v crosses a specific threshold V_θ (to connect back to biology: opening voltage-dependent K^+ and Ca^{2+}). If we take the probability that a neuron crosses this threshold per time step T we get the neurons output firing rate which we can also write in terms of the fluctuation distribution P_v

$$\nu_{\text{out}} \simeq \frac{p(v > V_\theta)}{T} = \frac{1}{2T} \int_{V_\theta}^{\infty} dv P(v), \quad (3.36)$$

which is just our transfer function F .

For the adiabatic time step T the obvious choice would be the autocorrelation time of the membrane potential fluctuations. An initial guess would be the membrane time constant τ_m . However, the autocorrelation time is only well approximated by τ_m when there is only one or a few synaptic events per time bin but gets less accurate with higher input frequency. This is a good approximation for controlled single cell experiments or models (as done in [1, 43]) but for especially population models the approximation no longer holds [87] (we will calculate this explicitly later in this section, in (3.54)).

With taking $T = \tau_v$, with τ_v the membrane potential autocorrelation time constant, and taking into account the Gaussian distribution for P_v , we can find [43]

$$F = \nu_{\text{out}} \simeq \frac{1}{2\tau_v} \operatorname{erfc} \left(\frac{V_\theta - \mu_v}{\sqrt{2}\sigma_v} \right), \quad (3.37)$$

with requiring because of the adiabatic time step that $\tau_v > \tau_m > \tau_s$ (see Table 3.1).

With (3.37), it is left to find the statistical moments describing the fluctuations μ_v, σ_v , the autocorrelation time τ_v , and a value for the threshold V_θ . Following [88], we propose a phenomenological threshold function instead of a hard threshold. This allows to take into account deviations and renders the formalism stable and prone to missmatches not accounted by theory. The function is defined as a general second order polynomial dependent on the fluctuation parameters

$$V_\theta^{\text{eff}}(\mu_V, \sigma_V, \tau_V^N) = P_0 + \sum_x P_x \cdot \frac{x - x^0}{\delta x^0} + \sum_{x,y} P_{xy} \cdot \frac{x - x^0}{\delta x^0} \frac{y - y^0}{\delta y^0}, \quad (3.38)$$

where $\tau_v^N = \tau_v / \tau_m$ is the normalised autocorrelation time.

This general form of (3.38) allows for capturing nonlinear effects [23, 87] without assuming a definite shape which would restrict the applicability to a subset of neuron types. However, the parameters P can not be derived analytically. Therefore, the idea is to reformulate (3.37) as

$$V_\theta^{\text{eff}}(\nu_{\text{out}}, \mu_V, \sigma_V, \tau_V^N) = \sqrt{2} \sigma_v \operatorname{erfc}^{-1}(2\tau_m \tau_v^N \cdot \nu_{\text{out}}) + \mu_v, \quad \forall \nu_{\text{out}} > 0,$$

to compute the phenomenological threshold space from single cell data, either experimental or computational. On this space the threshold (3.38) is fitted and the parameters P are determined heuristically.

What is left now is to find analytical functions describing the fluctuations

$$\{\mu_v, \sigma_v, \tau_v\} : \nu_{\text{in}} \rightarrow \nu_{\text{out}},$$

which are dependent on the input firing rate and map to the neurons output firing rate. With these found (1) the phenomenological threshold can be fitted, and after that (2) the transfer function can be calculated as a function also of incoming firing rate.

THE REMINDER OF THIS SECTION IS THE DERIVATION OF THESE FUNCTIONS. We start with the assumption that synaptic events are Poissonian (Section A.2) and the fact that PSPs superimpose we can get the mean μ_v and variance σ_v of the membrane potential $v(t)$ via campbell's theorem [52]. With including a sum over different synapse types s (here excitatory and inhibitory $\{e, i\}$), their respective number of synapses K_s and incoming firing rate ν_s at s we get

$$\mu_v \equiv \langle v(t) \rangle = E_L + \sum_{s \in \{e, i\}} K_s \nu_s \int dt \text{PSP}_s(t) \quad (3.39)$$

$$\sigma_v^2 = \sum_{s \in \{e, i\}} K_s \nu_s \int dt \text{PSP}_s^2(t), \quad (3.40)$$

where PSP_s is either an excitatory or inhibitory postsynaptic potential, and the number of synapses in a $G(N, p)$ Erdos-Renyi network is $K_s \equiv p_s N_s$, with p_s the probability of connections to and N_s the number of neurons of the population projecting to synapse s

In order to get a form for the PSPs we make use of the simplest linear conductance-based equation (3.2) [42] describing the free membrane potential v of our model neurons. This we extend by adding the adaptation current ω in the same fashion as for the AdEx such that then the resulting equation is just a linearised AdEx (3.4)

$$c_m \frac{dv}{dt} = g_L(E_L - v) - \omega + I_{\text{syn}}(t) \quad (3.41)$$

$$I_{\text{syn}}(t) = \sum_s (E_s - v_\mu) G_s(t),$$

where the synaptic current I_{syn} in our conductance-based models is again a function of time-dependent synaptic conductances G_s . With the above assumption it follows that G_s are just linear sums of all conductance changes per single synaptic event (kernels) g_s for all incoming spikes at all respective spike times t_{spike} such that

$$\begin{aligned} G_s(t) &= \sum_{t_{\text{spike}}} g_s(t - t_{\text{spike}}) \\ g_s(t) &= Q_s \theta(t) e^{-\frac{t}{\tau_s}}. \end{aligned} \quad (3.42)$$

All constants are the same ones as in the AdEx explained in [Section 3.2.2](#).

The idea now to get the statistical moments of the fluctuations via [\(3.39\)](#) and [\(3.40\)](#), is using [\(3.41\)](#) to compute the local change in v of a single synaptic event which we can set equal to an equivalent PSP of the same event.

We can reorder [\(3.41\)](#), and inserting the synaptic current, to group together a term describing all fluctuations, in shape akin to a general current-based equation

$$\tau_m(t) \frac{dv}{dt} = -v + \frac{g_L E_L + \sum_s E_s G_s(t) - \omega}{G_{\text{tot}}}, \quad (3.43)$$

with defining the effective membrane time constant $\tau_m(t) \equiv c_m/G_{\text{tot}}(t)$ and subsequently the total membrane conductance $G_{\text{tot}}(t) \equiv g_L + \sum_s G_s(t)$. The fraction now describes now fully the deviation via synaptic driven fluctuation from the equilibrium membrane potential at E_L .

In order now to enable analytical treatment of synaptic input we replace the synaptic conductances G_s of [\(3.42\)](#) with their mean values μ_G^s via [\(3.39\)](#) and taking g_s as a conductance PSP. It follows that

$$\mu_G^s \equiv \langle G_s(t) \rangle = \nu_s \int dt g_s(t) = \nu_s Q_s \tau_s K_s. \quad (3.44)$$

With this approximation we can take the mean of v in [\(3.43\)](#) and we find the first statistical moment for the fluctuation driven membrane potential

$$\mu_v = \frac{g_L E_L + \sum_s \mu_G^s E_s - \omega}{\hat{\mu}_G}, \quad (3.45)$$

where $\hat{\mu}_G \equiv \langle G_{\text{tot}} \rangle = g_L + \sum_s \mu_G^s$ is the mean of the total membrane conductance. Note that $\hat{\mu}_G$ predicts the ratio of excitatory and inhibitory input frequencies $\nu_{(e,i)}$ needed to achieve E-I balance (see [\[44\]](#)).

Now equivalently via [\(3.40\)](#) we can also compute the variances of the fluctuations $G_s(t)$, namely

$$\sigma_G^s = \sqrt{\frac{\nu_s K_s \tau_s}{2}} Q_s. \quad (3.46)$$

The approximation $\mu_G^s = \langle G_s \rangle$ only holds if the fluctuations are negligible which is the case if the ratio of mean and variance is small. with taking the ratio of [\(3.44\)](#) and [\(3.46\)](#) we get that $\mu_G^s / \sigma_G^s \propto \sqrt{\nu_s}$. Thus, the approximation for taking only into account the mean of fluctuations $G_s(t)$ and subsequently the derivation of μ_v improves with respective incoming synaptic firing rates $n\nu_s$.

Now with this statistical interpretation the effective membrane potential time constant becomes also time-independent $\tau_m(t) \rightarrow \tilde{\tau}_m = c_m/\hat{\mu}_G$, which at first order is approximately the mean effective time constant $\langle \tau_m \rangle$. Here again the ratio of mean and variance

can be determined to find that they are also proportional to nu_s [44] (both ratios are listed in Table 3.1).

With the above derivations of the mean of time constant, membrane potential, and fluctuations, we can approximate the response of membrane potential v_s to a single synaptic input spike in an active scenario (including general synaptic bombardment). We take the time evolution for the whole membrane potential (3.43) for v_s and the induced synaptic current via one synaptic event via (3.42) and setting $t_{\text{spike}} = 0$. This while staying in the statistical framework allows to formulate v_s without explicitly knowing the state of $v(t)$, and it follows that

$$\tilde{\tau}_m \frac{dv_s}{dt} = -(v_s - \mu_v) - \frac{(v_s - E_s)g_s(t)}{\hat{\mu}_G},$$

where $v_s(0) = \mu_v$.

With this the synaptic driving force $v_s(t) - E_s$ can now be approximated as a constant value resulting from the mean conductance bombardment: $\mu_v - E_s$. This constant will enable an analytical solution for the standard deviation σ_v and the autocorrelation time τ_v of synaptic fluctuations. First step is to level the previous equation by subtracting μ_v so that we describe only the trace of the postsynaptic potential of one synaptic event s relative to the mean potential ($v_s \rightarrow \text{PSP}_s$), and with reordering it follows

$$\tilde{\tau}_m \frac{d}{dt} \text{PSP}_s = -\text{PSP}_s + \frac{(E_s - \mu_v)g_s(t)}{\hat{\mu}_G}, \quad (3.47)$$

with still $t_{\text{spike}} = 0$ and correspondingly $\text{PSP}_s(0) = 0$.

Now the solution to (3.47) is the explicit equation for one postsynaptic potential, it follows to [87]

$$\text{PSP}_s(t) = U_s \frac{\tau_s}{\tilde{\tau}_m - \tau_s} \left[e^{\frac{-t}{\tilde{\tau}_m}} - e^{\frac{-t}{\tau_s}} \right], \quad (3.48)$$

where $U_s \equiv \frac{Q_s}{\hat{\mu}_G} (E_s - \mu_v)$ is the *effective* synaptic driving force.

With the trace of PSPs (3.48) we can now in principle compute the variance of the membrane potential σ_v via (3.39) and (3.40). However, in time space this is not solvable for more than one single synaptic event [44]. Therefore, we make use of shotnoise theory to calculate the power spectrum density of fluctuations P_v which is dependent on all PSPs [16], and which is importantly in frequency space q . It follows that

$$P_v(q) = \sum_s K_s v_s \|\text{PSP}_s(q)\|^2, \quad (3.49)$$

where $\text{PSP}_s(q)$ is the Fourier transform of $\text{PSP}_s(t)$ which follows via (3.48) to

$$\text{PSP}_s(q) = U_s \frac{\tau_s}{\tilde{\tau}_m - \tau_s} \left[\frac{\tilde{\tau}_m}{2\pi i \tilde{\tau}_m q + 1} - \frac{\tau_s}{2\pi i \tau_s q + 1} \right]. \quad (3.50)$$

Then setting P_v into (3.40) allows to define the variance in terms of the power spectrum density and subsequently of $\text{PSP}_s(q)$

$$\sigma_v^2 = \int_q P_v(q). \quad (3.51)$$

Now to compute the integral $\int P_v$ we first calculate at $q = 0$ the square modulus

$$\|\text{PSP}_s(0)\|^2 = (U_s \cdot \tau_s)^2,$$

and subsequently get as in [87]

$$\int_q \|\text{PSP}_s(q)\|^2 = \frac{\|\text{PSP}_s(0)\|^2}{2(\tilde{\tau}_m + \tau_s)} = \frac{(U_s \cdot \tau_s)^2}{2(\tilde{\tau}_m + \tau_s)}. \quad (3.52)$$

Taking to this the sum over synapses s and incoming firing rate, which we can both move out of the integral, we get via (3.51) the variance of membrane potential fluctuations

$$\sigma_v^2(\{\nu_s\}) = \sum_s K_s \nu_s \frac{(U_s \cdot \tau_s)^2}{2(\tilde{\tau}_m + \tau_s)}, \quad (3.53)$$

which only depends now on the at the synapses incoming firing rates ν_s .

With (3.45) and (3.53) we completely describe the statistical system of membrane potential fluctuations v . We exclude higher order activations via the employed restrictions on timescales τ_m and τ_s and especially the firing rate (see Table 3.1). However, to complete the transfer function (3.37) we still need the global autocorrelation time τ_v , which serves as a speed estimation for such fltuations. With exponential synaptic shotnoise, via (3.42), τ_v would not suffice to fully describe the autocorrelation function of fluctuations A . However, we can take an exponential apprximation of A such that then τ_v is a first order approximation.

For this we follow [88] and theorise the autocorrelation time as

$$\tau_v \equiv \frac{1}{2A(0)} \int d\tau A(\tau)^{-1}$$

where $A(\tau)$ is the autocorrelation function of membrane potential fluctuations with time lag τ .

We can rewrite this in terms of the exponential P_v (the power spectral densities (3.49) as already defined via shotnoise theory [16]), and get

$$\tau_v = \frac{1}{2} \left(\frac{\int_q P_v(q)}{P_v(0)} \right)^{-1}.$$

Then, with just setting in the already computed Fourier-transformed PSPs from above into (3.49) it follows the global autocorrelation time

$$\tau_v(\{\nu_s\}) = \sum_s K_s \nu_s (U_s \cdot \tau_s)^2 \cdot \sum_s \frac{\tilde{\tau}_m + \tau_s}{K_s \nu_s (U_s \cdot \tau_s)^2}, \quad (3.54)$$

which is now explicitly dependent on the presynaptic firing rates per synapse s .

If there is only one type of synapse $\{\nu_s\} = \nu_s$ then the above expression simplifies to $\tau_v = \tilde{\tau}_m + \tau_s$. With the assumption of $\tau_m > \tau_s$ we get that $\tau_v \approx \tau_m$ as a useful approximation (and which is also used for experimental studies [44, 88]).

All functions describing the statistics of membrane potential fluctuations now map the incoming or presynaptic frequencies ν_s to mean, variance and autocorrelation, and via (3.37) to the output firing rate of a cell $\nu_{\text{out}} = F(\{n\nu_s\})$. This completes the full mean-field formalism of (3.33) with the high conductance state transfer function F . Only thing left is to find parameters P of (3.38) via fitting to single cell data. This will be done in the results in Section 4.1.2.

Table 3.1: Formalism requirements via employed approximations and assumptions. For AdEx, mean-field, fluctuation modeling, and network (as sep. by the lines).

$\tau_\omega > \tau_m$	Mixed regime of the AdEx (Section 3.2.2)
$T > \tau_{\text{ac}} \approx 1\text{ms}$	No fluctuations (CLT, see Figure 4.4c)
$T < \max(\nu_{\text{AI}})^{-1} \approx 15\text{ms}$	with ν_{AI} the spontaneous cell firing rate range in thalamus [61]
$\Delta\nu = (NT)^{-1} \simeq 0.1\text{Hz}$	Firing rate resolution in the employed model
$\tau_\omega \gg T$	Adaptation dynamics timescale is independent of fluctuations in ν
$\tau_m > \tau_{(e,i)}$	$v(t)$ dynamics are not subject to single synaptic events (3.36) [43]
$\mu_G^s/\sigma_G^s \propto \sqrt{\nu_s} \stackrel{!}{<} 1$	Approximation for synaptic fluctuations (3.46)
$\langle \tau_{\text{eff}} \rangle/\sigma_\tau \propto \sqrt{\sum_s \nu_s} \stackrel{!}{<} 1$	Approximation for $v(t)$ timescale [44]
$G(N, p)$ Erdos-Renyi model	Random network (see Section A.2)
$p \approx 1/N$	Sparse connectivity in $G(N, p)$
Dynamics	AI regime & E-I balance [25, 44, 80]

3.4 ANALYSIS AND SIMULATIONS

In this final section, we describe the numerical methods employed for analysis and simulations. (Disclaimer: The Dynamical Analysis section is adapted from [51].)

Dynamical analysis

To obtain the steady-state and equilibrium firing point activities of the simulated spiking network, we calculate the averaged population activity over extended simulation times ($T > 5$ s) for constant Poissonian inputs. Oscillations are ruled out either by direct observation or through spectral analysis. For the mean-field model, the equilibrium activity is calculated as the population's firing rate after a transient period, up to the point where all eigenvalues of the Jacobian matrix (J) are negative, indicating stability. The Jacobian is defined over the variable set $X \in \{\nu_e, \nu_i, \omega_e, \omega_i\}$ and computed via numerical differentiation.

For bifurcation analysis, we use the same technique up to the bifurcation point. In the spindle section (Section 4.3), we utilize two populations each of thalamocortical relay (TC) and thalamic reticular (RE) neurons to capture and model the asynchronous irregular (AI) dynamics of spindle oscillations in the thalamus. Consequently, the state variables are expanded to $X \in \{\nu_e^1, \nu_e^2, \nu_i^1, \nu_i^2, \omega_e^1, \omega_e^2, \omega_i^1, \omega_i^2\}$. In this case and in Figure 4.11, the Jacobian eigenvalues for the mean-field model are complex up to the bifurcation point, suggesting a supercritical Andronov-Hopf bifurcation. Beyond the bifurcation point in the spiking network, instead of averaging firing rates, we average the extrema over a long simulation time, effectively capturing the amplitude of oscillations. The same approach is applied to the mean-field model.

The maximum Lyapunov exponents for spiking network activities are calculated numerically using the Rosenstein algorithm [58], which quantifies the divergence of nearby trajectories in phase space and is indicative of chaotic dynamics.

Numerical integration

Numerical integration is a method for solving general initial value problems: Let $x(t)$ be a function with its derivative $f(t, x) \equiv \dot{x}$ and an initial value of $x(t = 0) = x_0$, where $t \in [t_0, T]$. We impose an equidistant time-grid for t such that $t_n = t_{n-1} + h = t_0 + nh$, where h is the *time step* and t_0 is the initial time value.

The simplest numerical integration method, Euler's method, takes the line tangent $f(t_n)$ at the beginning of a time interval t_n as an estimate of the slope of the function x over the whole interval $[t_n, t_{n+1}]$. Therefore the area $h \cdot f$ approximates the integral of that interval and it follows

$$x(t_n + 1) = x_{n+1} = x_n + h \cdot f(t_n, x_n). \quad (3.55)$$

The error here however accumulates as this method is constantly either overestimating or underestimating the concavity of the solution function. To address this issue one can calculate the slope f at both endpoints of the interval $\{t_n, t_{n+1}\}$, where the slope at the right endpoint is calculated using the Euler's method approximation (3.55). This effectively introduces a step size of $h/2$ and actively works against over- and underestimation as the right tangent line is correcting the left tangent line in the opposite direction. It follows that

$$\begin{aligned} \tilde{x}_{n+1} &= x_n + h \cdot f(t_n, x_n) \\ x_{n+1} &= x_n + \frac{h}{2} [f(t_n, x_n) + f(t_{n+1}, \tilde{x}_{n+1})], \end{aligned} \quad (3.56)$$

where \tilde{x}_{n+1} is the Euler's method prediction and (3.56) is the effective correction. This is called Heun's method.

Numerical simulations

All simulations were conducted in Python. The mean-field simulations of the ODE system (3.27)–(3.29) utilized the `numpy` library, while the spiking single-cell and network simulations of the AdEx model (3.4) employed the `Brian2` library [72].

`Brian2` is a neural simulator designed to balance flexibility and performance, allowing for the integration of complex computational experiments beyond neuronal and network components. Key features of `Brian2` include: (1) Users define models using string-based equations, which reduces errors and increases reproducibility and readability. This facilitates rapid testing of new models in combination with existing neuronal equations. Additionally, constants and variables are stored with both their scale and physical units, ensuring dimensional consistency. (2) `Brian2` is a clock-driven simulator operating on an evenly spaced computational time grid. It integrates arbitrary differential equations at each time step, followed by event-driven updates such as spike generation mechanisms. (3) `Brian2` integrates model definitions, simulation protocols, data analysis, and more into a single, readable script, allowing for a complete and reproducible computational experiment.

One limitation of the clock-driven approach is that it can overestimate synchrony in the network if the time step dt is too large. Additionally, spikes are constrained by the time grid, introducing an approximation error of $O(dt)$, which corresponds to the total accuracy of the simulation. Consequently, there is often no need to employ high-order numerical integration methods, and a simple forward Euler method is sufficient in most cases [72]. However, we observed a slight accuracy improvement using the higher-order Heun's method (3.56) without significant computational overhead. Therefore, we employed Heun's method for integration in single-cell and network spiking simulations.

For the mean-field model, the time constant T (see (3.27)–(3.29)) governs the system's memory and dynamics. As $T \gg dt$, an explicit forward Euler method (3.55) for numerical integration is sufficient. The second-order mean-field requires calculating the derivatives of the transfer function F in firing space ($\partial_\nu F$). We compared analytical solutions with numerical derivatives of F and found no significant difference in accuracy. Therefore, we opted to use numerical derivatives for all simulations due to their simplicity and ease of implementation.

For generic inputs with a specific firing rate frequency f , we employed statistically generated Poisson-distributed spike trains with mean rate f . In the mean-field model, this corresponds to a constant input value of f .

4 | RESULTS AND ANALYSIS

DISCLAIMER: This thesis' results are published in a preprint paper [51] (see Author's note). The following chapter on main results is very similar to the publication. In more detail: All Figures and all text except some paragraphs and small changes are taken or slightly adapted from [51].

This chapter presents the main results of this study and thesis. It is divided into three parts: Model Construction and Validation ([Section 4.1](#)): We will systematically construct the single-cell, network, and mean-field models, in that order. This process will utilize the previously developed theory ([Chapter 3](#)) while validating all choices and parameters against experimental data and biological constraints (as described in [Chapter 2](#)). This part concludes with a comprehensive validation of the constructed mean-field model ([Section 4.1.3](#)). Investigation of Thalamic Behavior ([Section 4.2](#)): Using the validated models, we will examine thalamic behavior and its dependence on various brain states. Deep Sleep and Spindle Analysis ([Section 4.3](#)): We will explore the thalamic dynamics during deep sleep, with a particular focus on spindle oscillations. These latter two sections represent the primary investigations of this thesis, leveraging the models developed in the first part to provide insights into thalamic function across different physiological states.

4.1 THALAMIC MODEL

4.1.1 Cell level

For the cell parameters, we model two distinct states of the thalamus corresponding to high or low levels of the excitatory neuromodulator acetylcholine (ACh), as described in [Section 2.3.1](#). McCormick and Prince [46] and [48] demonstrated that low levels of ACh alter the firing patterns of TC cells, inhibiting single tonic firing and promoting bursting behavior. Given ACh's capability to act as a switch between tonic and bursting modes in TC cell relay, and its role in regulating overall physiological brain state (see [Section 2.3.3](#) and [13, 47, 67]), we define two distinct states in our model:

- Awake state: Characterized by the presence of ACh, corresponding to wakefulness, REM sleep, and high attentive states.
- Sleep state: Characterized by the absence of ACh, corresponding to non-REM sleep and low attentive states.

We fit the AdEx model ([3.4](#)) to recorded TC and RE cell traces from the studies by McCormick and Prince [46] and McCormick [48] ([Figure 2.3](#)), representing two distinct states: ACh present (awake) and ACh absent (sleep). Initial parameter values are derived from Destexhe [18], and the resulting optimized parameters are presented in [Table 4.1](#).

This phenomenological fit is validated across the entire parameter space using a *mean absolute error* (MAE) stability analysis, comparing real and simulated cell traces (see

Table 4.1: Used cell and synaptic parameters for TC and RE cells in awake (ACh) and sleep (no ACh) states, respectively. The last two parameters are for the spiking network only.

PARAM	AWAKE		SLEEP		DESCRIPTION
	TC	RE	TC	RE	
Q_e	1nS	4nS	-	-	exc. conductance increment
Q_i	6nS	1nS	-	-	inh. conductance increment
c_m	160pF	200pF	-	-	membrane capacitance
E_L	-65mV	-75mV	-70mV	-85mV	resting (leakage) potential
g_L	10nS	10nS	9.5nS	13nS	leak conductance
τ_w	200ms	200ms	270ms	230ms	adaptation time const.
a	0nS	8nS	14nS	28nS	membrane pot. adaptation
b	10pA	10pA	200pA	20pA	spike frequency adaptation
$\tau_{(e,i)}$	5ms	5ms	-	-	syn. time constants
E_e	0mV	0mV	-	-	exc. reversal potential
E_i	-80mV	-80mV	-	-	inh. reversal potential
V_t	-50mV	-45mV	-	-	threshold for the exp. onset
Δ	4.5mV	2.5mV	-	-	amplitude of the spike onset

[Figure A.2–A.5](#)). We implemented two manual parameter adjustments: (1) A hyperpolarized EL for RE cells in the sleep state. While this choice deviates from the best fit, as evidenced by the increased error shown in the second row of [Figure A.4](#), it was necessary to ensure biologically realistic, stable, and inhibition-controlled asynchronous irregular (AI) dynamics in the full network (see [Section 4.1.3](#)). (2) A stronger spike adaptation parameter b for TC cells, also in the sleep state. This adjustment is required for TC cells to exhibit bursting behavior in network simulations (see [Figure 4.6b](#)). While it leads to more pronounced bursting at the single-cell level, it does not significantly increase the error of the single-cell fit.

To demonstrate that the cells exhibit the correct behavior using the AdEx model (3.4) with the proposed cell parameters, [Figure 4.1b](#) presents four exemplary single-cell traces of RE and TC neurons. In these simulations, a constant, time-gated current was injected into the cell to evoke a firing response. This was achieved by setting a rectangular pulse as I_{syn} in (3.4) (I_{syn} generates tonic and burst firing via two different bifurcations depending on excitability state, see [Section 3.2.2](#) and [76]). The top row demonstrates the desired response types for the TC cell: tonic firing with awake parameters (modulating ACh), and burst firing with sleep parameters (low-level of ACh). The bottom row shows the RE cell's response, which exhibits burst firing in both parameter states. However, in the sleep state, the burst duration decreases while maintaining the same number of spikes, resulting in increased *burstiness*.

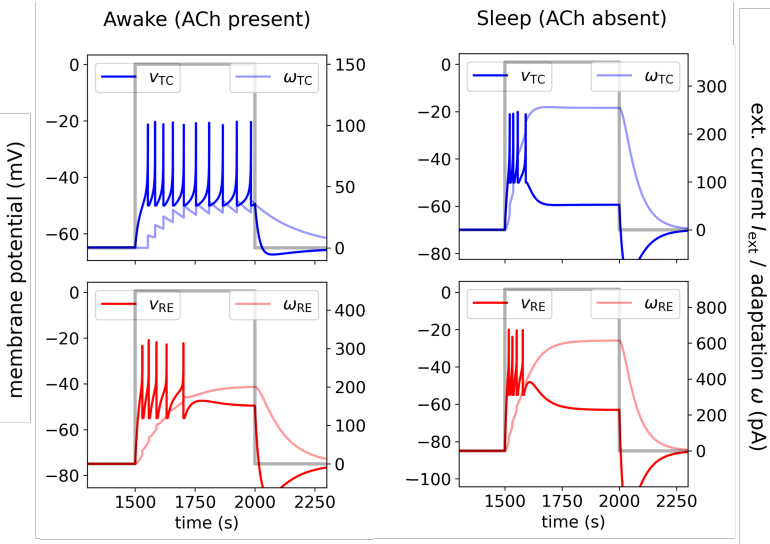


Figure 4.1: TC and RE single cell dynamics. Single cell traces from AdEx IF neurons (see Methods for details) of TC and RE response to the injected current in awake state (with ACh) and the same in sleep state (no ACh). The cell’s membrane potential v and adaptation current ω are shown in color for TC (blue) and RE cell (red), respectively. (Figure adapted from [51])

4.1.2 Population level

We model one thalamocortical relay (TC) and one connected reticular (RE) population of a generic thalamic nucleus (Section 2.2). We will model not a complete nucleus but a nucleus subpopulation. This is in agreement with newer studies suggesting multiple distinct parallel pathways per nucleus, with also interactions between themselves. We neglect interneurons, as we assume to be in the limit of large and sparsely connected networks. Then, their correlations become insubstantial, and interneurons are not contributing to population dynamics [67] (see also Section 2.2). One of the main goals of the thalamus mean-field is to be incorporated into large or whole brain models with, among others, already developed cortical mean-field models [23]. These describe populations of $\sim 10^4$ cortical neurons. To keep the scale difference between cortex and thalamus proportional, we employ a scale of 1/10 [53, 62] and therefore use $N=500$ neurons per population.

The network with its connections is depicted in Figure 4.2. We consider a randomly connected *Erdős-Rényi* network comparable to the statistical assumptions of the mean-field. TC and RE populations form a loop of excitation and inhibition. TC cells do not excite other TC cells but excite RE cells (in addition to outgoing axons to the cortex). In contrast, RE cells are connected in an inhibitory loop and also inhibit TC cells. We propose two external drives serving as inputs to the model: The *cortical* drive P (going to both populations) and the *sensory* drive S (going only to TC cells), modeling cortical signals and sensory stimuli to the thalamus, respectively.

For the synaptic and connection parameter values, we start with a sparse connection between populations of 5% and increments of $Q_e = 1\text{nS}$ to be close to the values of previous mean-field models (i.a. [23]) while keeping true to thalamic evident connections being local but sparse [40]. To model the dense net of locally self-inhibiting RE neurons in the TRN (refer to e.g. [41, 45]), we use a high $p=30\%$ and a balancing low

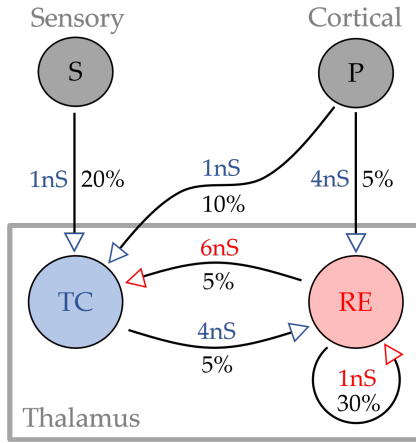


Figure 4.2: Employed network and connectivity structure. The chosen network structure of two thalamic populations (TC and RE cells of each $N = 500$), their synaptic increments Q , and connection probabilities p for all connection between the TC and RE population. The external inputs are shown in grey: The *cortical* drive P ($N=8000$) and the *sensory* stimulus drive S ($N=500$). The arrows mark the direction of synaptic transmission and if they act excitatory (blue) or inhibitory (red). (Figure adapted from [51])

$Q=1nS$. According to [61, 62] there are significant more axons going from cortex to TC than from cortex to RE cells, but the amplitude of connection are stronger, keeping the impactfulness of the role of TRN in the cortico-thalamic control. Last, the number and convergence of connections from RE to TC cells ensure strong inhibition [61].

Until now, the discussion applies to the cell and network structure of both the mean-field and the spiking model. Whereas the spiking model can now be readily simulated with the discussed parameter choices (implementation described in Section 3.4), the mean-field model is built on and requires the cell-specific transfer function F (3.37) to be fitted to data (Section 3.3.6). This will be done in multiple steps:

To get the transfer functions we fit the parameters $\{P\}$ on single cell simulations of TC and RE cells (in awake state) using the AdEx equations (3.4) and cell parameters as explained previously. The formalism translates excitatory and inhibitory input firing rates $\{\nu_e, \nu_i\}$ of a neuron into its fluctuation statistics $\{\mu_V, \sigma_V, \tau_V\}$ and then to its output firing rate (refer back to Section 3.3.6 for details and derivation; the following equations are all defined there).

The advantage of this semi-analytic approach is that –given either simulated or experimental data– we can calculate the phenomenological threshold $V_{\text{thr}}^{\text{eff}}$ (3.38) by rearranging the transfer function equation (3.37). The employed procedure is to first fit (3.38) linearly in the threshold space (depending on the topography of the threshold space, this fit can to be done nonlinearly too). However, here (3.45) has to be adjusted because the adaptation variable ω is unknown. Therefore, the (stationary) solution to the adaptation field equation (3.35) is used to calculate ω from the firing rate data. The resulting values for $\{P\}$ are then used as initial guesses for the fully nonlinear fit of (3.37) in the original firing rate space. This two-step process helps ensure a more robust fit by providing a good starting point for the nonlinear optimization.

For the fit we normalised the fluctuation regime the same way as done in previous works [23, 88] to ensure comparability especially for building large scale models ($\mu_V^0 = -60\text{mV}$, $\delta\mu_V^0 = 10\text{mV}$, $\sigma_V^0 = 4\text{mV}$, $\delta\sigma_V^0 = 6\text{mV}$ and $\tau_V^{N0} = 0.5$, $\delta\tau_V^{N0} = 1$).

In Figure 4.3, we show the fitted transfer functions F_μ for TC cells (top, blue) and RE cells (bottom, red) across the full range of excitatory input frequencies (ν_e) and a subset of three inhibitory input frequencies (ν_i). Each dot represents the averaged output frequency from single-cell simulations over 5 seconds. The sigmoid shape of the transfer function (3.37) is evident. Certain deviations from the fitted predictions via F are observed only at very high firing rates; a region of lesser biological relevance for the

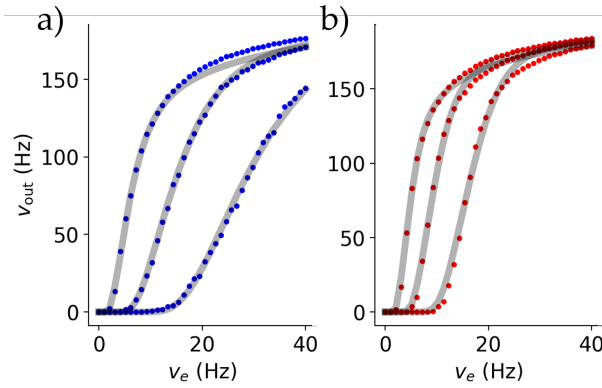


Figure 4.3: Transfer function fit. The fitted transfer functions for RE and TC cell for three different inhibitory inputs each with their corresponding single cell simulations. (a) is for TC and (b) for RE cell-type (awake state). The dots each represent the averaged firing rate of a cell over 100 runs. (Figure adapted from [51])

phenomena studied in this thesis. To improve statistics, the resulting single-cell firing rates were averaged over 100 runs.

4.1.3 Validation of the mean-field

After constructing and fitting the mean-field model, in this section, we will validate it by comparing its predictions of population activities with those of the spiking network. Furthermore, we will demonstrate its suitability for modeling both the awake and sleep states of the thalamus as defined in [Section 2.3.3](#).

The fit parameters of the mean-field's transfer function F , obtained using the fitting technique described in [Section 4.1.2](#), are depicted in [Table 4.2](#). These parameters are applied to both awake and sleep states, as the differences between these states are captured by other model components. They are used throughout this and the following sections (but not in [Section 4.3](#), where a different parameterization is required due to the specific generation of spindle oscillations).

Table 4.2: The fitting parameters P of V_{thr}^{eff} and their values. All values in mV.

CELL	P_0	P_μ	P_σ	P_τ	$P_{\mu\mu}$	$P_{\mu\sigma}$	$P_{\mu\tau}$	$P_{\sigma\sigma}$	$P_{\sigma\tau}$	$P_{\tau\tau}$
TC	-47.31	1.68	0.97	-3.46	0.47	-1.68	-6.46	3.43	-1.14	0.19
RE	-40.77	-1.98	-3.12	3.57	1.39	-0.38	-0.33	0.16	0.26	-0.53

The direct validation of the mean-field model is to compare the predicted mean firing rates ν_μ and their standard deviations σ_μ with the firing rates of the full spiking network, both representing the full thalamic substructure model (as depicted in [Figure 4.2](#)). This comparison is shown in [Figure 4.4a](#). Both populations receive an external constant *cortical* input of $P = 4\text{Hz}$ and a double Gaussian *sensory* stimulus S (definition in appendix; for the spiking model the input is a Poissonian spike train of mean $P!$). The spiking network provides the membrane potential evolution and spike times t_s for all the 1000 cells. The spikes of all neurons are shown as dots in the upper raster plot. By averaging $\{t_s\}$ over a specific bin time T_{bin} , we can calculate the time-dependent averaged firing rate of both spiking network (SN) populations. We use $T_{bin} = 5\text{ms}$ for all simulations except stated otherwise. To compare to the mean-field, in the formalism we have to employ a similar time window for the mean-fields time constant T , and we set $T = T_{bin}$. The choice of 5ms is justified by the following results and that this timescale is larger than correlation effects but smaller than adaptation and potentiation effects (for more details refer back to [Section 3.3](#) and see also [Table 3.1](#)).

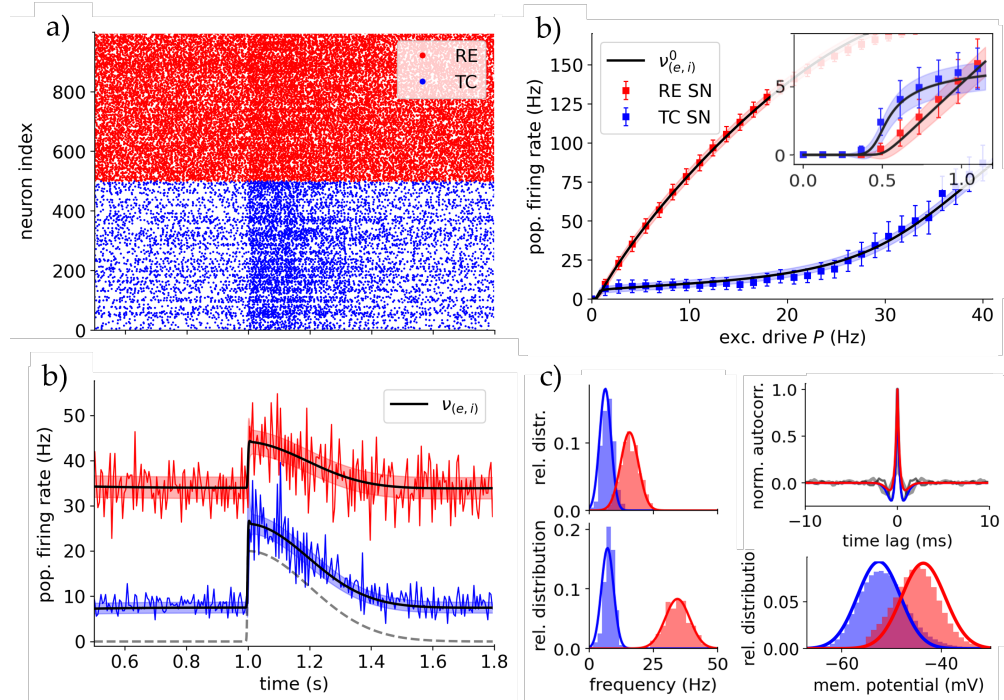


Figure 4.4: Validating the mean-field with spiking networks. (a) Comparison of the firing rate of the mean-field and the spiking network for constant cortical drive $P = 4\text{Hz}$ and a Gaussian stimulus coming from S . Top is the raster plot showing all spiking times $\{t_s\}$ for all neurons in the spiking network simulation. Bottom is the averaged mean firing rate of spiking network (blue/red lines) and predicted mean firing rate of the mean-field ν (black line) with its standard deviation (shaded blue/red areas). (b) Comparison of the mean firing rate and corresponding standard deviation of the spiking network and the mean-field over a range of cortical inputs. Each dot represents a spiking network simulation for 10s where the steady long time mean is calculated. The black lines correspond to the mean-fields fixpoints $\nu_{(e,i)}^0$, with the shaded areas being the standard deviations. The inset shows a zoom at the *silent* and *initial* regimes (see main text for further discussion). (c) Left column: The firing rate distributions of spiking network (histogram) and mean-field (line) for $P = \{2, 4\}\text{Hz}$. Bottom-right: Comparison of membrane potential distribution for 4Hz. Top-right: Autocorrelation of TC and RE population for spiking network (gray lines) and mean-field (blue/red lines). (Figure adapted from [51])

In Figure 4.4b, we vary the cortical drive P and compare the equilibrium population firing rates for TC and RE populations in both the spiking network and mean field over a 10-second simulation (methodology see Section 3.4). This analysis reveals four distinct regimes of TC response: The first regime with no activity. The second regime with a fast response to changes in P . The *inhibited* third regime with limited responses. And the fourth regime with strong TC cell responsiveness due to (biologically unrealistic) saturated RE cell activity. This justifies using a cortical drive $P > 1\text{Hz}$ for most simulations, ensuring a stable low-activity AI state, comparable to especially *in-vivo* experiments.

In Figure 4.4c, we compare the distribution of firing rates and membrane potentials. In the latter the refractory states are removed to get a realistic comparison with the mean-field. The fit between mean-field and spiking network distributions only diverges at high firing rates of close to 100Hz due to the discontinuous nature of simulating spiking models. The good agreement in not only firing rate but also membrane potential is significant. Equations (3.45) and (3.51) predict accurately the spiking populations

membrane potential statistics and will henceforth be used to compare with experimental data and methods.

In the same figure, top-right, there is depicted a comparison of auto-correlations of TC and RE populations activity in the stationary state corresponding to $P=4\text{Hz}$, showing a strong independence of population activity as expected from a inhibition-controlled network without excitatory-excitatory connections (see Appendix for definition). This also agrees with the important assumption that the models are in AI state. Additionally, with the autocorrelation's decay time as a lower limit, the choice of T_{bin} and T for $\tau=5\text{ms}$ is further justified.

Finally, we assess the robustness of the mean-field by varying global parameters ([Figure A.1](#) in appendix). This is done for adaptation parameters $\{b, a\}$, which exhibit the significant change between awake and sleep state, and synaptic excitatory conductance Q_e to validate its change for simulations in this study. We demonstrate that even far of the actual fitting point, the mean-field remains effective in capturing network dynamics. This validation allows us to use the mean-field approach for parameter space analysis and the study of the transition between awake and sleep states with just one mean-field parameter fit.

4.2 RESPONSIVENESS

4.2.1 Tonic and burst firing modes

We explore how bursting, which is modulated by acetylcholine (ACh) levels, impacts the response of thalamic neurons and their network. Our fit to biological bursting TC cells, based on data from [48], demonstrates that the AdEx model with our chosen parameter set successfully reproduces bursting behavior of single TC cells in the ACh-depleted (sleep) state. This is evident from the cell traces shown in [Figure 4.1](#).

We want to investigate the stability of those regimes and their dependence on model parameters. With the employed models ([Chapter 3](#)), the mechanism generating bursting is the slow adaptation current of the AdEx ([3.4](#)).

We introduce firing adaptation \mathcal{F} as a metric describing how adaptation shapes the response. Because the AdEx generates bursting-like behaviour via its adaptation current ω , we will see a good agreement between \mathcal{F} and burstiness.

We use the transfer function F ([3.37](#)). For the effect of adaptation mechanisms on the firing rate of a neuron type we can identify two crucial states described by F : The no-adaptation fixpoint (F_0): This state represents the firing rate of a cell in the absence of adaptation and corresponds to the cell's firing rate at the onset of a stimulus where the (slow) adaptation mechanisms have no impact yet. And the real-adaptation fixpoint (F_ω): Representing the cell's firing rate when it has fully adapted to its own and the stimulus influence. Then $F_0 - F_\omega$ reflects the change in firing rate of a cell from initial activity at the onset of a stimulus as it transitions towards full adaptation and slowing its firing rate.

Necessarily, the transfer function is firing-based and needs non-zero firing rate inputs (ν_e, ν_i) to yield results. Therefore, we calculate the fixpoints for a constant $\nu_e = 1\text{Hz}$. When considering high firing rates as decreased ISIs this metric is comparable to experi-

mental methods measuring burstiness (such as [84]). Concluding, we define the firing adaptation metric as

$$\mathcal{F} \equiv \frac{F_0 - F_\omega}{F_0}, \quad \text{where } \partial_t F_{\{0,\omega\}}(\nu_e = 1\text{Hz}) = 0. \quad (4.1)$$

With (4.1), we investigate the stability of bursting in TC cells and the dependence of bursting on model parameters. For this we use the level of firing adaptation to quantify the effect of adaptation mechanisms on the firing rate of neurons. The dependence of TC firing adaptation on membrane and spiking adaptation parameters and membrane polarization is shown in Figure 4.5a,b. Firing adaptation, and consequently bursting behavior, is strongest at high membrane adaptation levels and hyperpolarized membrane potentials. The awake state (high ACh) experiences nearly no firing adaptation, while the sleep state (low ACh) shows strong firing adaptation, consistent with the bursting behavior observed in Figure 4.1.

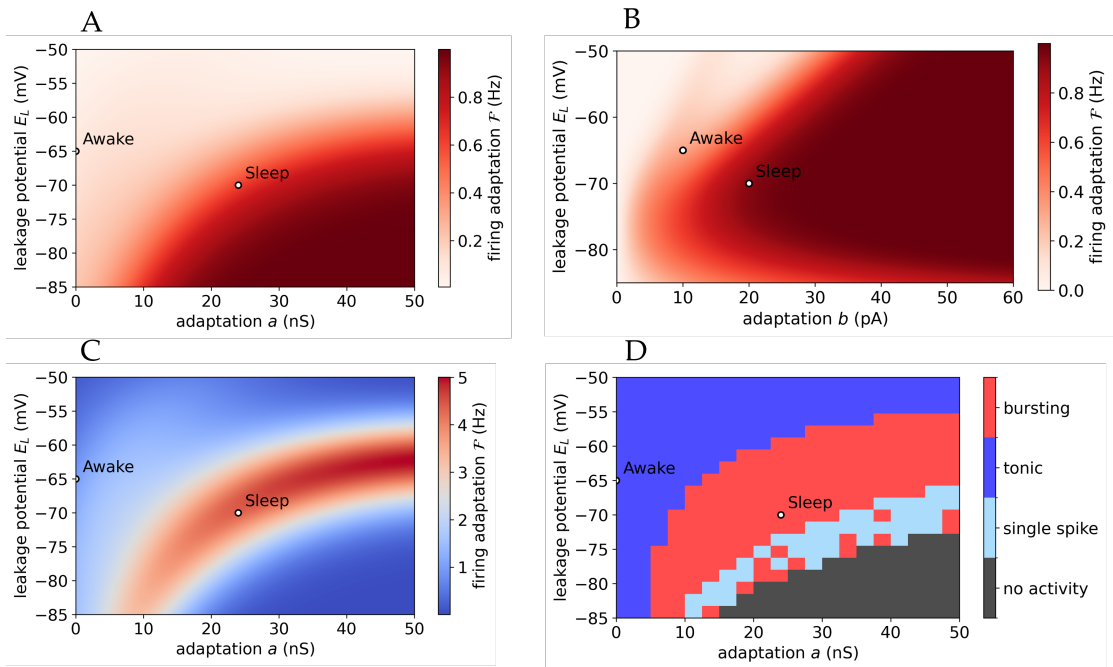


Figure 4.5: Firing adaptation and bursting of TC cells. (a) Parameter scan for firing adaptation \mathcal{F} for TC cells via the fitted transfer function (3.37) for resting potential and membrane adaptation a . Depicted are the parameter values for sleep and awake state. (b) Same as in (a) but for spiking adaptation b . (c) The scan of (a) but the firing adaptation \mathcal{F} is multiplied by the firing rate during the response (also via transfer function), revealing a split of bursting dynamics for the same input. (d) Parameter scan of TC single-cell simulations, showing the possible firing modes of tonic, bursting, single spikes, or no spikes as a response to a input current (see text). Similarity to firing adaptation in (a) and (c) is evident. (Figure taken from [51])

We want to improve on defining the states of ACh as tonic/bursting states and subsequently as awake and sleep states. For this we conducted a parameter scan using spiking network simulations of single TC cells mapping the different firing modes. Similar to [33] (and Figure 4.1) we injected the cell with a constant current for 1s. We classified firing patterns based on the number of spikes on a time scale relative to the adaptation time constant ($\tau_\omega \approx 200$ ms). The external current applied was proportional to E_L in order to induce activity (with $I = \{200\text{nA for } E_L = -50\text{mV}, 400\text{nA for } E_L = -85\text{mV}\}$).

[Figure 4.5d](#) presents the results, highlighting the four possible firing modes. The ACh-absent or sleep state exhibits stable bursting not susceptible to either adaptation or voltage perturbations while the ACh-present or awake state is deep in the tonic regime.

The scan shows a similar tendency of increased bursting as with increased firing adaptation. Note that the firing adaptation is not taking into account if there is actually a non-zero response to account for the single spikes or no activity response types of the single cell scan ([Figure 4.5d](#)). When integrating with \mathcal{F} the actual response amplitude we get however the same strip-region of bursting as in the single-cell scan (see [Figure 4.5c](#), the same holds for the scan in *b*).

Following, we aim to replicate experiments at single cell level on tonic and bursting states of TC cells, as documented in Sherman and Guillery [61, ch. 6] (see [Figure 2.4](#)). These experiments involved manipulating the membrane potential of recorded TC cells to force either a tonic mode (around -65mV , resting state) or a bursting mode (around -75mV , hyperpolarised state), in the absence of external stimuli. A grating retinal stimulus was applied, leading to an oscillatory firing rate response. In these experiments, TC cells in tonic mode exhibited a linear response throughout the stimulus period, while TC cells in bursting mode showed strong responses primarily during the initial phase of each stimulus cycle, with reduced activity in later phases.

We recreated this behaviour computationally in our proposed spiking network with an oscillatory sensory drive S , with amplitude of 10Hz and frequency of 2Hz . The network was set in awake state emulating a lightly anaesthetised state as in experiment. To model the thalamus *in-vivo*, a constant external cortical drive of $P = 4\text{Hz}$ was applied (the *inhibited* regime, [Figure 4.4d](#)). Subsequently, we recorded one single cell with each awake and sleep parameters. While the proposed awake and sleep states are not identical to the artificially set tonic and bursting modes in the experiment, the switch via acetylcholine (ACh) generates a similar polarization.

The recorded cell's response was calculated by averaging the spike times over 40 simulations for a time bin of 15s . This *firing rate* is depicted in the first row of each [Figure 4.6a,b](#) for the awake state and sleep state, respectively. We observe the same response patterns as in the experiment for awake and sleep parameters, although with slightly lower response amplitudes in the sleep state compared to the hyperpolarized state of the experiment. This can be attributed to the absence of T-channels and low-threshold spikes in the AdEx model [61]. In [Figure 4.6b](#) there is also depicted, in light blue, the response in sleep state with the unchanged adaptation parameters ($b = 20\text{pA}$), which does not show the correct behavior.

The effects, however, are quite small and functionally not so different between awake and sleep states. We would expect stronger effects of bursting in the responsiveness when adaptation effects are significantly slower than changes in the input and subsequently membrane potential (as is the case for single cells, [Figure 4.1b](#) for a rectangular pulse). To investigate this at the network level, thalamic response to faster changing stimuli is tested. In [Figure 4.6c](#), a split-Gaussian with steep left-hand std. is depicted (at $t_0 = 1.5\text{s}$ with std. $\sigma_l = 2\text{ms}$ and amplitude $A = 20\text{Hz}$, see [Equation A.6](#); inhibited regime). TC response is two-fold at an initial peak and then quickly adapts. This response curve is nonlinear and does not follow the shape of the stimulus faithfully anymore. This *peak* response is a direct effect of TC cells bursting at the onset of the stimulus, as shown in the inset for a random TC cell of the spiking network simulation. Similar to the single cells definition of showing bursting ([Figure 4.1b](#)), also the TC population activity vanishes after the initial peak for a sustained input (no cortical drive, [Figure 4.6d](#)). The initial bursting of TC cells is captured by the mean-field mainly via its second order moments,

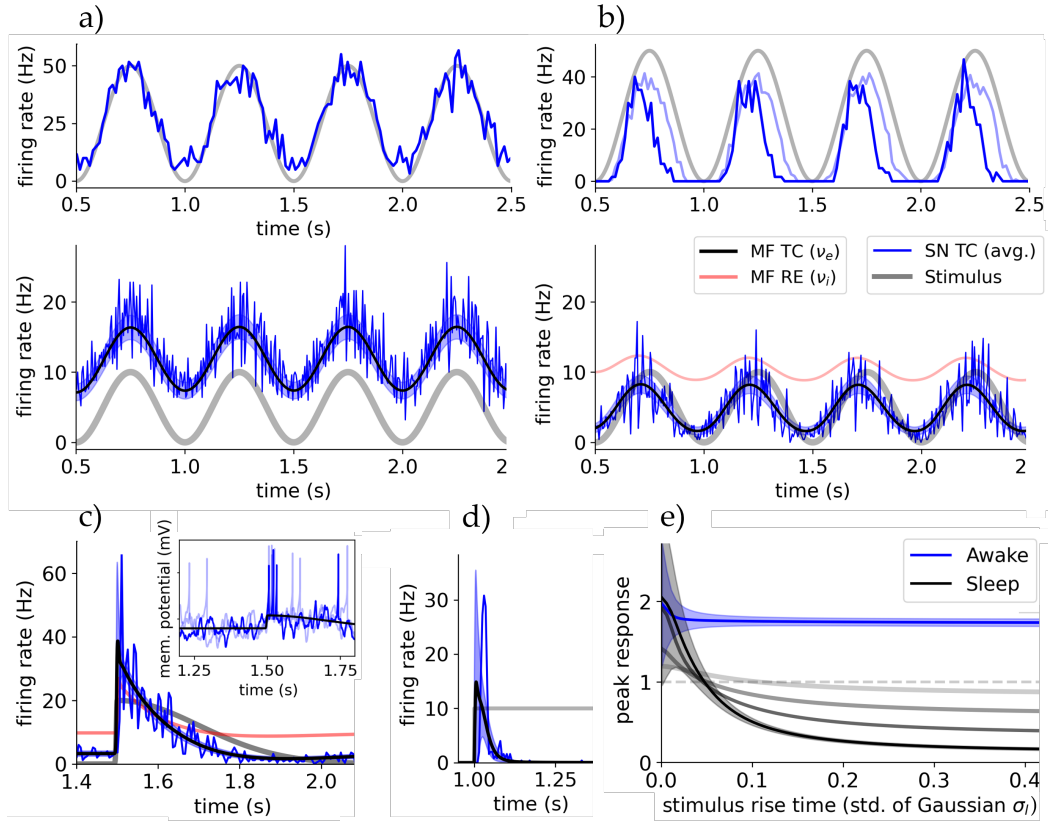


Figure 4.6: Bursting of TC cells renders thalamic response nonlinear in sleep state. (a) Top row: Single cell and population response to a strong oscillatory sensory drive S in awake state. Bottom row: Activities of spiking network (TC population, blue) and mean-field (TC population, black line with color-shaded std., RE population, red line). The grading stimulus is pictured in light grey. The single cell recording of the top rows is taken from this network simulation. RE activity is of same frequency and phase as TC activity but with amplitude $\sim 50\text{Hz}$ (not shown). (b) The same setup as in (a) but in sleep state (TC bursting, see main text). The single cell recording is done in the network of (a) which was in awake state to be close to the experiment. (Dark blue is sleep state and light blue is sleep state with lower adaptation $b=20\text{pA}$.) The single cell traces in (a) and (b) reproduce the experiments of Sherman and Guillory [61, ch. 6]. (c) Thalamic response of spiking network and mean-field to a fast changing stimulus (split-Gaussian with steep left-hand std. σ_l). Inset shows trace of 3 random TC cells of the spiking simulation, showing bursting at the onset of the stimulus ($t_0 = 1.5\text{s}$; mV per s). (d) Rectangular stimulus in absence of cortical drive showing that TC activity vanishes after initial burst. (e) The maximum amplitude of response (peak), relative to the incoming stimulus amplitude, as a function of the ‘slope’ of stimulus (left std. σ_l of split-Gaussian; amplitude 10Hz and right std. 0.2s). Depicted is the response for awake and sleep state and in sleep state for different applied cortical constant drives (from black to gray: {1, 2, 4, 10}Hz). (Figure adapted from [51])

namely autocovariance c (blue shaded areas in plot) and autocorrelation C next to a smaller increase in mean firing rate ν .

In conclusion, both single-cell and population-level response of TC cells appears linear in awake state (ACh present) with enhanced stimulus amplitude, while in sleep state (ACh absent) response is linear but of reduced amplitude for slowly changing stimuli, and nonlinear for quickly changing stimuli. In addition, and as evident from Figure 4.6c,

both spiking network and mean-field model capture the bursting of TC cells, resulting in a “bursting” population response. This enhances stimulus detection in low attention states for significant sensory inputs and the transmission of mostly time-dependent information such as oscillations in sleep state.

4.2.2 Cortical and sensory input

We will now examine how thalamic responsiveness depends on background cortical activity and how the two different biological inputs to the thalamus (sensory and cortical) modulate its behavior.

Referring back to [Figure 4.6d](#), we observe a modulating role of cortical input, which in the sleep state can render the typically nonlinear TC response (due to bursting) linear by removing the dependence on stimulus change at high cortical drives (gray lines in plot). This suggests that the cortex could potentially generate a time window where external information is temporarily transferred faithfully during usually non-attentive states. This observation is consistent with previous findings on cortical modulation of thalamic responsiveness but attributes a simple and direct *wake-up-call* function to the cortex.

Moving on, we are interested in the differences between the two drives. In [Figure 4.7a](#), the (stationary) firing rate response of the TC cell population in the mean-field model for different constant inputs in awake state is displayed, with both cortical and sensory drives. We applied a small constant cortical input $P = 1\text{Hz}$ to be in a low activity AI state comparable to *in-vivo* ([Figure 4.4d](#)). In case of sensory stimuli, the response is strongly proportional to the input, and we identify that the slope of this response is influenced by the cortical drive P .

In [Figure 4.7b](#) we see this dependency is inversely proportional, where we conducted simulations for varying cortical drive amplitudes and observed that the gain (slope of the linear response curve) decreases as P increases. In the sleep state, the response remains relatively constant, slightly decreasing with P , contrasting the awake state’s high gain for all cortical inputs. The cortical drive removes the firing rate-dependency of thalamic response to stimuli in awake like states but does not alter it in sleep state. This is in agreement with studies which assumed the cortical role in the thalamus to be modulating thalamic response similar to noise [5], and with our study on synaptic noise (see next [Section 4.2.3](#)).

For cortical input, the response is nonlinear but exhibits multiple linear regions, as seen in [Figure 4.4c](#). The threshold at around 25Hz serves as a turning point (the end of the *inhibited* regime, at which the RE population firing rate saturates). Inputs below this threshold do not provoke a strong sustained response, while inputs above do. The RE population’s strong response to changes in the *inhibited* regime nearly nullifies TC and therefore thalamic response.

These behaviors are evident in the TC population’s response to a rectangular pulse stimulus from either P or S in [Figure 4.7c](#). Notably, low cortical inputs can even be repressive, with only larger amplitudes triggering robust and sustained responses, particularly in the awake state (in agreement with studies such like Crandall, Cruikshank, and Connors [15]). In sleep state for both inputs or with low cortical inputs in awake state, responses are highly nonlinear, emphasizing the transfer of gradients rather than absolute values. The initial activity spikes at the onset of the input are created by the delay it takes the RE population to react to both stimulus and TC excitation to inhibit

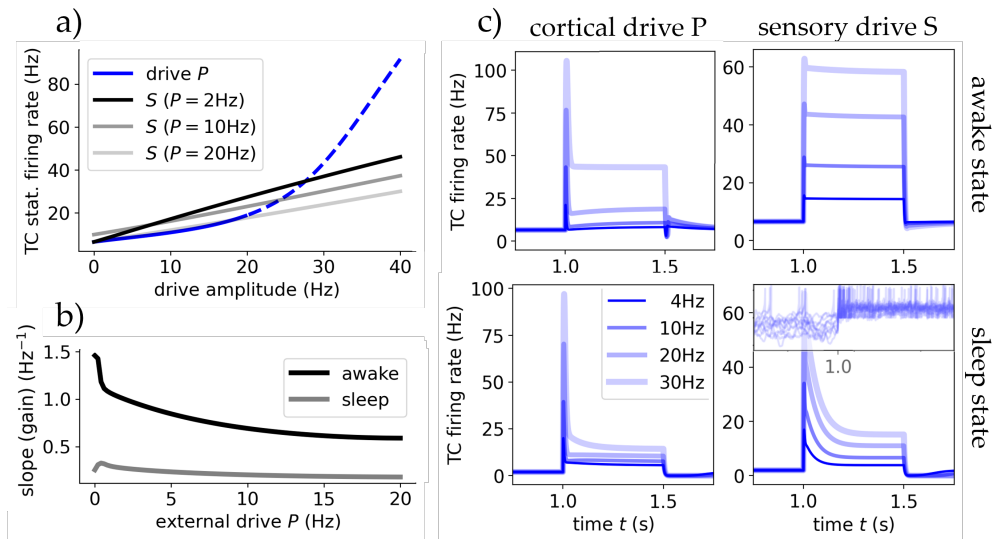


Figure 4.7: The thalamus responsiveness depends on external input origin. (a) The steady state output firing rate of the TC population after reaching equilibrium for different drives P and S. Blue is for inputs coming from cortical drive P, where solid marks the *inhibited regime* and dashed the *blow-up regime*. Black are for sensory drive S, with varying degrees of cortical input. TC cells respond linearly for sensory stimuli, whereas cortical stimuli are nonlinear only showing a strong proportionality after $\sim 20\text{Hz}$. (b) Cortical drive removes thalamic response dependency on stimulus frequency. The gradients of the sensory input response curves (black in (a)) as a function of cortical input P for awake and sleep state. (c) The TC populations response to a rectangular stimulus of varying amplitude coming from either drive in both states. In the bottom-right there are also depicted 10 randomly chosen single cell traces to connect the population spike with single cell burst-like behaviour. (Figure adapted from [51])

TC activity and –to a lesser extent– by the delayed adaptation mechanisms of both RE and TC populations. This is magnified in sleep state by stronger adaptation effects and resulting single cell bursting (see last Section 4.2.1). This mechanism allows the thalamus to respond to cortical input and modulation despite its strong inhibiting effect via the TRN.

Concluding, only in awake state and for sensory input, or with cortical control for sensory input at sleep state, thalamic responsiveness is linear while only temporal information is transferred for cortical input and sensory input at sleep states without cortical control.

4.2.3 Synaptic noise

Building on our previous analysis of thalamic responsiveness, we now turn our attention to the role of synaptic noise. We have analyzed how the responsiveness of thalamic cells depends on different firing modes and input sources. However, it has been shown that the level of synaptic noise (background activity) can significantly alter these responses. In this section, we analyze the role of noise, manifesting as background synaptic and subthreshold membrane potential fluctuations, and how it influences response properties and firing modes. We begin by replicating single-cell findings from Wolfart et al. [84]. They observed that synaptic noise controls TC neuron response and behavior, and notably,

that such noise removes the dependency of TC cell responses on both membrane voltage and input frequency.

We recreated this computationally at single cell level. Figure 4.8a shows the response of single TC cells in awake state to a Poissonian spike train of 5Hz with varying excitatory synaptic strength (Q_e), reflecting the experimental setup. We observe the same step-like function in the static case without external synaptic noise: going from no activity to single spike response to double spike response or bursts at high conductances (regions separated by dashed lines). With noise the response function becomes smoother and the partition of the aforementioned regimes becomes blurred. The time-dependent noise was implemented as an Ornstein-Uhlenbeck (OU) process entering the cells membrane potential as a synaptic current (see Section A.2).

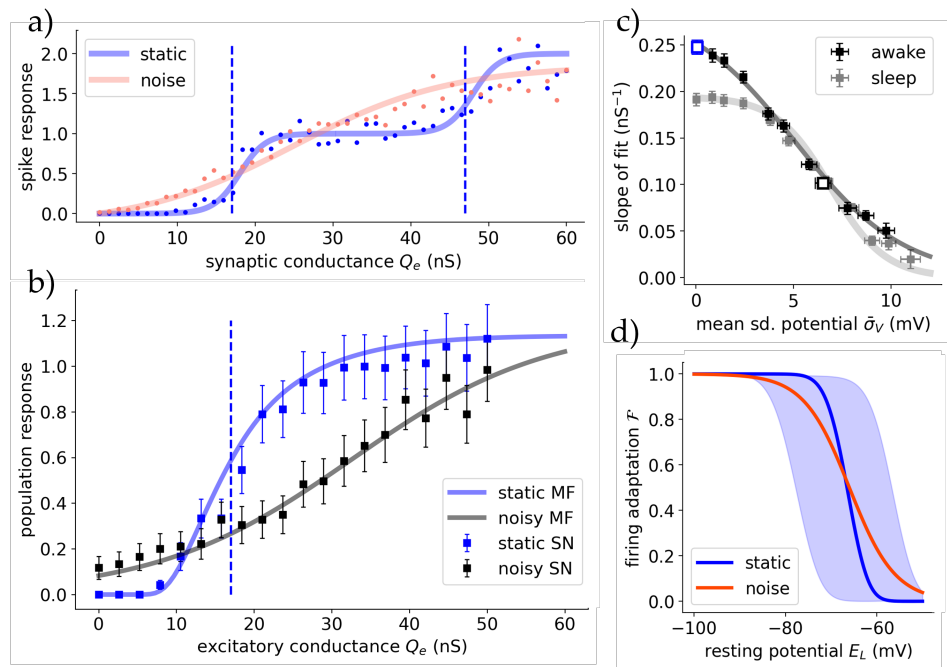


Figure 4.8: Synaptic noise modulates the dependence of thalamic responsiveness on voltage.

(a) Response to a 5Hz Poissonian spike train for different values of excitatory synaptic strength Q_e for simulated spiking single cells in awake state. The noise was injected as an OU-like current in the membrane potential via I_{syn} . The dots represent each the spikes per receiving incoming spike, averaged over 100 runs for 10s each. The lines correspond to sigmoidial fits, where the blue dashed lines mark the shift fit parameter depicting the center of the slope. Reproducing Fig. 4a of [84]. (b) The same setup but with the full thalamic spiking network (squares) and the mean field (lines), showing the relative response to a 10Hz Poissonian spike train. The dotted line marks the slope center of the single cell simulations going from no spikes to a one-to-one spike response. For the mean-field the synaptic noise was added as an additional time-dependent conductance into the formalism (see main text). (c) The (maximum) slopes of the mean-field response curves (b) plotted against the standard deviation of the membrane potential predicted by the mean-field. Showing a proportionality between fluctuations and the slope of the response function. At high noise levels the difference between awake and sleep state vanishes. The two cases from (b) are drawn as empty blue/black boxes. (d) Synaptic noise reduces the dependency of TC firing adaptation (sim. burstiness) on cell state (polarisation). Shaded area is the standard deviation induced by small conductance noise (5nS), and orange the average. Reproducing Fig. 5b of [84]. (Figure adapted from [51])

To translate this behaviour to the population level we did simulations of the full spiking network of the employed thalamic substructure. A constant Poissonian input of 15Hz was inserted into all cells, coming from just one source; comparable to dynamical patch clamps at single cell level. The stationary firing rate output of the TC population was measured for different synaptic strengths Q_e . The resulting response function is depicted in [Figure 4.8b](#) for the static and noisy case for both spiking network and mean-field.

For the mean-field, the noise-dependent shape of the response function is passively included in the definition of the transfer function ([3.37](#)), with its slope being controlled by the standard deviation of the subthreshold membrane potential (σ_V). However, to recreate the experiment, which employed a time-dependent external noise, we extended the formalism by adding two additional static synaptic conductances $\tilde{\mu}_{G(e,i)}$. Those are modelled as OU-type functions averaged for each time bin T . The conductance noise was implemented in the mean-field via adding the mean of OU-type noise (x) in a time window corresponding to T to the static conductances μ_G (see methods). The resulting conductances including noise are then:

$$\tilde{\mu}_{G(e,i)}(t) = \mu_{G(e,i)}(t) + [x(t)_{(e,i)}]_T \quad (4.2)$$

The specific parameters for x used for the synaptic noisy case in simulations are $\mu = 0\text{nS}$, $\theta = 5\text{ms}^{-1}$, and especially $\sigma_i = 200\text{nS}$ and $\sigma_e = 60\text{nS}$ for the amplitudes.

Both spiking network and mean-field show that the TC populations response function has its maximum slope at the same place as the first step at single cell level from no activity to single spike response (the first dashed line in [Figure 4.8a](#) and the dashed line in [Figure 4.8b](#), respectively). Furthermore, the effect of synaptic noise is the same for population response as in the single-cell experiment, decreasing the response functions maximum slope.

How the maximum slope of the response function depends on this noise is depicted in [Figure 4.8c](#). Here instead of the injected noise the noise-dependent membrane potential subthreshold fluctuations averaged over all runs ($\bar{\sigma}_V$) is shown. In sleep state the population response slope is $\sim 20\%$ less steep for the static case or small noise. Strong synaptic noise and subsequent membrane potential fluctuations decrease the slope as expected. Additionally, synaptic noise diffuses the response differences of awake and sleep state at intermediate noise levels and removes nearly all dependence of thalamic response on conductance at high noise levels ($\bar{\sigma}_V > 10\text{mV}$), where the response function is nearly constant (at a value dependent on the ratio of excitatory and inhibitory noise $\tilde{\mu}_{Ge}/\tilde{\mu}_{Gi}$).

Additionally, the effect of synaptic noise on the firing adaptation \mathcal{F} of TC cells was tested in [Figure 4.8d](#). Noise diffuses the state transition between no firing adaptation and strong firing adaptation for different levels of membrane potential polarization. As in [Section 4.2.1](#) we can refer to the similarity of \mathcal{F} to *burstiness*, and hypothesize that strong noise allows for firing adaptation and also bursting for membrane potential levels showing no bursting without noise, this would be in agreement with experimental studies ([[84](#)] Fig. 5b therein).

Previously, we showed that synaptic noise modifies thalamic response dependency on voltage and conductance. There, input frequency was fixed. Further following [[84](#)], we proceed to investigate how noise changes the thalamus' response in respect to input frequency.

For this, single TC cells were simulated for extended duration with incoming Poissonian spike trains of 10Hz, modelling a generic input from retinal ganglion cells in-vivo. Here the *retinal* input conductances were fixed. During simulation, for each output spike

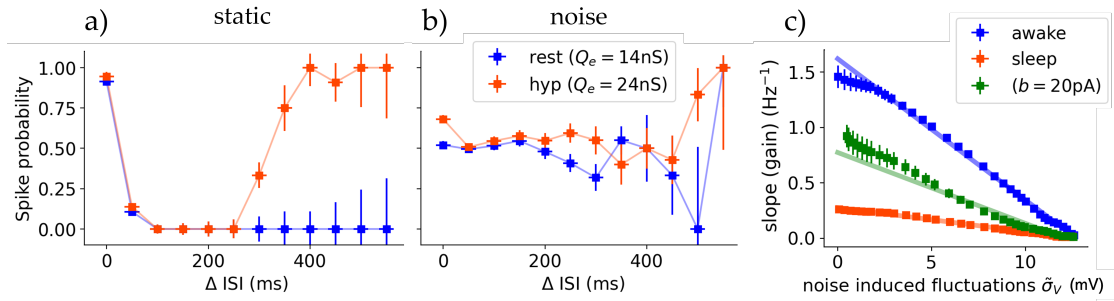


Figure 4.9: Synaptic noise removes the dependence of thalamic response on frequency. (a) A single TC cell's spike response probability dependent on the interspike interval (Δ ISI) between input spikes. The input is a Poissonian spike train with a mean frequency of 10Hz, comparable to an in-vivo retinal input. This recreates computationally the experiment of Figure 4 in [84]. For both resting ($E_L = -65\text{ mV}$) and hyperpolarized ($E_L = -70\text{ mV}$) state the spike response is nearly 100% at low ISI's and therefore only reacting to *summed* input spikes. In hyperpolarized state, with T-channel adjusted synaptic conductance, the TC cell responds to also high ISI's with a nearly one-to-one probability. See legend in (b). (b) Same setup as in (a) but with additional synaptic noise (see main text). Frequency-dependent response is greatly removed. (c) The mean-fields thalamic response gradient (gain) to gated sensory stimuli of 10Hz as a function of synaptic noise via noise induced membrane potential fluctuations. For the awake state and the sleep state with $b \in \{20, 200\}\text{ pA}$. Regardless of state, noise linearly leads to a reduced thalamic response dependency on stimulus frequency. The shaded lines are linear fits. (Figure adapted from [51])

of the recorded TC cell, the interspike interval (Δ ISI) of the retinal input between the spike which results in the spike response and the preceding one is measured. This way the spike probability or response can be measured as a function of input frequency. Because of the increasingly more rare occurrence of large ISI's ($\Delta > 400\text{ ms}$) in a Poissonian spike train of 10Hz, the following plots are cut off at 550ms. Until then reasonable long simulation times provide distinguishable uncertainties. Figure 4.9a shows the results for a TC cell without additional synaptic noise. At resting potential (awake state, $E_L = -65\text{ mV}$ with $Q_e = 14\text{ ns}$) spike response only occurred at summed input spikes with $\Delta < 50\text{ ms}$ with an all-or-none character. At hyperpolarized potential (awake state, $E_L = -70\text{ mV}$ with $Q_e = 24\text{ ns}$) not only input spike summation evoked a response but also ISI's with duration longer than 300ms. These even show higher spike probability compared to spike summation at low ISI's. The difference in input conductances Q_e was necessary to account for equal number of spikes between both states, where the high conductance in the hyperpolarized state captures the effects of T-channels. In the presence of synaptic noise this changes drastically and both TC cells at resting and at hyperpolarized levels exhibit the same spike response, completely independent of input frequency (see Figure 4.9b). Remarkably, with noise spike probability is significantly lower even with spike summation ($\text{ISI} \rightarrow 0\text{ ms}$), independent of polarization. These results exactly reproduce the experimental results of [84].

Moving to population level, we present thalamic stimulus response as a function dependent on synaptic noise. Noise acts in a similar way on the frequency dependent response as cortical input (see Section 4.2.2). In the same manner, in Figure 4.9c the slope of the linear response of the TC population as a function of input amplitude is depicted (gain). As with modulating cortical input (refer Figure 4.7), noise decreases response. However, different to the control of cortical input, where the gain saturates at 0.7 Hz^{-1} ,

noise linearly reduces gain until a complete banishment of frequency dependence at very high noise levels ($\tilde{\sigma}_V > 12\text{mV}$). This holds true for all states. In the awake state the loss of gain per membrane fluctuation is $(-0.12 \pm 0.01)\text{gain/mV}$. For the sleep state the loss is $(-0.028 \pm 0.003)\text{gain/mV}$. Finally, we see that the noise required to equalize the dependence on frequency between awake and sleep state is significantly higher than for equalizing the dependence on voltage (induced subthreshold fluctuations of 12mV and 4mV, respectively).

4.3 SPINDLES

Spindle oscillations are one of the main activity dynamics of the thalamus during slow-wave sleep or anesthesia [69], strongly influencing the responsiveness of the thalamus in such states (see Section 2.3.4). These originate from the superposition of multiple cellular and circuit properties. In ACh depleted conditions such as during sleep, T-channel currents promote bursts after hyperpolarization (as modeled in [19] for a Hodgkin-Huxley model), and barrages of IPSPs occur in strongly connected subgroups within the TRN [65]. This creates two self-sustained loops: an inhibitory self-loop within TRN neurons, and a loop connecting RE and TC cells (see colored connections in Figure 4.10c). The rebound bursts caused by this circuit arrangement generate spindle oscillations, as shown by experiments and computational models [21, 69].

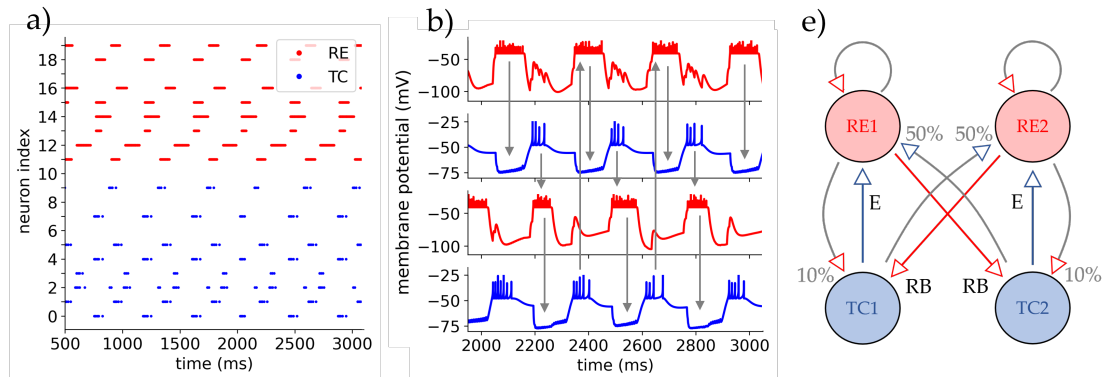


Figure 4.10: Spindle oscillations are generated by TC-RE connections and missing excitatory-excitatory links in the thalamus. (a) Raster plot of a simulation for the small network showing all 20 neurons. (b) Four neurons showing anti-phase burst firing with rebound bursts of the TC cells as a possible generator of spindles. Cell traces are taken from the simulation in (a) with a small network ($N = 20$). The arrows show the loop of activity propagation between RE and TC cells with rebound bursts and direct excitation. These pathways translate to the four colored connections in (e). (e) The 4-structure used for the mean-field connections. The colored arrows mark the main pathway of propagation with rebound bursts (RB) and direct excitation (E) as transmitters. The non-significant connections are marked in grey with their respective relative strength shown in percentages of the original connection probability. The RE populations keep their local self-loop. (Figure adapted from [51])

Computational models demonstrated that a 4-neuron structure of TC and RE neurons exhibits self-sustained oscillations with all characteristics of spindles, as shown first for Hodgkin-Huxley type models [22] and later using AdEx models [18]. These oscillations rely on a loop where a TC cell triggers a burst in an RE cell which, in turn, causes

a rebound burst in another TC cell, completing the cycle. In their study however the oscillations waned with increased network size.

In this study, we show that the proposed models in a sleep-like state indeed show spindles at all scales, validating them as thalamic models. In contrast to Destexhe [18], we aim for robust spindles at population scales. To enhance rebound bursting we promote burst firing by adjusting the reset membrane potential (V_r) below the sodium spike threshold onset: $V_r = -48\text{mV}$ for TC and $V_r = -42\text{mV}$ for RE cell. This yields sustained burst firing without sustained activation, mimicking T-channel like activation and IPSP barrages in RE cells. Accordingly we re-calibrate the mean-field fit to accommodate the change in V_r . (The original fit produces spindles too, but with unrealistic amplitudes.) The resulting fit parameters are depicted in [Table 4.3](#).

Table 4.3: The fitting parameters for the **spindle-adapted mean-field** of $V_{\text{thr}}^{\text{eff}}$ and their values. All values in mV.

CELL	P_0	P_μ	P_σ	P_τ	$P_{\mu\mu}$	$P_{\mu\sigma}$	$P_{\mu\tau}$	$P_{\sigma\sigma}$	$P_{\sigma\tau}$	$P_{\tau\tau}$
TC	-51.17	3.94	15.53	-7.15	0.35	-7.57	-1.19	-13.61	9.47	29.44
RE	-45.84	3.53	-16.90	41.75	0.34	2.02	-5.23	19.44	49.70	-93.53

In [Figure 4.10a](#) we illustrate oscillatory dynamics in a small network of 20 neurons, revealing a generating 4-loop structure inside the network (b). We employed the burst-adjusted sleep parameters but with synaptic parameters from [18]. To invoke activity, an initial kick of Poissonian input of high frequency to only a random subset of neurons was applied.

Moving to the network size of $N=1000$ neurons used in this study, we employ our full parameter set ([Table 4.1](#)) and the same initial kick. We show in [Figure 4.11a](#) that the full spiking network shows self sustained oscillations.

For the mean-field to produce self-sustained oscillations we employ the 4-structure as seen at single cell level (from [18]) and justify its need also at the population level. This is further supported by studies such as [47]. They showed the mechanism behind the generation and specific frequency of oscillations in the thalamus is the delay in the propagation of activity between different TC neurons. Thalamic relay cell clusters have no connection to themselves and so RE neurons serve as intermitter. The slow adaptation mechanics governing rebound bursts are therefore generating the slow $\sim 10\text{Hz}$ spindle oscillations.

In order to implement this, we construct two RE and two TC populations and keep all connections active, but reduce the connection probability of links which are antagonistic to this propagation via rebound bursts. This can be seen as two close but locally separated subgroups of relay neurons. The resulting structure is depicted in [Figure 4.10c](#). (Note: If the connections are set homogeneous then this network is acting exactly like a mean-field with just two populations.) The main links for the propagation are colored and labeled with their mechanism of propagation: RE induced rebound bursts and TC excitation. To initiate the spindles here also a kick of high activity going to only one or two populations was necessary, in agreement with the spiking network. Additionally, T was set to 15ms to have similar phases and shapes with the spiking network. The averaged spiking network and resulting mean-field activities of the populations are depicted in [Figure 4.11b](#). In [Figure 4.11c](#) the Fourier spectrum of spiking network and mean-field is compared, and we can see the transient into the stable limit cycle in phase space.

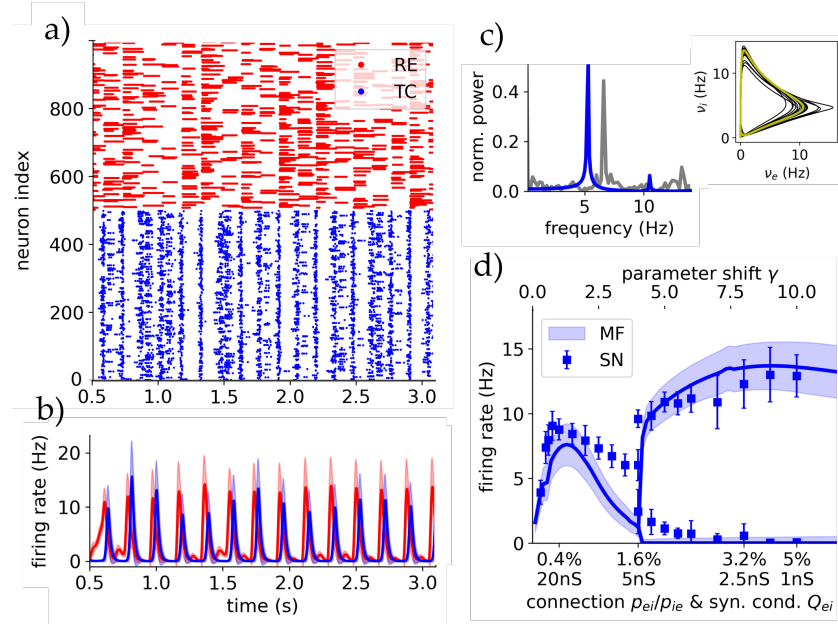


Figure 4.11: Spindle oscillations in a sleep-like state generate a highly unresponsive thalamic state. (a) Raster plot of the full-scale spiking network with 1000 neurons for spindle parameters (ACh/sleep state with rebound burst). (b) Mean-field oscillations: Firing rates and standard deviations of both TC and RE populations. (d) Fourier spectrum for spiking network (grey) and mean field (blue) of the TC population activity. Inset right: Phase plane in the TC and RE firing rate space. Yellow is the stable limit cycle and black the transient. (d) Bifurcation diagram showing the suggested Andronov-Hopf bifurcation that occurs when gradually increasing the connection probability in the network, for spiking network and mean-field. This corresponds to a parameter shift from the parameters used in [18] with $\gamma=1$ to the parameters used in this paper with $\gamma=10$. (Figure adapted from [51])

In contrast to these oscillations occurring at larger ($N = 1000$) scales, in [18] small networks generated spindles in SR-like dynamics while at scales of $N > 40$ neurons population activity produced self-driven steady states with AI dynamics. In Figure 4.11d we show a bifurcation diagram transitioning between connection and balancing synaptic parameters from [18] ($\gamma=1$) to our parameter values (Table 4.1, $\gamma=10$). Showing that sufficient connections are necessary for spindles at larger scales. The Jacobian eigenvalues calculated at the steady points of the mean-field up to the bifurcation point are complex. This together with the transition into a stable limit cycle suggests a supercritical Andronov-Hopf bifurcation as the origin of spindles.

This self-sustained oscillation is remarkably robust in regards to perturbations of all kinds of inputs, with even oscillatory inputs producing the same frequency spindles. This renders the thalamus' responsiveness in this spindle-adjusted sleep state relatively independent of external input. Only prolonged and constant inputs of a duration longer than multiple spindle periods destroy the synchronisation and create steady state AI dynamics, with the spindles however starting again after the input stops. Furthermore, the bifurcation diagram in connection with [18], shows that thalamic function and responsiveness can be drastically altered depending on specific order parameters, such as here with network and synaptic parameters.

This structural explanation of thalamic oscillations suggests that while individual neurons remain in a fluctuation-driven, AI state in large networks, the oscillations

emerge at the population level. This population-level emergence of oscillations, despite individual neuronal variability, is also supported by experimental evidence (see e.g. [12]).

5 | DISCUSSION

DISCLAIMER: The following discussion is adapted from [51].

In this study, we introduced a biologically realistic mean-field model of the thalamus, capturing the population dynamics of thalamocortical relay (TC) neurons and thalamic reticular (RE) neurons in two physiological states: the *awake* state, characterized by high levels of acetylcholine (ACh) neuromodulation typical of wakefulness and REM sleep, and the *sleep* state, marked by low levels of ACh neuromodulation characteristic of NREM sleep (based on [46, 48]). This model enabled us to investigate the state-dependent responsiveness of the thalamus across micro to meso scales. By doing so, we have enhanced our understanding of thalamic function, particularly in relation to the complex interplay between single-cell properties and emergent network dynamics.

Our mean-field model employs the master-equation formalism introduced by El Boustani and Destexhe [25] and incorporates slow adaptation mechanisms [23]. We constructed it using a bottom-up approach following the formalism described by Zerlaut et al. [88], which includes a subthreshold-dependent transfer function [44]. The thalamic network structure we built is faithful to experimental observations, demonstrating that both the mean-field and spiking network exhibit the desired balanced excitation-inhibition state with asynchronous irregular (AI) dynamics and a realistic dominant RE activity.

After building the model (in Section 4.1), in Section 4.1.3, we successfully confirmed the mean-field's predictive accuracy through comparison with the spiking network, verifying its ability to replicate the dynamic behavior and population distribution of thalamic cells. Notably, we demonstrated that the mean-field model can predict the network's subthreshold activity, enabling modeling experiments using intracellularly injected currents. Additionally, we proved its validity beyond the fitting point, necessitating only one fit for a wide range of parameters and allowing for investigating phase transitions between different brain states with the same model.

We then applied this validated model to investigate thalamic responsiveness and its dependence on internal and external states. Our investigation focused on three key aspects of thalamic function:

First, in Section 4.2.1, we analyzed the critical role of bursting in TC cells, extending the single-cell findings of Sherman and Guillery [61] to the population level. Bursting in TC cells arises due to the activation of low-threshold T-type calcium channels following hyperpolarization, resulting in a rapid sequence of action potentials. We demonstrated that in the sleep state, thalamic response is generally reduced, except for significant (rapidly changing) stimuli. In these cases, the timing of stimuli is primarily transmitted via a strong and fast thalamic response, generated by TC cell bursting and delayed inhibition of RE cells. This finding aligns with the hypothesis that bursting serves to generate alerting signals during low-attention states [61] and supports the role of the thalamus in generating and distributing oscillations during NREM sleep [69]. Importantly, our results validate that the mean-field model successfully captures the crucial nonlinear thalamic feature of bursting. This transition between tonic and bursting firing patterns in TC cells provides a mechanism for state-dependent modulation of sensory information

transmission to the cortex, potentially explaining the thalamus's role in attention and arousal regulation.

Second, in [Section 4.2.2](#), we examined the influence of external inputs on thalamic response. Our model demonstrates, in agreement with experimental findings [15], an important distinction in the processing of inputs based on their origin: sensory-like stimuli experience a more linear response and are therefore transferred more faithfully than cortical-like inputs, which generate a nonlinear response due to the activation of the inhibitory TRN. In the sleep-like state, however, the relay of information becomes strongly nonlinear regardless of input origin. Additionally, we identified two key modulatory effects of cortical input: (1) In the awake state, cortical inputs activate the TRN, which inhibits TC neurons and represses thalamic responsiveness. This mechanism may serve to filter out irrelevant sensory information during focused attention. (2) In the sleep state, cortical inputs can depolarize TC neurons, shifting them from bursting to tonic firing modes, thus promoting a linear response to sensory stimuli. This effect could allow the cortex to rapidly increase thalamic responsiveness, enabling faithful transfer of sensory input following significant stimuli that trigger arousal. These findings align with the *predictive coding theory* [55]. They suggest that the thalamic response to sensory stimuli reflects a combination of feedforward stimulus inputs with predictions or memories mediated by the cortex. This interaction between bottom-up sensory information and top-down cortical modulation may be crucial for adaptive sensory processing across different brain states.

Third, in [Section 4.2.3](#), we investigated the role of synaptic noise in thalamic response. For the first time, we successfully modeled the experimental findings of Wolfart et al. [84], demonstrating that synaptic noise acts as a controller for responsiveness at the population level. We showed that the TC cells' step-like response function for single spikes translates effectively to their collective response at the population scale, sharing the same conductance threshold. This property allows the thalamus to fine-tune its responsiveness to external stimuli at both cellular and population levels. Additionally, we found that noise diffuses transitions between states of tonic and bursting firing at the single-cell level and between awake and sleep states at the population level. Importantly, we demonstrated that noise diminishes the thalamic response dependency on both voltage and frequency in an equivalent manner for both single-cell and population levels. We highlight the interesting similarity between synaptic noise and cortical input in their control of stimulus transfer and their ability to render stimulus response less dependent on stimulus frequency—a similarity often presumed but not explicitly demonstrated [5]. These insights underscore the critical importance of integrating conductance-based subthreshold fluctuation dynamics into meso- to macro-scale modeling approaches. Our findings suggest that such integration is essential for accurately capturing the nuanced and state-dependent information processing capabilities of the thalamus in large-scale brain models.

Finally, in [Section 4.3](#), we demonstrated the successful reproduction of spindle-like oscillations in a sleep-like state, providing crucial validation for our thalamic model's ability to capture complex, state-dependent dynamics. We emphasize the necessity of specific substructures within the thalamus, such as reciprocal connections between TC and RE neurons, for generating realistic oscillations at all scales while individual neurons remain in the asynchronous irregular (AI) regime, consistent with experimental observations [12]. This finding highlights the model's capacity to bridge single-neuron and population-level behaviors. In this spindle-oscillation state, thalamic responsiveness to inputs is highly suppressed, with only strong and prolonged cortical inputs temporarily

creating AI dynamics during their activation. This selective responsiveness may play a role in sleep-dependent memory consolidation and sensory gating. Importantly, our results demonstrate that connection probability and synaptic conductance can have a profound impact on population dynamics, introducing new phase transitions and population-level behaviors. This sensitivity to network parameters provides a potential mechanism for the flexible modulation of thalamic function across different brain states and cognitive demands.

6

CONCLUSION AND OUTLOOK

In conclusion, this study underscores the value of integrating single-cell dynamics with thalamic-specific structures at the population level to understand the complex role of thalamic responsiveness. By advancing our comprehension of thalamic function and its influence on perception, attention, and cognition, we bridge the gap between cellular and synaptic properties and overall brain dynamics, particularly in sensory processing. This work has important implications for connecting computational neuroscience with the study of neural disorders and the development of neural implants and prosthetics.

More specifically, by offering this biologically realistic and experimentally grounded mean-field model of the thalamus, which integrates thalamic dynamics with cortical feedback, we provide an essential starting point for future research in a wide field of applications:

(1) Neuromodulation: Further investigation into the neuromodulatory role of acetylcholine (ACh) in TC and RE neurons and its impact on thalamic responsiveness and spindle generation is warranted. As we showed in this study, the connection between physiological states and ACh is persistent at both the single-cell and population levels. However, we did not explore this in detail, focusing mainly on reproducing experiments and demonstrating their population coding effect. Future work could involve larger parameter scans (building on [Figure 4.5](#)) to define parameter regions especially useful for modeling. Another direct step would be to fit the transfer function to real neural activity data of TC and RE neurons, for example, via dynamic clamp recordings.

(2) Cortical input: A deeper analysis of the effects of cortical input on thalamic function is essential, possibly exploring the concept of cortical input as a form of structured noise [\[5\]](#) and its implications for thalamic information processing. A thalamo-cortical expansion (see point 4) to simulate cortical input would be particularly interesting, allowing us to study the bidirectional interactions between the cortex and thalamus in a more detailed manner.

(3) While we demonstrated the generation of spindles in this model, the next step is to investigate how spindles affect thalamic responsiveness and influence sensory modulation. Connected to this is the analysis of transitions between the investigated physiological states and how these transitions interact with the generation of oscillations. Since we required another fit for the spindle-sleep state, this would involve either obtaining an awake-state fit that can capture the sustained barrages of RE neurons or extending the AdEx model to include the dynamics of T-type calcium channels. This extension would also involve modifications to the mean-field formalism, but with the realistic assumption of slow channel effects, it could be treated similarly to slow adaptation effects ([Section 3.3.5](#)). Additionally, exploring the role of specific network motifs in spindle generation and propagation presents a promising avenue. Finally, it would be interesting to determine if the proposed model can capture slower delta waves and to understand how cell states differ between delta and spindle oscillations, connecting directly to achieving a more complete picture of different sleep phase transitions [\[41\]](#).

(4) Model Expansions: Several potential expansions of our model could significantly enhance our understanding of brain-wide dynamics: 4.1) Parallel Thalamic Mean-Field

Models: Developing parallel thalamic mean-field models to capture the diversity of thalamic nuclei and their functions. An initial step was already taken in the spindle case (Section 4.3). This would allow us to model different thalamic regions with specific properties and roles in sensory processing and cognition.

4.2) Integration into a Full Thalamo-Cortical Loop: Integrating our thalamic model into a full thalamo-cortical loop is particularly interesting and readily implementable, as the thalamic mean-field model developed in this study is directly integrable with previously developed cortical models [23]. This integration will enable the investigation of cortical control in a more realistic dynamical setting and directly relate thalamic responsiveness to its effect on cortical responses to stimuli. Additionally, since spindle and delta waves are primarily recorded via the cortex, a thalamo-cortical model of whole-brain oscillations is more realistic. This could also help answer the longstanding question of whether these oscillations require thalamo-cortical feedback or are purely generated and distributed by the thalamus. An extension to a retino-thalamo-cortical model to study visual processing pathways would be especially interesting for retinal prosthetics and applications in computer vision in connection with image detection models.

4.3) Inclusion in Large-Scale Brain Models: Finally, including our thalamic model in large-scale brain models represents the final scale extension, which should be readily achievable. Of particular importance is *The Virtual Brain* [59], which connects mean-field models via real connectomics data. Until now, only cortical mean-field models have been included [32]. During this study, several other brain regions have been modeled using the same mean-field framework, namely the basal ganglia, hippocampus, and striatum [74, 75]. All these regions require the thalamus to connect them to each other, the cortex, and sensory input. Combining these models with connectome-based connections promises the possibility of investigating whole-brain dynamics with realistic structure and connections to single-cell parameters and effects such as neuromodulators. This will bridge the gap between molecular and cellular neuroscience and cognitive neuroscience, as well as imaging techniques such as EEG and MEG.

By pursuing these future directions, we can continue to deepen our understanding of thalamic function and its crucial role in sensory processing, cognitive states, and overall brain dynamics. This work will not only advance our knowledge of the thalamus but also contribute to the development of more sophisticated neural models and potentially inform new neuroprosthetic and neuropharmaceutical approaches.

A | APPENDIX

A.1 A NEUROSCIENCE PRIMER

Neuroscience is the study of the nervous system, encompassing the brain, spinal cord, and peripheral nerves. At the heart of neuroscience lies the neuron, the fundamental processing and memory unit of the nervous system. For a comprehensive introduction, see [41, ch: 1–2].

Neurons

Neurons are specialized cells that transmit information through electrical and chemical signals. They consist of three main parts: The **cell body** (or SOMA) the nucleus and other organelles essential for cellular function. It integrates incoming signals and generates outgoing signals to the axon. **Dendrites** are branch-like extensions that receive synaptic inputs from other neurons and transmit these signals toward the cell body. **Axons** are long, slender projection that conducts electrical impulses, known as *action potentials*, away from the cell body toward other neurons, muscles, or glands. Neurons are interconnected via *synapses*, specialized junctions that facilitate communication between neurons. These connections form complex neural networks that underlie all neural functions. Simplifying, the neuron can be modeled electrically as an RC circuit, where the lipid bilayer of the cell membrane acts as a capacitor, and ion channels provide conductance pathways, maintaining the membrane potential out of equilibrium.

Membrane Potential

The membrane potential V_m is the electrical potential difference across the neuron's plasma membrane, arising from the distribution of ions on either side of the membrane. At rest, neurons typically maintain a resting membrane potential of approximately -70mV , with the inside of the cell being negative relative to the outside.

The **Nernst equation** describes the equilibrium potential E_{ion} for a particular ion species across the membrane:

$$E_{\text{ion}} = \frac{RT}{zF} \ln \left(\frac{[\text{ion}]_{\text{outside}}}{[\text{ion}]_{\text{inside}}} \right),$$

where R is the universal gas constant, T is the absolute temperature in Kelvin, z is the valence of the ion, F is Faraday's constant, $[\text{ion}]_{\text{outside}}$ and $[\text{ion}]_{\text{inside}}$ are the extracellular and intracellular ion concentrations, respectively.

Action potentials

An *action potential* is a rapid, transient change in the membrane potential of a neuron. It serves as the basic unit of communication within the nervous system. The action potential

is generated by the opening and closing of voltage-gated ion channels in the neuron's membrane and involves several key phases: **Resting State:** The neuron maintains a resting membrane potential around -70mV due to the uneven distribution of ions across the membrane. **Depolarization:** When a stimulus depolarizes the membrane to a threshold (typically around -55mV), voltage-gated sodium (Na^+) channels open, allowing Na^+ ions to flow into the neuron, further depolarizing the membrane. **Repolarization:** At the peak of the action potential (around $+30\text{mV}$), voltage-gated sodium channels inactivate, and voltage-gated potassium (K^+) channels open, allowing K^+ ions to flow out of the neuron, repolarizing the membrane. **Hyperpolarization:** The membrane potential briefly becomes more negative than the resting potential due to the continued efflux of K^+ ions before the potassium channels close. **Return to Resting Potential:** The membrane potential returns to the resting level through the action of leak channels and the sodium-potassium pump (Na^+/K^+ ATPase), which restores the ionic gradients.

The Hodgkin-Huxley model provides a quantitative description of the ionic currents underlying the action potential, it and its successors are described in [Section 3.2](#).

Ion Channels

Ion channels are integral membrane proteins that allow ions to pass through the cell membrane, thereby influencing the neuron's electrical properties. Different types of ion channels play crucial roles in generating and regulating action potentials: **Voltage-Gated Ion Channels:** Open or close in response to changes in membrane potential. They are critical in the initiation and propagation of action potentials. Examples include voltage-gated sodium, potassium, calcium, and chloride channels. **Ligand-Gated Ion Channels:** Open or close in response to the binding of specific neurotransmitters or ligands. They mediate synaptic transmission by converting chemical signals into electrical signals. **Mechanically-Gated Ion Channels:** Open or close in response to mechanical stimuli, such as pressure or stretching. They are important in sensory systems like touch and hearing.

The flow of ions through these channels generates ionic currents that can be described by Ohm's law for ion channels: $I_{\text{ion}} = g_{\text{ion}}(V_m - E_{\text{ion}})$, where I_{ion} is the ionic current, g_{ion} is the conductance of the ion channel, V_m is the membrane potential, and E_{ion} is the equilibrium potential for that ion.

Synapses

A *synapse* is a specialized junction that allows communication between neurons in the nervous system. Synapses can be classified into two main types: chemical synapses and electrical synapses.

At **Chemical Synapses**, action potentials arriving at the presynaptic axon terminal trigger the release of neurotransmitter molecules into the synaptic cleft, a tiny gap between the presynaptic and postsynaptic neurons. This process involves:

1. **Neurotransmitter Release:** Depolarization opens voltage-gated calcium (Ca^{2+}) channels, allowing Ca^{2+} influx, which triggers synaptic vesicle fusion with the presynaptic membrane and neurotransmitter release.
2. **Neurotransmitter Binding:** Neurotransmitters diffuse across the synaptic cleft and bind to receptors on the postsynaptic neuron.

3. **Postsynaptic Potential:** Binding of neurotransmitters induces ion channel opening, leading to excitatory or inhibitory postsynaptic potentials (EPSPs or IPSPs), altering the postsynaptic membrane potential.
4. **Termination:** Neurotransmitter action is terminated by reuptake, enzymatic degradation, or diffusion away from the synapse.

The synaptic current can be modeled as: $I_{\text{syn}} = g_{\text{syn}}(V_m - E_{\text{syn}})$, where g_{syn} is the synaptic conductance, and E_{syn} is the synaptic reversal potential, which depends on the type of neurotransmitter (e.g., glutamate, GABA).

Synaptic strength can change over time through mechanisms of synaptic plasticity, such as long-term potentiation (LTP) and long-term depression (LTD), which are thought to underlie learning and memory. The changes in synaptic strength can be modeled by adjusting g_{syn} over time based on activity-dependent rules.

Electrical Synapses (Gap Junctions) involve direct electrical coupling between neurons through gap junctions, allowing ions and small molecules to pass directly from one cell to another. They enable rapid and bidirectional signal transmission but are less common than chemical synapses.

Neuromodulators

Neuromodulators are signaling molecules that modulate the activity of neurons and neural circuits, influencing various brain functions, including mood, cognition, arousal, and behavior. They act by binding to specific receptors on the neuron's membrane, often leading to changes in membrane potential or altering the sensitivity of ion channels and synaptic transmission.

Neuromodulators differ from neurotransmitters in that they often have broader, longer-lasting effects and can act over larger areas of the brain. Examples include:

Acetylcholine (ACh): Involved in attention, learning, and memory. It can modulate neuronal excitability and synaptic plasticity. **Dopamine:** Plays roles in reward, motivation, and motor control. **Serotonin:** Involved in mood regulation, appetite, and sleep. **Norepinephrine (Noradrenaline):** Associated with arousal, alertness, and stress responses.

Neuromodulation can be mathematically modeled by introducing modulation terms in the equations governing neuronal excitability, such as adjusting the maximal conductances or kinetics of ion channels.

A.2 MATHEMATICAL APPENDIX

Conventions and notation

EINSTEIN SUMMATION CONVENTION We adopt Einstein's summation convention, where repeated indices in a term imply summation over all possible values of those indices. For example:

$$y_\mu = \partial^\lambda \partial_\lambda x_\mu = \sum_\lambda \partial^\lambda \partial_\lambda x_\mu.$$

If the indices run over a and b (i.e., $\lambda \in a, b$), this expands to:

$$y_\mu = \partial^a \partial_a x_\mu + \partial^b \partial_b x_\mu.$$

SETS Sets are denoted using curly braces. For example, ξ represents a set containing elements ζ .

HEAVISIDE STEP FUNCTION The Heaviside step function, denoted by $\theta(x)$ or $\mathcal{H}(x)$, is defined as:

$$\theta(x) = \begin{cases} 1, & \text{if } x \geq 0 \\ 0, & \text{if } x < 0. \end{cases}$$

It can also be represented in terms of the Dirac delta function $\delta(x)$:

$$\theta(x) = \int_{-\infty}^x \delta(t), dt.$$

PARTIAL DERIVATIVES Partial derivatives with respect to a variable x^μ are denoted as:

$$\partial_\mu \equiv \frac{\partial}{\partial x^\mu}.$$

Similarly, higher-order partial derivatives follow this notation:

$$\partial_{\mu\nu} \equiv \frac{\partial^2}{\partial x^\mu \partial x^\nu}.$$

KRONECKER DELTA The Kronecker delta $\delta_{\mu\nu}$ is a function of two variables μ and ν , defined as:

$$\delta_{\mu\nu} = \begin{cases} 1, & \text{if } \mu = \nu \\ 0, & \text{if } \mu \neq \nu. \end{cases}$$

DIRAC DELTA FUNCTION The Dirac delta function $\delta(x)$ is a generalized function (or distribution) defined by its sifting property:

$$\int_{-\infty}^{\infty} \delta(x - x_0) f(x), dx = f(x_0),$$

for any smooth function $f(x)$. It is characterized by:

$$\delta(x) = 0 \quad \text{for } x \neq 0, \quad \text{and} \quad \int_{-\infty}^{\infty} \delta(x), dx = 1.$$

FLOOR FUNCTION When dealing with exponents that are inherently non-integer terms, it is understood that the floor function $\lfloor x \rfloor$ is used to take the greatest integer less than or equal to x .

DETERMINANT The determinant of a square matrix A is denoted as $\det(A)$ or $|A|$.

FOURIER TRANSFORM The Fourier transform of a function $f(t)$ is defined using the following convention:

$$F(q) = \int_{-\infty}^{\infty} f(t), e^{-2\pi i q t}, dt.$$

The inverse Fourier transform is then given by:

$$f(t) = \int_{-\infty}^{\infty} F(q), e^{2\pi i q t}, dq.$$

PROBABILITY AND STATISTICS

- $p(\xi)$ denotes the probability density function (PDF) of a continuous random variable ξ , or the probability mass function (PMF) if ξ is discrete.
- $P(\xi)$ represents the cumulative distribution function (CDF) of ξ , giving the probability that the variable takes a value less than or equal to ξ .
- The expected value (mean) of ξ is denoted by $\langle \xi \rangle$ or $\mathbb{E}[\xi]$.

Key statistical quantities are defined as follows:

Quantity	Definition
Mean	$\langle \xi \rangle = \begin{cases} \sum_{\xi} p(\xi) \xi, & \text{(discrete)} \\ \int_{-\infty}^{\infty} \xi p(\xi) d\xi, & \text{(continuous)} \end{cases}$
Variance	$\sigma^2 = \langle (\xi - \langle \xi \rangle)^2 \rangle = \langle \xi^2 \rangle - \langle \xi \rangle^2$
Covariance	$\text{cov}(\xi, \eta) = \langle (\xi - \langle \xi \rangle)(\eta - \langle \eta \rangle) \rangle = \langle \xi \eta \rangle - \langle \xi \rangle \langle \eta \rangle$
Correlation Coefficient	$\rho_{\xi \eta} = \frac{\text{cov}(\xi, \eta)}{\sigma_{\xi} \sigma_{\eta}}$

VECTOR AND MATRIX NOTATION

- Vectors are denoted by bold lowercase letters (e.g., \mathbf{v}), with components v_i .
- Matrices are denoted by uppercase letters (e.g., A), with elements A_{ij} .
- The transpose of a matrix A is denoted by A^T .
- The identity matrix is denoted by I .

INNER PRODUCT AND NORMS

- The inner product of two vectors \mathbf{u} and \mathbf{v} in \mathbb{R}^n is given by $\mathbf{u} \cdot \mathbf{v} = \sum_{i=1}^n u_i v_i$.
- The Euclidean norm of a vector \mathbf{v} is $|\mathbf{v}| = \sqrt{\mathbf{v} \cdot \mathbf{v}}$.

DIFFERENTIAL OPERATORS

- The gradient operator is denoted by ∇ .
- The Laplacian operator is $\nabla^2 = \nabla \cdot \nabla$.

OTHER NOTATIONS

- The set of real numbers is denoted by \mathbb{R} .
- The set of integers is denoted by \mathbb{Z} .
- The natural logarithm is denoted by $\ln(x)$.
- Exponential functions are denoted by $\exp(x)$.
- The imaginary unit is denoted by i , where $i = \sqrt{-1}$.

Markov Process

A Markov process is a stochastic process characterized by the Markov property, which states that the future state of the system depends only on its present state and not on its past history. This memoryless property is mathematically expressed as:

$$P[\xi(t+1) | \xi(t), \xi(t-1), \dots, \xi(0)] = P[\xi(t+1) | \xi(t)],$$

where $P[\xi(t+1) | \xi(t), \xi(t-1), \dots, \xi(0)]$ is the conditional probability of the system being in state $\xi(t+1)$ at time $t+1$ given all previous states, and it equals $P[\xi(t+1) | \xi(t)]$, the probability conditioned only on the current state.

Closure Problem

The statistical closure problem arises in the context of hierarchical equations for statistical moments, where the equation for a moment of order n , denoted $\langle \xi^n \rangle$, depends on higher-order moments such as $\langle \xi^{n+1} \rangle$. This creates an open-ended hierarchy that cannot be solved without additional assumptions or approximations. The problem was first encountered in the study of turbulent flows, where the mean velocity field depends on the Reynolds stress, involving correlations between velocity fluctuations.

Various approaches have been developed to address the closure problem, including the *quasi-normal approximation*, mean-field theories, and renormalized perturbation techniques similar to those used in quantum field theory. The quasi-normal approximation assumes that higher-order moments can be expressed in terms of lower-order moments by assuming the random variables follow a Gaussian distribution. Specifically, it allows even-order moments $\langle \xi^{2n} \rangle$ to be expressed in terms of products of second-order moments due to the properties of Gaussian distributions:

$$\langle \xi^{2n} \rangle = (2n - 1)!! (\langle \xi^2 \rangle)^n,$$

where $(2n - 1)!!$ is the double factorial.

However, because Gaussian distributions are fully characterized by their first two moments (mean and variance), this approach works well for even-order moments but does not directly address odd-order moments. As a result, additional methods or approximations are needed to close the hierarchy at odd orders, often leading researchers to limit their analysis to moments up to $n = 2$.

Erdős-Rényi network

The Erdős-Rényi (ER) model is a fundamental model in network theory used to describe random graphs. It consists of two closely related variants: The $G(N, M)$ model: In this model, all graphs with exactly N nodes and M edges are equally likely. It represents a random network where the total number of edges is fixed. And the $G(N, p)$ model: This variant constructs a graph by connecting each pair of N nodes independently with probability p . In this model, the number of edges is a random variable following a binomial distribution. In the $G(N, p)$ model, the probability of generating a specific graph with exactly m edges is given by:

$$P(\text{Graph with } m \text{ edges}) = p^m (1-p)^{\binom{N}{2}-m}.$$

This formula arises because each of the $\binom{N}{2}$ possible edges can either be present (with probability p) or absent (with probability $1-p$), independently of all other edges.

Stirling's Formula

Stirling's formula is an approximation used to estimate the factorial of a large number n . It is particularly useful in probability and statistics for simplifying expressions involving factorials. The formula is given by:

$$n! \approx n^n e^{-n} \sqrt{2\pi n}. \quad (\text{A.1})$$

In logarithmic form, which is often more convenient for calculations, Stirling's approximation is:

$$\ln n! \approx n \ln n - n + \frac{1}{2} \ln(2\pi n). \quad (\text{A.2})$$

Stirling's formula provides an accurate approximation for large n , and the relative error decreases as n increases.

Error function

The error function $\text{erf}(z)$ and the complementary error function $\text{erfc}(z)$ are important functions in probability, statistics, and partial differential equations. They are defined as:

$$\text{erf}(z) = \frac{2}{\sqrt{\pi}} \int_0^z e^{-t^2} dt, \quad \text{erfc}(z) = 1 - \text{erf}(z) = \frac{2}{\sqrt{\pi}} \int_z^\infty e^{-t^2} dt. \quad (\text{A.3})$$

The error function maps real numbers to values in $(-1, 1)$, i.e., $\text{erf} : \mathbb{R} \rightarrow (-1, 1)$.

For a normally distributed random variable ξ with mean $\mu = 0$ and standard deviation σ , the probability that ξ falls within the interval $[-z, z]$ is given by:

$$P(\xi \in [-z, z]) = \text{erf}\left(\frac{z}{\sigma\sqrt{2}}\right). \quad (\text{A.4})$$

In the case of a standard normal distribution ($\sigma = 1$), this simplifies to:

$$P(\xi \in [-z, z]) = \text{erf}\left(\frac{z}{\sqrt{2}}\right). \quad (\text{A.5})$$

Gaussian stimulus

The double Gaussian stimulus used as an input is defined as

$$G(t, t_0) = A[\theta(t_0 - t)e^{\frac{-(t-t_0)^2}{2\sigma_l^2}} + \theta(t - t_0)e^{\frac{-(t-t_0)^2}{2\sigma_r^2}}], \quad (\text{A.6})$$

with t_0 the peak of the stimulus and with amplitude A and slopes $\sigma_{l,r}$ of the left and right half-side Gaussian, respectively. This formulation allows the stimulus to have asymmetric rise and decay times, which can model more realistic input signals in neural systems where the onset and offset dynamics differ.

Ornstein-Uhlenbeck noise

The Ornstein-Uhlenbeck (OU) process is a type of stochastic process used to model systems with a tendency to revert to a mean value over time. It is a continuous-time analog of the discrete-time AR(1) process and is often used to represent colored noise with temporal correlations in neuroscience and other fields. The OU process is defined by the stochastic differential equation (SDE):

$$\frac{dx}{dt} = \theta(\mu - x) + \sigma \frac{dW}{dt}, \quad (\text{A.7})$$

where μ is the mean reversion level, θ the mean reversion rate, and σ the amplitude of the standard Wiener process $W(t)$, or white noise.

In computational neuroscience, the OU process is used to model synaptic input currents or membrane potential fluctuations that have temporal correlations, providing a more realistic representation of neuronal input compared to uncorrelated white noise.

A.3 AUXILIARY CALCULATIONS

Statistical moments

$$\begin{aligned} \partial_t \langle m_\mu \rangle &= \partial_t \prod_\alpha \int_0^{1/T} dm_\alpha m_\mu P_t(\{m_\gamma\}) \\ &= \partial_t \prod_\alpha \int_0^{1/T} dm_\alpha m_\mu \partial_t P_t(\{m_\gamma\}) \\ &= \partial_t \prod_\alpha \int_0^{1/T} dm_\alpha \prod_\beta \int_0^{1/T} dm'_\beta [m_\mu P_t(\{m_\gamma\}) W(\{m_\gamma\} | \{m'_\gamma\}) \\ &\quad - m_\mu P_t(\{m'_\gamma\}) W(\{m'_\gamma\} | \{m_\gamma\})] \\ &= \partial_t \prod_\alpha \int_0^{1/T} dm_\alpha \prod_\beta \int_0^{1/T} dm'_\beta (m'_\mu - m_\mu) P_t(\{m_\gamma\}) W(\{m'_\gamma\} | \{m_\gamma\}) \\ &= \partial_t \prod_\alpha \int_0^{1/T} dm_\alpha a_\mu(\{m_\gamma\}) P_t(\{m_\gamma\}) \\ &= \langle a_\mu(\{m_\gamma\}) \rangle \end{aligned}$$

$$\bar{a}_\mu(\{\langle m_\gamma \rangle, \langle \omega_\gamma \rangle\}) = \prod_\beta \int_0^{1/T} \int_{\Omega} dm'_\beta d\omega'_\beta (m'_\mu - \langle m_\mu \rangle) W(\{m'_\gamma, \omega'_\gamma\} | \{m_\gamma, \omega_\gamma\}) \quad (\text{A.8})$$

$$\bar{a}_{\mu\nu}(\{\langle m_\gamma \rangle, \langle \omega_\gamma \rangle\}) = \prod_\beta \int_0^{1/T} \int_{\Omega} dm'_\beta d\omega'_\beta (m'_\mu - \langle m_\mu \rangle)(m'_\nu - \langle m_\nu \rangle) W(\{m'_\gamma, \omega'_\gamma\} | \{m_\gamma, \omega_\gamma\}) \quad (\text{A.9})$$

Non-dimensionalization of the AdEx

$$\begin{aligned} \bar{v}(\bar{t}) &\equiv \frac{v(t) - V_t}{\Delta} \\ \bar{\omega}(\bar{t}) &\equiv \frac{\omega(t) + a(E_L - V_t)}{g_L \Delta} \\ \bar{\tau}_\omega &\equiv \frac{\tau_\omega}{\tau_m} \\ \bar{a} &\equiv \frac{a}{g_L} \\ \bar{I} &\equiv \frac{I}{g_L \Delta} + (1 + \frac{a}{g_L}) \frac{E_L - V_t}{\Delta} \\ \bar{t} &\equiv \frac{t}{\tau_m} \\ \bar{b} &\equiv \frac{b}{g_L \Delta} \\ \bar{V}_r &\equiv \frac{V_r - V_t}{\Delta} \end{aligned}$$

SUPPLEMENTARY FIGURES

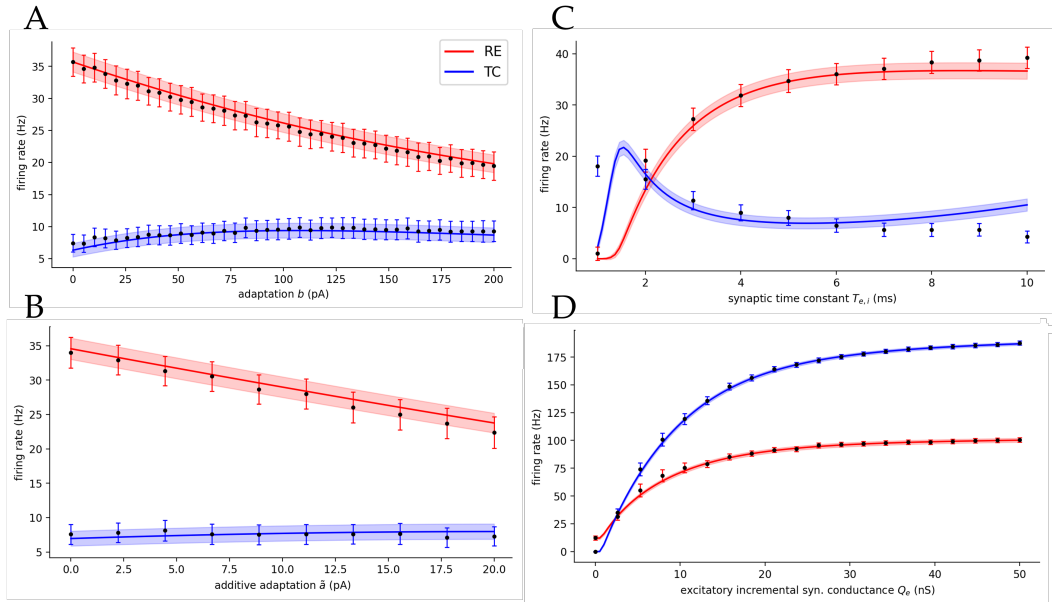


Figure A.1: Global parameter analysis for mean-field and spiking network. Black markers represent equilibrium population firing rates of the spiking network. Colored line and shaded area represent the mean-fields mean and standard deviation, respectively. (a) Spiking adaptation parameter. (b) Membrane potential adaptation parameter as shift of the original parameters to keep the difference between TC and RE adaptations, securing stable dynamics. (a) and (b) ensure the mean-fields fit validity between awake and sleep state. (c) Synaptic exponential delay time constant of both populations. (d) Excitatory incremental synaptic conductance for TC only. This allows modeling dynamic clamp-like techniques and changing or *injecting* conductances without necessitating a new fit. (Figure taken from [51])

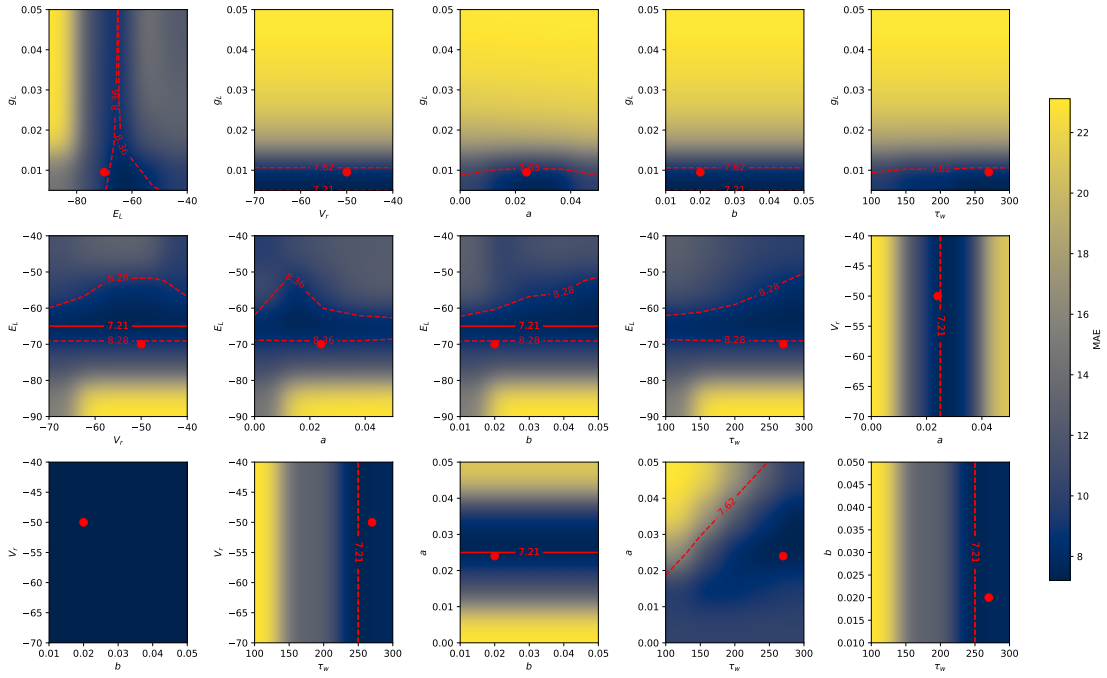


Figure A.2: Parameter space fit for TC without ACh. The mean absolute error (MAE) between the AdEx (3.4) and the TC cell traces in absence of ACh from [46]. Red lines mark minimum MAE (solid lines) and 5% deviation from said minimum (dashed lines). The employed parameter values are marked as the red dot. (see units in Figure A.4, Figure taken from [51])

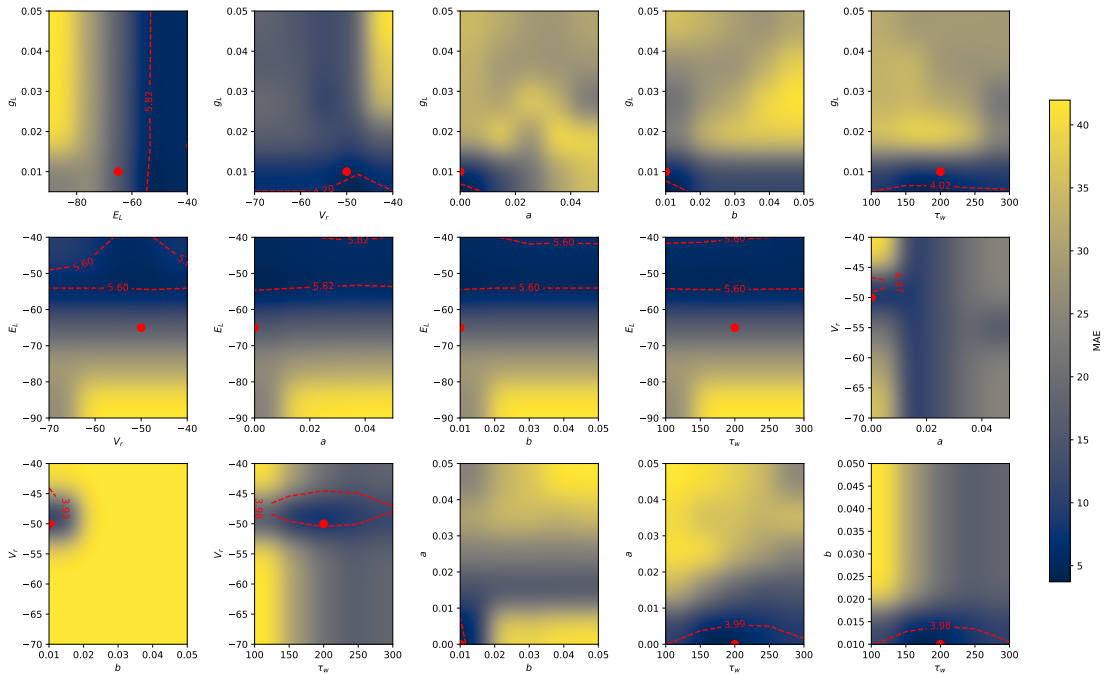


Figure A.3: Parameter space fit for TC with ACh. (see caption in Figure A.2 and units in Figure A.4, Figure taken from [51])

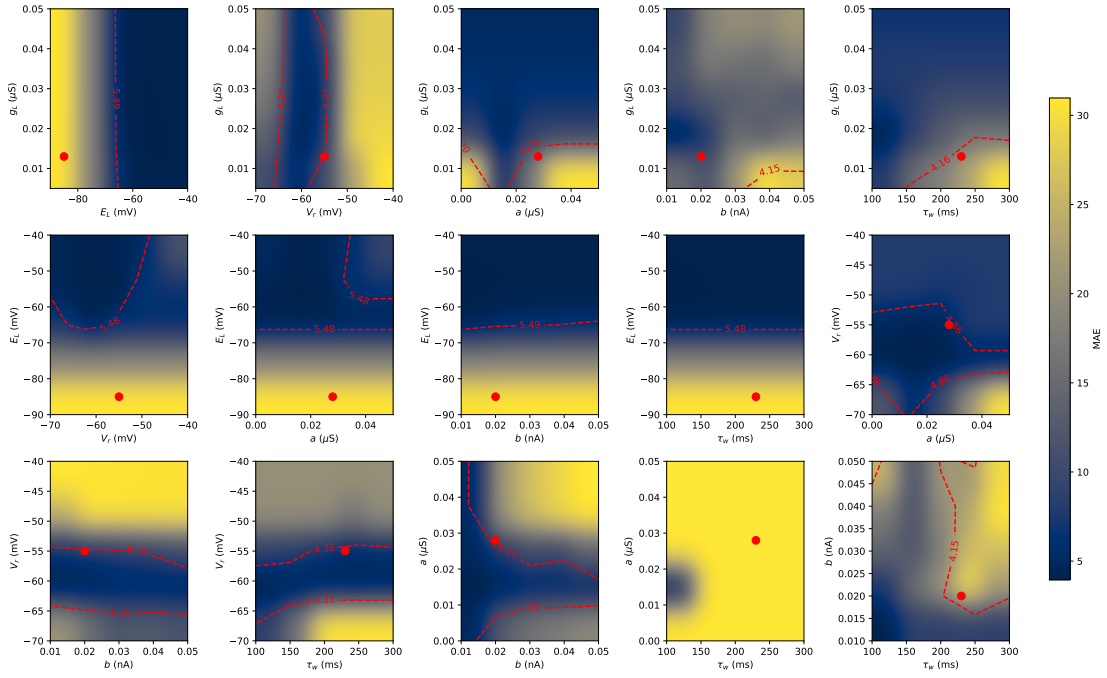


Figure A.4: Parameter space fit for RE without ACh. (see caption in Figure A.2) The chosen value of E_L marks the biggest MAE. Here we still chose to take a hyperpolarised value to account for the reduced excitability in RE neurons with ACh absent [46] and to inhibit also the population response to keep the stability of the network (see main text). (Figure taken from [51])

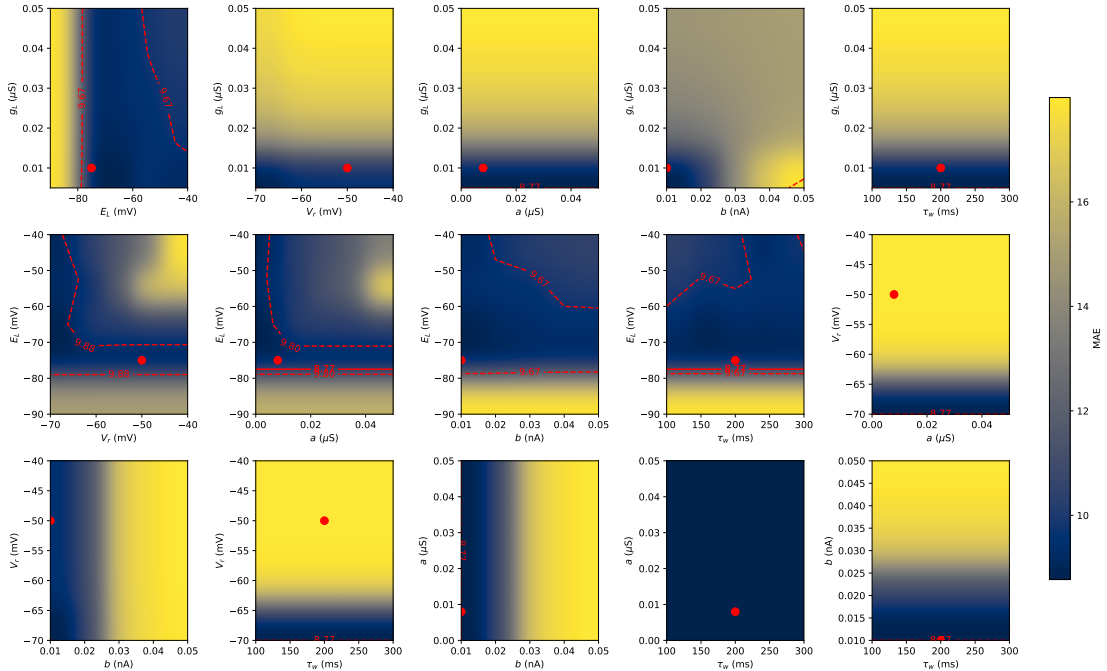


Figure A.5: Parameter space fit for RE with ACh. (see caption in Figure A.2, Figure from [51])

BIBLIOGRAPHY

- [1] Daniel J. Amit and Nicolas J.-B. Brunel. "Model of global spontaneous activity and local structured activity during delay periods in the cerebral cortex." In: *Cerebral cortex* 7 3 (1997), pp. 237–52.
- [2] Daniel J. Amit, Hanoch Gutfreund, and H. Sompolinsky. "Spin-glass models of neural networks". In: *Phys. Rev. A* 32 (2 Aug. 1985), pp. 1007–1018. doi: [10.1103/PhysRevA.32.1007](https://doi.org/10.1103/PhysRevA.32.1007). URL: <https://link.aps.org/doi/10.1103/PhysRevA.32.1007>.
- [3] Amos Arieli et al. "Dynamics of Ongoing Activity: Explanation of the Large Variability in Evoked Cortical Responses". In: *Science* 273.5283 (1996), pp. 1868–1871. doi: [10.1126/science.273.5283.1868](https://doi.org/10.1126/science.273.5283.1868). URL: <https://www.science.org/doi/abs/10.1126/science.273.5283.1868>.
- [4] Danielle S. Bassett, Perry Zurn, and Joshua I. Gold. "On the nature and use of models in network neuroscience". In: *Nature Reviews Neuroscience* 19 (2018), pp. 566–578. url: <https://api.semanticscholar.org/CorpusID:205569660>.
- [5] Sébastien Béhuret et al. "Cortically-Controlled Population Stochastic Facilitation as a Plausible Substrate for Guiding Sensory Transfer across the Thalamic Gateway". In: *PLoS computational biology* 9 (Dec. 2013), e1003401. doi: [10.1371/journal.pcbi.1003401](https://doi.org/10.1371/journal.pcbi.1003401).
- [6] Timothy Bellay et al. "Irregular spiking of pyramidal neurons organizes as scale-invariant neuronal avalanches in the awake state". In: *eLife* 4 (July 2015). Ed. by Frances K Skinner, e07224. ISSN: 2050-084X. doi: [10.7554/eLife.07224](https://doi.org/10.7554/eLife.07224). URL: <https://doi.org/10.7554/eLife.07224>.
- [7] Michael Breakspear. "Dynamic models of large-scale brain activity". In: *Nature Neuroscience* 20 (2017), pp. 340–352. URL: <https://api.semanticscholar.org/CorpusID:20538785>.
- [8] R. Brette. "Philosophy of the Spike: Rate-Based vs. Spike-Based Theories of the Brain." In: *Front Syst Neurosci.* 9.10 (Nov. 2015). doi: [10.3389/fnsys.2015.00151](https://doi.org/10.3389/fnsys.2015.00151).
- [9] Romain Brette and Wulfram Gerstner. "Adaptive Exponential Integrate-and-Fire Model As An Effective Description Of Neuronal Activity". In: *Journal of neurophysiology* 94 (Dec. 2005), pp. 3637–42. doi: [10.1152/jn.00686.2005](https://doi.org/10.1152/jn.00686.2005).
- [10] RE Brown et al. "Control of sleep and wakefulness." In: *Physiol Rev.* 92.3 (2012), pp. 1087–187. doi: [10.1152/physrev.00032.2011](https://doi.org/10.1152/physrev.00032.2011).
- [11] Nicolas Brunel. "Dynamics of Sparsely Connected Networks of Excitatory and Inhibitory Spiking Neurons". In: *Journal of Computational Neuroscience* 8 (Jan. 2000). doi: [10.1023/A:1008925309027](https://doi.org/10.1023/A:1008925309027).
- [12] Nicolas Brunel and Vincent Hakim. "Sparsely synchronized neuronal oscillations". In: *Chaos: An Interdisciplinary Journal of Nonlinear Science* 18.1 (Mar. 2008), p. 015113. ISSN: 1054-1500. doi: [10.1063/1.2779858](https://doi.org/10.1063/1.2779858). URL: <https://doi.org/10.1063/1.2779858>.

- [13] Manuel A. Castro-Alamancos and Barry W. Connors. "Cellular Mechanisms of the Augmenting Response: Short-Term Plasticity in a Thalamocortical Pathway". In: *Journal of Neuroscience* 16.23 (1996), pp. 7742–7756. ISSN: 0270-6474. DOI: [10.1523/JNEUROSCI.16-23-07742.1996](https://doi.org/10.1523/JNEUROSCI.16-23-07742.1996). URL: <https://www.jneurosci.org/content/16/23/7742>.
- [14] Stephen Coombes. "Coombes, S.: Waves, bumps, and patterns in neural field theories. Biol. Cybern. 93(2), 91–108". In: *Biological cybernetics* 93 (Sept. 2005), pp. 91–108. DOI: [10.1007/s00422-005-0574-y](https://doi.org/10.1007/s00422-005-0574-y).
- [15] Shane R. Crandall, Scott J. Cruikshank, and Barry W. Connors. "A Corticothalamic Switch: Controlling the Thalamus with Dynamic Synapses". In: *Neuron* 86.3 (2015), pp. 768–782. ISSN: 0896-6273. DOI: <https://doi.org/10.1016/j.neuron.2015.03.040>. URL: <https://www.sciencedirect.com/science/article/pii/S0896627315002640>.
- [16] D. J. Daley and D. Vere-Jones. *An Introduction to the Theory of Point Processes*. 2nd ed. Probability and Its Applications. Springer New York, NY, 2003. ISBN: 978-0-387-95541-4. DOI: [10.1007/b97277](https://doi.org/10.1007/b97277).
- [17] Peter Dayan and L.F. Abbott. *Theoretical Neuroscience: computational and mathematical modeling of neural systems*. Ed. by Terrence J. Sejnowski and Tomaso Poggio. MIT press, 2001. ISBN: 0-262-04199-5.
- [18] Alain Destexhe. "Self-sustained asynchronous irregular states and Up–Down states in thalamic, cortical and thalamocortical networks of nonlinear integrate-and-fire neurons". In: *Journal of computational neuroscience* 27 (July 2009), pp. 493–506. DOI: [10.1007/s10827-009-0164-4](https://doi.org/10.1007/s10827-009-0164-4).
- [19] Alain Destexhe, Diego Contreras, and Terrence Sejnowski. "A Model of Spindle Rhythmicity in the Isolated Thalamic Reticular Nucleus". In: *J Neurophysiol* 72 (Aug. 1994).
- [20] Alain Destexhe, Michael Rudolph, and Denis Paré. "The high-conductance state of neocortical neurons in vivo". In: *Nature Reviews Neuroscience* 4 (2003), pp. 739–751.
- [21] Alain Destexhe and Terrence J. Sejnowski. *Thalamocortical Assemblies*. Oxford University Press, Oxford UK, 2001. ISBN: 0-19-852425-0.
- [22] Alain Destexhe et al. "Ionic mechanisms underlying synchronized oscillations and propagating waves in a model of ferret thalamic slices." In: *Journal of Neurophysiology* 76 (1996), pp. 2049–2070.
- [23] Matteo DiVolo et al. "Biologically Realistic Mean-Field Models of Conductance-Based Networks of Spiking Neurons with Adaptation". In: *Neural Computation* 31.4 (Apr. 2019), pp. 653–680. ISSN: 0899-7667. DOI: [10.1162/neco_a_01173](https://doi.org/10.1162/neco_a_01173). URL: https://doi.org/10.1162/neco%5C_a%5C_01173.
- [24] Guy Doron et al. "Spiking Irregularity and Frequency Modulate the Behavioral Report of Single-Neuron Stimulation". In: *Neuron* 81.3 (2014), pp. 653–663. ISSN: 0896-6273. DOI: <https://doi.org/10.1016/j.neuron.2013.11.032>. URL: <https://www.sciencedirect.com/science/article/pii/S089662731301129X>.
- [25] Sami El Boustani and Alain Destexhe. "A Master Equation Formalism for Macroscopic Modeling of Asynchronous Irregular Activity States". In: *Neural Computation* 21.1 (Jan. 2009), pp. 46–100. ISSN: 0899-7667. DOI: [10.1162/neco.2009.02-08-710](https://doi.org/10.1162/neco.2009.02-08-710). URL: <https://doi.org/10.1162/neco.2009.02-08-710>.

- [26] Laura M. J. Fernandez and Anita Lüthi. "Sleep Spindles: Mechanisms and Functions". In: *Physiological Reviews* 100.2 (2020). PMID: 31804897, pp. 805–868. doi: [10.1152/physrev.00042.2018](https://doi.org/10.1152/physrev.00042.2018). URL: <https://doi.org/10.1152/physrev.00042.2018>.
- [27] Fabio Ferrarelli et al. "Reduced Sleep Spindle Activity in Schizophrenia Patients". In: *The American journal of psychiatry* 164 (Apr. 2007), pp. 483–92. doi: [10.1176/appi.ajp.164.3.483](https://doi.org/10.1176/appi.ajp.164.3.483).
- [28] Paul T Francis et al. "The cholinergic hypothesis of Alzheimer's disease: a review of progress". In: *Journal of Neurology, Neurosurgery & Psychiatry* 66.2 (1999), pp. 137–147. doi: [10.1136/jnnp.66.2.137](https://doi.org/10.1136/jnnp.66.2.137). URL: <https://jnnp.bmjjournals.org/content/66/2/137>.
- [29] Richard Gast, Helmut Schmidt, and Thomas Knösche. "A Mean-Field Description of Bursting Dynamics in Spiking Neural Networks with Short-Term Adaptation". In: *Neural Computation* 32 (July 2020), pp. 1–20. doi: [10.1162/neco_a_01300](https://doi.org/10.1162/neco_a_01300).
- [30] TC Gent et al. "Thalamic dual control of sleep and wakefulness." In: *Nat Neurosci.* 21.7 (2018), pp. 974–984. doi: [10.1038/s41593-018-0164-7](https://doi.org/10.1038/s41593-018-0164-7).
- [31] Iris Ginzburg and Haim Sompolinsky. "Theory of correlations in stochastic neural networks". In: *Phys. Rev. E* 50 (4 Oct. 1994), pp. 3171–3191. doi: [10.1103/PhysRevE.50.3171](https://doi.org/10.1103/PhysRevE.50.3171). URL: <https://link.aps.org/doi/10.1103/PhysRevE.50.3171>.
- [32] Jennifer Goldman et al. "A comprehensive neural simulation of slow-wave sleep and highly responsive wakefulness dynamics". In: *Frontiers in Computational Neuroscience* 16 (Jan. 2023), p. 1058957. doi: [10.3389/fncom.2022.1058957](https://doi.org/10.3389/fncom.2022.1058957).
- [33] Domenico Guarino and Alain Destexhe. "Modeling central neuromodulation". To be published. 2024.
- [34] Domenico Giulio Guarino. "Functional roles of the corticothalamic feedback loop". 2018USPCBo83. PhD thesis. 2018. URL: <http://www.theses.fr/2018USPCB083/document>.
- [35] Anne Marie Himmelheber, Martin Sarter, and John P Bruno. "Increases in cortical acetylcholine release during sustained attention performance in rats". In: *Cognitive Brain Research* 9.3 (2000), pp. 313–325. ISSN: 0926-6410. doi: [https://doi.org/10.1016/S0926-6410\(00\)00012-4](https://doi.org/10.1016/S0926-6410(00)00012-4). URL: <https://www.sciencedirect.com/science/article/pii/S0926641000000124>.
- [36] AL Hodgkin and AF Huxley. "A quantitative description of membrane current and its application to conduction and excitation in nerve". In: *J Physiol.* 4.117 (1952). doi: [10.1113/jphysiol.1952.sp004764](https://doi.org/10.1113/jphysiol.1952.sp004764).
- [37] E.M. Izhikevich. "Which model to use for cortical spiking neurons?" In: *IEEE Transactions on Neural Networks* 15.5 (2004), pp. 1063–1070. doi: [10.1109/TNN.2004.832719](https://doi.org/10.1109/TNN.2004.832719).
- [38] Llinás R. Jahnson H. "Ionic basis for the electro-responsiveness and oscillatory properties of guinea-pig thalamic neurones in vitro." In: *J Physiol.* 349 (1984), pp. 227–247. doi: [10.1113/jphysiol.1984.sp015154](https://doi.org/10.1113/jphysiol.1984.sp015154).
- [39] BE Jones. "From waking to sleeping: neuronal and chemical substrates." In: *Trends Pharmacol. Sci.* 11.26 (2005), pp. 578–86. doi: [10.1016%2Fj.tips.2005.09.009](https://doi.org/10.1016%2Fj.tips.2005.09.009).
- [40] Edward G Jones. "Principles of thalamic organization". In: *The thalamus*. Springer, 1985, pp. 85–149.

- [41] Eric R. Kandel, James H. Schwartz, and Thomas M. Jessell, eds. *Principles of Neural Science*. 3rd ed. New York: Elsevier, 1991.
- [42] Christof Koch. *Biophysics of Computation: Information Processing in Single Neurons*. Oxford University Press, Nov. 1998. ISBN: 9780195104912. DOI: [10.1093/oso/9780195104912.001.0001](https://doi.org/10.1093/oso/9780195104912.001.0001). URL: <https://doi.org/10.1093/oso/9780195104912.001.0001>.
- [43] Alexandre Kuhn, Ad Aertsen, and Stefan Rotter. "Higher-Order Statistics of Input Ensembles and the Response of Simple Model Neurons". In: *Neural computation* 15 (Feb. 2003), pp. 67–101. DOI: [10.1162/089976603321043702](https://doi.org/10.1162/089976603321043702).
- [44] Alexandre Kuhn, Ad Aertsen, and Stefan Rotter. "Neuronal Integration of Synaptic Input in the Fluctuation-Driven Regime". In: *Journal of Neuroscience* 24.10 (2004), pp. 2345–2356. ISSN: 0270-6474. DOI: [10.1523/JNEUROSCI.3349-03.2004](https://doi.org/10.1523/JNEUROSCI.3349-03.2004). URL: <https://www.jneurosci.org/content/24/10/2345>.
- [45] Seung-Chan Lee et al. "Two Functionally Distinct Networks of Gap Junction-Coupled Inhibitory Neurons in the Thalamic Reticular Nucleus". In: *Journal of Neuroscience* 34.39 (2014), pp. 13170–13182. ISSN: 0270-6474. DOI: [10.1523/JNEUROSCI.0562-14.2014](https://doi.org/10.1523/JNEUROSCI.0562-14.2014). URL: <https://www.jneurosci.org/content/34/39/13170>.
- [46] D. McCormick and D Prince. "Acetylcholine induces burst firing in thalamic reticular neurones by activating a potassium conductance". In: *Nature* 319 (1986), pp. 402–405. URL: <https://doi.org/10.1038/319402a0>.
- [47] David A McCormick, Matthew J McGinley, and David B Salkoff. "Brain state dependent activity in the cortex and thalamus". In: *Current Opinion in Neurobiology* 31 (2015). SI: Brain rhythms and dynamic coordination, pp. 133–140. ISSN: 0959-4388. DOI: <https://doi.org/10.1016/j.conb.2014.10.003>. URL: <https://www.sciencedirect.com/science/article/pii/S0959438814002037>.
- [48] David A. McCormick. "Cholinergic and noradrenergic modulation of thalamocortical processing". In: *Trends in Neurosciences* 12.6 (1989), pp. 215–221. ISSN: 0166-2236. DOI: [https://doi.org/10.1016/0166-2236\(89\)90125-2](https://doi.org/10.1016/0166-2236(89)90125-2). URL: <https://www.sciencedirect.com/science/article/pii/0166223689901252>.
- [49] Anna S. Mitchell et al. "Advances in Understanding Mechanisms of Thalamic Relays in Cognition and Behavior". In: *Journal of Neuroscience* 34.46 (2014), pp. 15340–15346. ISSN: 0270-6474. DOI: [10.1523/JNEUROSCI.3289-14.2014](https://doi.org/10.1523/JNEUROSCI.3289-14.2014). URL: <https://www.jneurosci.org/content/34/46/15340>.
- [50] F. Nissl. "Die Grosshirnanteile des Kaninchens." In: *Archiv für Psychiatrie und Nervenkrankheiten* 52 (1913), pp. 867–953. DOI: [10.1007/BF02160485](https://doi.org/10.1007/BF02160485).
- [51] J Overwiening et al. "A Multi-Scale Study of Thalamic State-Dependent Responsiveness". In: *bioRxiv* (preprint, 2024). In review. DOI: [10.1101/2023.12.02.567941](https://doi.org/10.1101/2023.12.02.567941). URL: <https://www.biorxiv.org/content/early/2024/06/29/2023.12.02.567941>.
- [52] Athanasios Papoulis. "Probability, Random Variables and Stochastic Processes". In: McGraw-Hill, Inc., 1965. ISBN: 0-07-040477-5.

- [53] Didier Pinault and Martin Deschênes. "Projection and innervation patterns of individual thalamic reticular axons in the thalamus of the adult rat: A three-dimensional, graphic, and morphometric analysis". In: *Journal of Comparative Neurology* 391.2 (1998), pp. 180–203. doi: [10.1002/\(SICI\)1096-9861\(19980209\)391:2;1-2](https://doi.org/10.1002/(SICI)1096-9861(19980209)391:2;1-2). URL: <https://onlinelibrary.wiley.com/doi/abs/10.1002/%28SICI%291096-9861%2819980209%29391%3A2%3C180%3A%3AAID-CNE3%3E3.0.CO%3B2-Z>.
- [54] Eion J. Ramcharan, James W. Gnadt, and S. Murray Sherman. "Burst and tonic firing in thalamic cells of unanesthetized, behaving monkeys". In: *Visual Neuroscience* 17.1 (2000), pp. 55–62. doi: [10.1017/S0952523800171056](https://doi.org/10.1017/S0952523800171056).
- [55] R. Rao and D. Ballard. "Predictive coding in the visual cortex: a functional interpretation of some extra-classical receptive-field effects." In: *Nat Neurosci* 2 (1999), pp. 79–87. doi: [10.1038/4580](https://doi.org/10.1038/4580).
- [56] Björn Rasch and Jan Born. "About sleep's role in memory". In: *Physiol Rev.* 2.93 (2013). doi: [10.1152/physrev.00032.2012](https://doi.org/10.1152/physrev.00032.2012).
- [57] Jerzy E Rose and Clinton N Woolsey. "Organization of the mammalian thalamus and its relationships to the cerebral cortex". In: *Electroencephalography and clinical neurophysiology* 1.1-4 (1949), pp. 391–404.
- [58] Michael T. Rosenstein, James J. Collins, and Carlo J. De Luca. "A practical method for calculating largest Lyapunov exponents from small data sets". In: *Physica D: Nonlinear Phenomena* 65.1 (1993), pp. 117–134. ISSN: 0167-2789. doi: [https://doi.org/10.1016/0167-2789\(93\)90009-P](https://doi.org/10.1016/0167-2789(93)90009-P). URL: <https://www.sciencedirect.com/science/article/pii/016727899390009P>.
- [59] Paula Sanz-Leon et al. "Mathematical framework for large-scale brain network modeling in The Virtual Brain". In: *NeuroImage* 111 (2015), pp. 385–430. ISSN: 1053-8119. doi: <https://doi.org/10.1016/j.neuroimage.2015.01.002>. URL: <https://www.sciencedirect.com/science/article/pii/S1053811915000051>.
- [60] Thomas Schreiner et al. "The human thalamus orchestrates neocortical oscillations during NREM sleep". In: *Nat Commun* 13 (2022). doi: <https://doi.org/10.1038/s41467-022-32840-w>.
- [61] Murray Sherman and Rainer Guillery. *Exploring the Thalamus and Its Role in Cortical Function*. Jan. 2009. ISBN: 9780262316231. doi: [10.7551/mitpress/2940.001.0001](https://doi.org/10.7551/mitpress/2940.001.0001).
- [62] Murray S. Sherman and Christof Koch. "The control of retinogeniculate transmission in the mammalian lateral geniculate nucleus". In: *Experimental Brain Research* 63 (2004), pp. 1–20. URL: <https://api.semanticscholar.org/CorpusID:3220019>.
- [63] Guillary RW Sherman SM. "The role of the thalamus in the flow of information to the cortex." In: *Philos Trans R Soc Lond B Biol Sci.* 357.1428 (2002), pp. 1695–1708. doi: [10.1098/rstb.2002.1161](https://doi.org/10.1098/rstb.2002.1161).
- [64] C.S. Sherrington. *The integrative action of the nervous system*. New Haven: Yale University Press, 1906.
- [65] Yousheng Shu and David A. McCormick. "Inhibitory interactions between ferret thalamic reticular neurons." In: *Journal of neurophysiology* 87.5 (2002), pp. 2571–6. URL: <https://api.semanticscholar.org/CorpusID:18553357>.
- [66] Sherman SM. "Thalamocortical interactions." In: *Current Opinion in Neurobiology* 22.4 (2012), pp. 575–579. doi: [10.1016/j.conb.2012.03.005](https://doi.org/10.1016/j.conb.2012.03.005).

- [67] M Steriade et al. "Abolition of spindle oscillations in thalamic neurons disconnected from nucleus reticularis thalami". In: *J Neurophysiol.* 54(6) (1985), pp. 1473–1497. doi: <https://doi.org/10.1152/jn.1985.54.6.1473>.
- [68] M. Steriade, Igor Timofeev, and F. Grenier. "Natural Waking and Sleep States: A View From Inside Neocortical Neurons". In: *J Neurophysiol* 85 (May 2001), pp. 1969–85. doi: [10.1152/jn.2001.85.5.1969](https://doi.org/10.1152/jn.2001.85.5.1969).
- [69] Mircea Steriade. *Neuronal Substrates of Sleep and Epilepsy*. Cambridge University Press, 2003. doi: [10.1017/CBO9780511541711](https://doi.org/10.1017/CBO9780511541711).
- [70] Mircea Steriade. *Acetylcholine systems and rhythmic activities during the waking–sleep cycle*. 2004. doi: [10.1016/S0079-6123\(03\)45013-9](https://doi.org/10.1016/S0079-6123(03)45013-9).
- [71] Sejnowski TJ Steriade M McCormick DA. "Thalamocortical oscillations in the sleeping and aroused brain." In: *Science* 262.5134 (1993), pp. 679–685. doi: [10.1126/science.8235588](https://doi.org/10.1126/science.8235588).
- [72] Marcel Stimberg, Romain Brette, and Dan FM Goodman. "Brian 2, an intuitive and efficient neural simulator". In: *eLife* 8 (Aug. 2019). Ed. by Frances K Skinner, e47314. ISSN: 2050-084X. doi: [10.7554/eLife.47314](https://doi.org/10.7554/eLife.47314).
- [73] Jordy Tasserie et al. "Deep brain stimulation of the thalamus restores signatures of consciousness in a nonhuman primate model". In: *Science Advances* 8.11 (2022), eabl5547. doi: [10.1126/sciadv.abl5547](https://doi.org/10.1126/sciadv.abl5547). URL: <https://www.science.org/doi/abs/10.1126/sciadv.abl5547>.
- [74] Federico Tesler et al. "A multiscale model of striatum microcircuit dynamics". In: *bioRxiv* (2023), pp. 2023–12.
- [75] Federico Tesler et al. "Multiscale modelling of neuronal dynamics in hippocampus CA1". In: *bioRxiv* (2024), pp. 2024–04.
- [76] Jonathan Touboul and Romain Brette. "Dynamics and bifurcations of the adaptive exponential integrate-and-fire model". In: *Biological cybernetics* 99 (Dec. 2008), pp. 319–34. doi: [10.1007/s00422-008-0267-4](https://doi.org/10.1007/s00422-008-0267-4).
- [77] N.G. Van Kampen. *Stochastic Processes in Physics and Chemistry*. 3rd ed. Elsevier B.V., 2007. ISBN: 978-0-444-52965-7. doi: [10.1016/B978-0-444-52965-7.X5000-4](https://doi.org/10.1016/B978-0-444-52965-7.X5000-4).
- [78] Jonathan D. Victor et al. "Mean-field modeling of thalamocortical dynamics and a model-driven approach to EEG analysis". In: *Proceedings of the National Academy of Sciences* 108.supplement_3 (2011), pp. 15631–15638. doi: [10.1073/pnas.1012168108](https://doi.org/10.1073/pnas.1012168108). URL: <https://www.pnas.org/doi/abs/10.1073/pnas.1012168108>.
- [79] Tim P. Vogels and L. F. Abbott. "Signal Propagation and Logic Gating in Networks of Integrate-and-Fire Neurons". In: *Journal of Neuroscience* 25.46 (2005), pp. 10786–10795. ISSN: 0270-6474. doi: [10.1523/JNEUROSCI.3508-05.2005](https://doi.org/10.1523/JNEUROSCI.3508-05.2005). URL: <https://www.jneurosci.org/content/25/46/10786>.
- [80] C. van Vreeswijk and H. Sompolinsky. "Chaos in Neuronal Networks with Balanced Excitatory and Inhibitory Activity". In: *Science* 274.5293 (1996), pp. 1724–1726. doi: [10.1126/science.274.5293.1724](https://doi.org/10.1126/science.274.5293.1724). URL: <https://www.science.org/doi/abs/10.1126/science.274.5293.1724>.
- [81] A. E. Walker. *The primate thalamus*. Oxford, England: Univ. Chicago Press, 1938. ISBN: 1938-06223-000.

- [82] Chaoming Wang, Shangyang Li, and Si Wu. "Analysis of the Neuron Dynamics in Thalamic Reticular Nucleus by a Reduced Model". In: *Frontiers in Computational Neuroscience* 15 (2021). ISSN: 1662-5188. doi: [10.3389/fncom.2021.764153](https://doi.org/10.3389/fncom.2021.764153). URL: <https://www.frontiersin.org/articles/10.3389/fncom.2021.764153>.
- [83] Ralf D. Wimmer et al. "Thalamic control of sensory selection in divided attention". In: *Nature* 526.7605 (2015). doi: [10.1038/nature15398](https://doi.org/10.1038/nature15398). URL: <https://doi.org/10.1038/nature15398>.
- [84] Jakob Wolfart et al. "Synaptic background activity controls spike transfer from thalamus to cortex". In: *Nature Neuroscience* 8 (2005), pp. 1760–1767. URL: <https://api.semanticscholar.org/CorpusID:1352493>.
- [85] Rikuhiro G. Yamada and Hiroki R. Ueda. "Molecular Mechanisms of REM Sleep". In: *Frontiers in Neuroscience* 13 (2020). ISSN: 1662-453X. doi: [10.3389/fnins.2019.01402](https://doi.org/10.3389/fnins.2019.01402). URL: <https://www.frontiersin.org/journals/neuroscience/articles/10.3389/fnins.2019.01402>.
- [86] W. Yang et al. "Thalamus-driven functional populations in frontal cortex support decision-making." In: *Nat Neurosci* 25 (2022), pp. 1339–1352. doi: [10.1038/s41593-022-01171-w](https://doi.org/10.1038/s41593-022-01171-w).
- [87] Y. Zerlaut et al. "Modeling mesoscopic cortical dynamics using a mean-field model of conductance-based networks of adaptive exponential integrate-and-fire neurons." In: *J Comput Neurosci* 45-61.44 (2018). doi: [10.1007/s10827-017-0668-2](https://doi.org/10.1007/s10827-017-0668-2).
- [88] Yann Zerlaut et al. "Heterogeneous firing rate response of mice layer V pyramidal neurons in the fluctuation-driven regime". In: *The Journal of Physiology* 594 (May 2016). doi: [10.1113/JP272317](https://doi.org/10.1113/JP272317).

GLOSSARY

ANTERIOR An anatomical term indicating the *front* or forward-facing direction of an organism or structure; in humans, it refers to the direction toward the face or eyes.

CLOSURE PROBLEM The statistical closure problem is an open hierarchy of statistical equations in which the equation for a moment contains the unknown higher-order moment (see [Section A.2](#) for more details).

DEEP BRAIN STIMULATION Deep brain stimulation (DBS) is a reversible neurosurgical procedure used to treat various neurological and psychiatric disorders. It involves implanting electrodes into specific brain regions and delivering controlled electrical impulses to modulate the activity of targeted neural circuits. DBS has been shown to effectively alleviate symptoms associated with conditions such as Parkinson's disease, essential tremor, dystonia, obsessive-compulsive disorder, epilepsy, and treatment-resistant depression. Additionally, recent studies indicate that stimulation of the thalamus may help restore consciousness in unconscious patients.

DEFAULT MODE NETWORK The Default Mode Network (DMN) is a network of interconnected brain regions that are active during restful wakefulness when an individual is not focused on the external environment, such as during daydreaming or mind-wandering. Discovered using functional magnetic resonance imaging (*fMRI*), the DMN is associated with higher-order cognitive functions including autobiographical memory, future planning, social cognition, self-referential thought, and aspects of consciousness. Key regions of the DMN include the medial prefrontal cortex, posterior cingulate cortex, precuneus, and lateral parietal cortex, which exhibit strong functional connectivity during rest.

ERDOS-RENYI MODEL The Erdos-Renyi model describes a random network in which all graphs on a random but fixed vertex set with a random but fixed number of edges are equally likely (see [Section A.2](#) for more details).

GAP JUNCTIONS Gap junctions allow for the direct passage of ions and small molecules, such as neurotransmitters, second messengers, and metabolites, between interconnected neurons. Through the passage of ions, particularly potassium and sodium ions, gap junctions allow electrical signals to spread directly from one neuron to another. This process helps synchronize the electrical activity of interconnected neurons, promoting coordinated firing patterns and network oscillations.

GRAY MATTER Refers to the regions of the central nervous system that primarily contain cell bodies, dendrites, un-myelinated axons, glial cells, and synapses. It appears gray due to the presence of cell bodies and capillaries. It serves as the site of information processing and integration in the central nervous system.

HYPERPOLARIZATION A change in a neuron's membrane potential that makes it more negative relative to the resting potential. Hyperpolarization decreases the likelihood of generating an action potential, thereby inhibiting neuronal activity.

IN VITRO *In vitro* refers to studies and experiments conducted on biological cells or tissues outside their normal biological context, typically in a controlled laboratory environment such as petri dishes or test tubes. In neuroscience, this includes studies of cultured neurons, brain slices, or isolated synapses.

IN VIVO *In vivo* refers to studies and experiments conducted within living organisms. In neuroscience, this includes research on brain functions using techniques such as neuroimaging, electrophysiological recordings in awake animals or humans, and behavioral studies.

LATERAL An anatomical term referring to a position or direction away from the midline of the body; toward the *side* of an organism or structure.

MEDIAL An anatomical term indicating a position or direction toward the midline or center of the body; structures that are closer to the midline are considered medial.

NEUROTRANSMITTERS Neurotransmitters are chemical messengers that transmit signals across synapses—the specialized junctions between neurons or between neurons and other target cells (e.g., muscle or gland cells). They are released from synaptic vesicles in the presynaptic neuron and bind to specific receptors on the postsynaptic cell, modulating neuronal activity and influencing physiological processes and behaviors. Neurotransmitters can have excitatory or inhibitory effects on the postsynaptic neuron, depending on the receptors they activate.

NEUROMODULATORS Neuromodulators are signaling molecules in the nervous system that regulate the activity of neurons and neural networks, modulating various brain functions such as arousal, attention, learning, memory, and mood. Unlike classical neurotransmitters, which typically transmit signals directly and rapidly across synapses, neuromodulators often have more diffuse effects over longer time scales, influencing the overall excitability and plasticity of neural circuits. Examples include dopamine, serotonin, norepinephrine, acetylcholine, and certain neuropeptides. Neuromodulators act by binding to specific receptors on neurons, leading to changes in membrane potential, ion channel function, synaptic transmission, or gene expression.

NUCLEUS In neuroscience, a nucleus (plural: nuclei) refers to a distinct cluster of neuronal cell bodies within the central nervous system (CNS), particularly within the brain and spinal cord. Neuronal nuclei are groups of neurons that share similar functions, connectivity patterns, or neurotransmitter characteristics, and often serve as processing centers for specific types of information.

POISSONIAN Describes processes that follow a Poisson probability distribution, which models the number of events occurring within a fixed interval of time or space when these events occur independently and at a constant average rate. In neuroscience, Poissonian processes are often used to model the firing of neurons (*spike trains*), under the

assumption that spikes occur randomly and independently over time, consistent with the population coding principle (see below).

POPULATION CODING PRINCIPLE A principle in neuroscience stating that information is represented by the collective activity of a population of neurons rather than by individual neurons. In this framework, the precise timing of individual spikes is less important than the overall firing rate of the population. This concept is supported by observations that population firing rates correlate with behavioral outputs and sensory inputs (see [55]).

RECEPTIVE FIELD A receptive field is the specific region of sensory space (e.g., area of the visual field, region of skin) in which a stimulus will modify the firing of a particular neuron. For a sensory neuron, the receptive field is the area where stimulation leads to a response in that neuron. This concept extends throughout the nervous system; higher-order neurons have receptive fields that are combinations of the receptive fields of the neurons that provide input to them. For example, a retinal ganglion cell's receptive field is determined by the group of photoreceptors that synapse onto it, and the receptive field of a thalamic relay neuron is determined by the retinal ganglion cells that project to it.

RETINA The retina is a thin layer of neural tissue lining the inner surface of the back of the eye. It contains specialized cells, including photoreceptors (rods and cones), that detect light and convert it into electrical signals. These signals are processed by retinal interneurons and transmitted to the brain via retinal ganglion cells whose axons form the optic nerve. The retina performs initial processing of visual information before it reaches the brain, particularly the lateral geniculate nucleus (LGN) and visual cortex.

SYNAPTIC CONDUCTANCE Synaptic conductance is a measure of how easily ions can flow through synaptic channels when a synapse is activated, reflecting the synaptic strength. It determines the size and duration of synaptic currents in the postsynaptic neuron, thereby influencing neuronal communication and signal integration.

T-CHANNELS T-type calcium channels (T-channels) are a type of voltage-gated calcium channel that activate (open) at relatively low membrane potentials (near the resting potential). They are transient in nature, contributing to pacemaking activities and low-threshold spikes in neurons. In thalamic neurons, T-channels play a crucial role in generating burst firing during states of hyperpolarization, enabling signal transmission and rhythmic oscillations.

WHITE MATTER White matter refers to regions of the central nervous system that are composed mainly of myelinated axons. The myelin sheath, rich in lipids, gives white matter its characteristic color. White matter serves as the communication pathways within the brain and spinal cord, transmitting electrical signals between different gray matter areas, which contain neuronal cell bodies.

DECLARATION OF ACADEMIC INTEGRITY

I hereby confirm that this thesis on *A biologically realistic Mean-field model of the Thalamus* is solely my own work and that I have used no sources or aids other than the ones stated. All passages in my thesis for which other sources, including electronic media, have been used, be it direct quotes or content references, have been acknowledged as such and the sources cited.

Münster, 8 October 2024

Jorin Overwiening

I agree to have my thesis checked in order to rule out potential similarities with other works and to have my thesis stored in a database for this purpose.

Münster, 8 October 2024

Jorin Overwiening

COLOPHON

This document was typeset using the typographical look-and-feel `classicthesis` developed by André Miede. The style was inspired by Robert Bringhurst's seminal book on typography "*The Elements of Typographic Style*". `classicthesis` is available for both `LATEX` and `LyX`:

<https://bitbucket.org/amiede/classicthesis/>